

DTIC FILE COPY

AD-A230 609



①

**S** DTIC  
ELECTE  
JAN 08 1991  
**D**

ANALYSIS AND TESTING OF A  
BISTATIC RADAR CROSS SECTION  
MEASUREMENT CAPABILITY FOR THE  
AFIT ANECHOIC CHAMBER

THESIS

Timothy D. McCool  
Captain, USAF

AFIT/GE/90D-37

**DISTRIBUTION STATEMENT A**  
Approved for public release  
Distribution Unlimited

DEPARTMENT OF THE AIR FORCE  
AIR UNIVERSITY  
**AIR FORCE INSTITUTE OF TECHNOLOGY**

Wright-Patterson Air Force Base, Ohio

91 1 3 092

1

DTIC  
ELECT  
JAN 08 1981  
S  
D

ANALYSIS AND TESTING OF A  
BISTATIC RADAR CROSS SECTION  
MEASUREMENT CAPABILITY FOR THE  
AFIT ANECHOIC CHAMBER

THESIS

Timothy D. McCool  
Captain, USAF

AFIT/GE/90D-37

Approved for public release; distribution unlimited

**ANALYSIS AND TESTING OF A  
BISTATIC RADAR CROSS SECTION  
MEASUREMENT CAPABILITY FOR THE  
AFIT ANECHOIC CHAMBER**

**THESIS**

**Presented to the Faculty of the School of Engineering  
of the Air Force Institute of Technology  
Air University  
In Partial Fulfillment of the  
Requirements for the Degree of  
Master of Science in Electrical Engineering**

**Timothy D. McCool  
Captain, USAF**

**December 1990**

Approved For	
NTIS - GPO	
DEF. T.O.	
Unrestricted	
JAN 1991	
By	
Date	
Dist	
A-1	

**Approved for public release; distribution unlimited**



## *Acknowledgements*

First and foremost, I express my sincere gratitude to those in my life who are my love and inspiration, my wonderful wife Sue and two beautiful children, Christy and Megan. Without your support and encouragement, this would not have been possible. Thank you for being there and enduring the many sacrifices the last eighteen months, I love you!

Throughout this research, valuable assistance was provided by many individuals. Most important is my thesis advisor, Capt Philip Joseph, who I extend my utmost appreciation. His technical knowledge, intuition and guidance were essential to the ultimate completion of the project at hand. As well, I offer my thanks to my thesis committee members, Maj Harry Barksdale and Dr. Vittal Pyati, whose doors were always open if help was needed.

My thesis sponsor, Dr. Brian Kent of WRDC/SNA, deserves a special thanks for his unending support provided during this research endeavor. I spent many hours at the "Barn", with the staff there always willing to provide a helping hand. I am deeply indebted to Richard Porter who provided invaluable assistance along the way, from marking the AFIT chamber using a transit to providing me the luxury of using the computer system whenever I needed it. Likewise, a

special thanks to Dave Frasher, who was always willing to provide the equipment necessary to complete this research effort.

Stan Bashore and Jack Stunkel, of my sponsor's support contractor (Mission Research Corporation), were very helpful. Stan provided invaluable technical advice and assistance in numerous areas of this research. The computer help provided was essential in completing the bistatic RCS prediction plots. Jack constructed the target mounts I used for all the measurements. I pestered him countless times after damaging the mounts, and he was always helpful in providing another mount.

Two other people deserve special thanks for helping me with this research, Capts Dave Carroll and Brian Sanders, fellow LO classmates. Dave provided the knowledge and necessary tools required to get RCS-BSC2 up and running on the school computer network. Finally, I must offer my appreciation to Brian, whose assistance in the AFIT chamber proved invaluable. From helping me characterize the chamber with a probe to the much needed help with Hewlett-Packard basic programming as well as writing the data transfer program used between the Zenith and HP computers, I offer my sincerest thank you. He was always willing to help, even with his research ongoing.

To all of the above people, I want to say THANK YOU!

Timothy D. McCool

## *Table of Contents*

	Page
Acknowledgements . . . . .	ii
Table of Contents . . . . .	iv
List of Figures . . . . .	vii
List of Tables . . . . .	xii
Abstract . . . . .	xiii
I. Introduction . . . . .	1
Background . . . . .	1
Problem Statement . . . . .	4
Approach . . . . .	4
Measurement Summary . . . . .	5
Summary of Current Knowledge . . . . .	7
Theoretical . . . . .	7
Experimental . . . . .	8
Organization . . . . .	9
II. RCS Measurement Theory . . . . .	11
Introduction . . . . .	11
Theory . . . . .	11
RCS . . . . .	11
Scattering Regions . . . . .	13
Scattering Prediction Technique . . . . .	14
Measurement Considerations . . . . .	16
Calibration Equation . . . . .	16

	Page
Target Zone . . . . .	19
Downrange Amplitude Variation . . . . .	20
Crossrange Phase Variation . . . . .	20
Error Signals . . . . .	21
III. AFIT RCS Measurement System . . . . .	24
Introduction . . . . .	24
Chamber Description . . . . .	24
Physical Layout . . . . .	24
Measurement Equipment . . . . .	27
Software . . . . .	29
Target Zone . . . . .	30
Monostatic Target Zone. . . . .	31
Bistatic Target Zone. . . . .	32
Noise Floor and Calibration . . . . .	32
Bistatic RCS Measurement Approach . . . . .	37
Characterizing the Chamber . . . . .	38
Monostatic Time Domain . . . . .	39
Bistatic Time Domain . . . . .	39
IV. Relevant Software . . . . .	53
Measurement Software . . . . .	53
Data Transfer Software . . . . .	56
Prediction Software . . . . .	56
First Order UTD Analysis of 2D Strip . . . . .	58

	Page
V. Data Analysis and Validation . . . . .	65
Spheres . . . . .	67
Square Flat Plates . . . . .	70
Triangle Flat Plates . . . . .	73
Five Sided Flat Plates . . . . .	74
Reciprocity . . . . .	76
Bistatic Measurements Using Different Transmit Antennas . . . . .	77
Noise Floor Measurements . . . . .	78
Error Analysis . . . . .	79
VI. Conclusions and Recommendations . . . . .	81
Summary . . . . .	81
Conclusions . . . . .	81
Recommendations . . . . .	82
Appendix A. Predicted and Measured RCS of Targets .	84
Appendix B. Procedure for Performing Bistatic Measurements in AFIT's Far-field RCS Chamber . . . . .	130
Set of Instructions . . . . .	131
Additional Items Required	133
Appendix C. Software Listing . . . . .	134
Section I. UTD Flat Plate Prediction Code . . . . .	135
Section II. BISP Code . . . . .	139
Section III. ARMS Bistatic Code . . . . .	147
Section IV. Data Transfer Code . . . . .	158
Bibliography . . . . .	161
Vita . . . . .	163



## *List of Figures*

Figure	Page
1. Monostatic and bistatic radar geometry . . . . .	3
2. UTD geometry for wedge diffraction . . . . .	15
3. Crossrange phase variation in target zone, modeling transmitter as a point source. . . . .	22
4. Side view of AFIT far-field RCS chamber . . . . .	25
5. Top view of AFIT far-field RCS chamber . . . . .	26
6. AFIT RCS chamber measurement equipment . . . . .	28
7. Crossrange extent of target zone versus frequency, monostatic case. . . . .	31
8. Crossrange extent of target zone versus frequency, bistatic case. . . . .	33
9. Monostatic noise floor; range gate of 7 nsec, vertical polarization, and averaging factor of 32 . . . . .	35
10. Bistatic noise floor; bistatic angle of 45 degrees, range gate of 7 nsec, and averaging factor of 32 . . . . .	35
11. Bistatic noise floor; bistatic angle of 90 degrees, range gate of 7 nsec, and averaging factor of 32 . . . . .	36
12. Bistatic noise floor; bistatic angle of 135 degrees, range gate of 7 nsec, and averaging factor of 32 . . . . .	36
13. Time domain measurement, monostatic case . . . . .	40
14. Time domain measurement for bistatic angle of 45 degrees, X-band antenna transmitting . . . . .	43
15. Time domain measurement for bistatic angle of 45 degrees, AEL antenna transmitting . . . . .	44
16. Time domain measurement for bistatic angle of 45 degrees, Flam and Russell antenna transmitting . . . . .	45
17. Time domain measurement for bistatic angle of 90 degrees, X-band antenna transmitting . . . . .	46

Figure		Page
18.	Time domain measurement for bistatic angle of 135 degrees, X-band antenna transmitting . . . .	47
19.	Time domain measurement with time scale expanded for bistatic angle of 135 degrees . . .	48
20.	Definition of strip geometry used in UTD analysis	59
21.	Target geometry used for RCS predictions and measurements . . . . .	65
22.	Targets used . . . . .	66
23.	Measured RCS: 2.5" sphere, monostatic, 10 GHz, Vertical Polarization . . . . .	85
24.	Measured RCS: 2.5" sphere, $\beta=45^\circ$ , 10 GHz, Vertical Polarization, AEL antenna transmitting	86
25.	Measured RCS: 2.5" sphere, $\beta=45^\circ$ , 10 GHz, Vertical Polarization, X-band antenna transmitting	87
26.	Measured RCS: 2.5" sphere, $\beta=90^\circ$ , 10 GHz, Vertical Polarization . . . . .	88
27.	Measured RCS: 2.5" sphere, $\beta=135^\circ$ , 10 GHz, Vertical Polarization . . . . .	89
28.	Measured RCS: 6" sphere, monostatic, 10 GHz, Vertical Polarization . . . . .	90
29.	Measured RCS: 6" sphere, $\beta=45^\circ$ , 10 GHz, Vertical Polarization, AEL antenna transmitting . . . . .	91
30.	Measured RCS: 6" sphere, $\beta=45^\circ$ , 10 GHz, Vertical Polarization, X-band antenna transmitting . . . .	92
31.	Measured RCS: 6" sphere, $\beta=90^\circ$ , 10 GHz, Vertical Polarization . . . . .	93
32.	Measured RCS: 6" sphere, $\beta=135^\circ$ , 10 GHz, Vertical Polarization . . . . .	94
33.	Comparison of monostatic RCS predictions: 3.5" square flat plate, 10 GHz, Vertical Polarization	95
34.	Measured RCS: 3.5" square flat plate, monostatic, 10 GHz, Vertical Polarization . . . .	96

Figure		Page
35.	Comparison of bistatic RCS predictions: 3.5" square flat plate, $\beta=45^\circ$ , 10 GHz, Vertical Polarization . . . . .	97
36.	Measured RCS: 3.5" square flat plate, $\beta=45^\circ$ , 10 GHz, Vertical Polarization, AEL antenna transmitting . . . . .	98
37.	Measured RCS: 3.5" square flat plate, $\beta=45^\circ$ , 10 GHz, Vertical Polarization, X-band antenna transmitting . . . . .	99
38.	Comparison of bistatic RCS predictions: 3.5" square flat plate, $\beta=90^\circ$ , 10 GHz, Vertical Polarization . . . . .	100
39.	Measured RCS: 3.5" square flat plate, $\beta=90^\circ$ , 10 GHz, Vertical Polarization . . . . .	101
40.	Comparison of bistatic RCS predictions: 3.5" square flat plate, $\beta=135^\circ$ , 10 GHz, Vertical Polarization . . . . .	102
41.	Measured RCS: 3.5" square flat plate, $\beta=135^\circ$ , 10 GHz, Vertical Polarization . . . . .	103
42.	Comparison of monostatic RCS predictions: 6" square flat plate, 10 GHz, Vertical Polarization . . . . .	104
43.	Measured RCS: 6" square flat plate, monostatic, 10 GHz, Vertical Polarization . . . . .	105
44.	Comparison of bistatic RCS predictions: 6" square flat plate, $\beta=45^\circ$ , 10 GHz, Vertical Polarization . . . . .	106
45.	Measured RCS: 6" square flat plate, $\beta=45^\circ$ , 10 GHz, Vertical Polarization, AEL antenna transmitting . . . . .	107
46.	Measured RCS: 6" square flat plate, $\beta=45^\circ$ , 10 GHz, Vertical Polarization, X-band antenna transmitting . . . . .	108
47.	Comparison of bistatic RCS predictions: 6" square flat plate, $\beta=90^\circ$ , 10 GHz, Vertical Polarization . . . . .	109

Figure		Page
48.	Measured RCS: 6" square flat plate, $\beta=90^\circ$ , 10 GHz, Vertical Polarization . . . . .	110
49.	Comparison of bistatic RCS predictions: 6" square flat plate, $\beta=135^\circ$ , 10 GHz, Vertical Polarization . . . . .	111
50.	Measured RCS: 6" square flat plate, $\beta=135^\circ$ , 10 GHz, Vertical Polarization . . . . .	112
51.	Predicted RCS: 6" triangle flat plate, monostatic, 10 GHz, Vertical Polarization . . . .	113
52.	Measured RCS: 6" triangle flat plate, monostatic, 10 GHz, Vertical Polarization . . . .	114
53.	Predicted RCS: 6" triangle flat plate, $\beta=45^\circ$ , 10 GHz, Vertical Polarization . . . . .	115
54.	Measured RCS: 6" triangle flat plate, $\beta=45^\circ$ , 10 GHz, Vertical Polarization . . . . .	116
55.	Predicted RCS: 6" triangle flat plate, $\beta=90^\circ$ , 10 GHz, Vertical Polarization . . . . .	117
56.	Measured RCS: 6" triangle flat plate, $\beta=90^\circ$ , 10 GHz, Vertical Polarization . . . . .	118
57.	Predicted RCS: 6" triangle flat plate, $\beta=135^\circ$ , 10 GHz, Vertical Polarization . . . . .	119
58.	Measured RCS: 6" triangle flat plate, $\beta=135^\circ$ , 10 GHz, Vertical Polarization . . . . .	120
59.	Predicted RCS: Five sided flat plate, monostatic, 10 GHz, Vertical Polarization . . . .	121
60.	Measured RCS: Five sided flat plate, monostatic, 10 GHz, Vertical Polarization . . . .	122
61.	Predicted RCS: Five sided flat plate, $\beta=45^\circ$ , 10 GHz, Vertical Polarization . . . . .	123
62.	Measured RCS: Five sided flat plate, $\beta=45^\circ$ , 10 GHz, Vertical Polarization, X-band antenna transmitting . . . . .	124
63.	Measured RCS: Five sided flat plate, $\beta=45^\circ$ , 10 GHz, Vertical Polarization, Flam & Russell antenna transmitting . . . . .	125

Figure		Page
64.	Predicted RCS: Five sided flat plate, $\beta=90^\circ$ , 10 GHz, Vertical Polarization . . . . .	126
65.	Measured RCS: Five sided flat plate, $\beta=90^\circ$ , 10 GHz, Vertical Polarization . . . . .	127
66.	Predicted RCS: Five sided flat plate, $\beta=135^\circ$ , 10 GHz, Vertical Polarization . . . . .	128
67.	Measured RCS: Five sided flat plate, $\beta=135^\circ$ , 10 GHz, Vertical Polarization . . . . .	129

## *List of Tables*

Table	Page
1. Initial instrument states of HP 8510 network analyzer for RCS measurements . . . . .	52
2. Exact sphere data from BISPH at 10 GHz . . . . .	55
3. Exact sphere data from BISPH at 10 GHz and vertical polarization . . . . .	68
4. RCS for 2.5 inch Sphere (10 GHz, Ver Pol) . . . . .	69
5. RCS for 6 inch Sphere (10 GHz, Ver Pol) . . . . .	69
6. Main Lobe Peak RCS for 3.5 inch Square Flat Plate (10 GHz, Ver Pol) . . . . .	72
7. Main Lobe Peak RCS for 6 inch Square Flat Plate (10 GHz, Ver Pol) . . . . .	73
8. Main Lobe Peak RCS for Triangle Flat Plate (10 GHz, Ver Pol) . . . . .	74
9. Main Lobe Peak RCS for 5 sided Flat Plate (10 GHz, Ver Pol) . . . . .	76
10. Peak RCS from the spheres and square flat plates at $\beta = 45^\circ$ using different transmit antennas (10 GHz, Ver Pol) . . . . .	78
11. RCS of 5 inch sphere at 10 GHz and Vertical Polarization . . . . .	80

## *Abstract*

This research effort examined the feasibility of performing bistatic radar cross section (RCS) measurements in the AFIT anechoic chamber. The capability was established to measure the bistatic RCS of a target versus frequency and versus target azimuth angle. In either case, one of the three bistatic angles (angle between transmit and receive antennas) is available: 45°, 90°, and 135°.

Accurate bistatic RCS measurements were obtained using a CW radar and utilizing background subtraction, bistatic calibration, and software range gating. Simple targets were selected for validation purposes since their bistatic RCS could be predicted. These consisted of spheres and flat plates (square, triangular, and five sided).

Several computer codes were utilized for system validation. Two codes based on the Uniform Theory of Diffraction were used to predict the scattering from the flat plates. A program using a Mie series solution provided the exact scattering for the spheres, which were used for both RCS predictions and system calibration.

# ANALYSIS AND TESTING OF A BISTATIC RADAR CROSS SECTION MEASUREMENT CAPABILITY FOR THE AFIT ANECHOIC CHAMBER

## *1. Introduction*

### *Background*

The radar cross section (RCS) of a target is a ratio of the radar energy scattered in a particular direction away from a target to that which is incident on the target. The RCS of targets has become increasingly important in recent years with the emphasis the military has placed on the design of low observable or stealth technology platforms. Monostatic radars, as shown in Figure 1, dominate the radar systems in use today. Thus, the emphasis in reducing an objects monostatic RCS has prevailed. One method used to reduce the echo properties of these platforms is through shaping. By shaping an object, incident electromagnetic energy from the radar transmitter can be scattered in directions other than that of the expected location of the radar receiver. Shaping that reduces the RCS of an object in the backscatter direction, often creates an enhanced



radar return in bistatic directions (9:190).

As shown in Figure 1, a bistatic radar has its transmit and receive antennas separated by some bistatic angle. In bistatic radar scattering, the electromagnetic wave arrives at the target from the source and scatters in all directions, one of which is detected by the receiver. It follows that bistatic RCS measurements are performed to determine the scattering from a target at a particular bistatic geometry. These measurements are often accomplished on low monostatic RCS targets to determine their detectability in bistatic conditions (1:1).

Bistatic measurements are inherently more difficult than backscatter measurements (6:243). The simple addition of another antenna creates problems in several areas when performing bistatic measurements (4:148). One particular area of concern, as an example, is the direct feeding of the electromagnetic signal from the transmit antenna to the receive antenna. The signal received from this direct path can corrupt the measurement in certain situations. This will be discussed in more detail later.

While monostatic RCS measurements have become commonplace, details concerning bistatic measurements has lagged considerably behind. With the focus on monostatic measurements, the available literature is abundant. Conversely, documentation concerning bistatic measurements is minimal. The limited amount of data available on

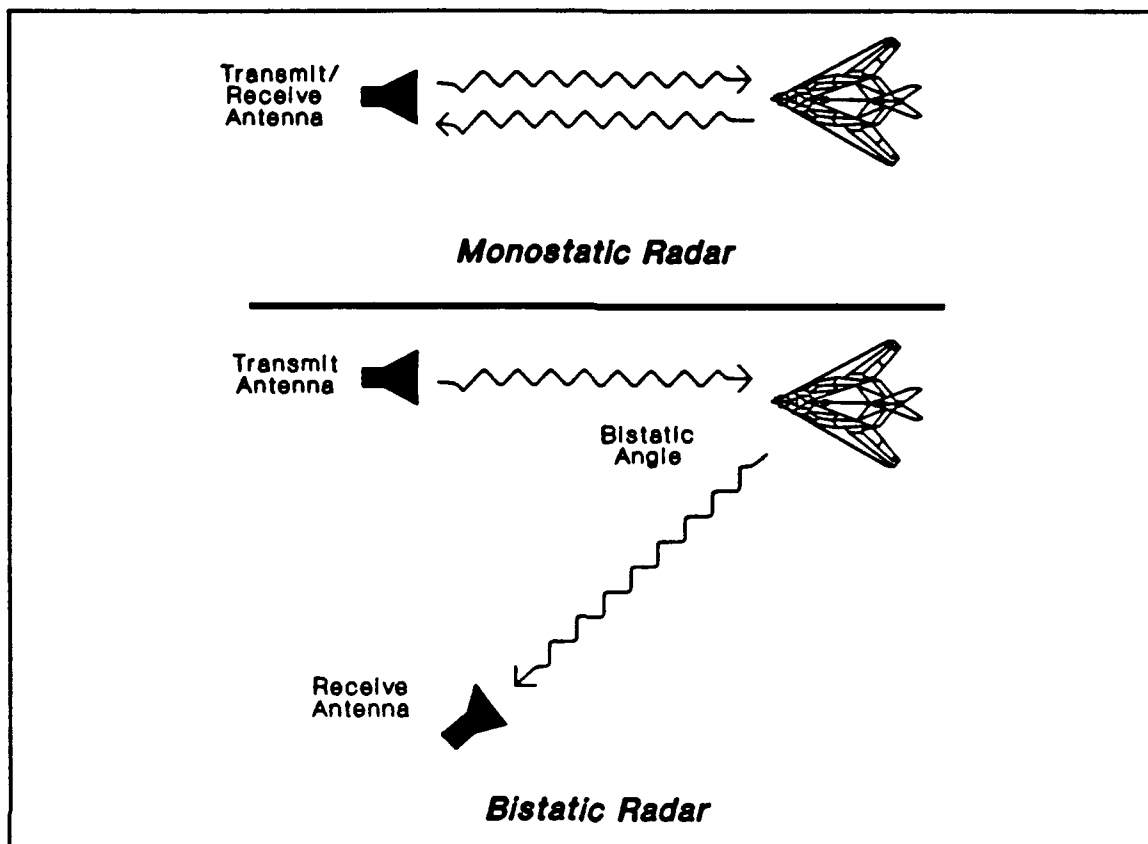


Figure 1. Monostatic and bistatic radar geometry

bistatic measurements combined with the current interest by the military in the bistatic RCS of targets result in the need for further research in this subject area.

Recent research concerning bistatic scattering and measurements has been accomplished at the Wright Research and Development Center's (WRDC) far-field range by several WRDC engineers and two Air Force Institute of Technology (AFIT) students (13; 17; 19). During 1987 and 1988 similar measurements were performed on a larger scale by the Air Force's 6585th Test Group at the Radar Target Scattering

(RATSCAT) outdoor facility (1).

AFIT has a far-field RCS measurement range used by graduate students for research and course work. It has been developed and used exclusively for monostatic measurements. Since each measurement facility has unique equipment, the requirements and methodology to perform a particular type of measurement varies between measurement ranges. Despite the increasing importance of bistatic scattering characteristics, AFIT's capability to provide experimental work to their students in this area is nonexistent.

#### *Problem Statement*

The purpose of this research is to expand the measurement capability of the AFIT far-field RCS range. The objective is to establish the capability to perform accurate bistatic radar cross section measurements using AFIT's far-field RCS range.

#### *Approach*

To accomplish the above objective, a feasibility study was first performed on the AFIT chamber system configuration to determine allowable target dimensions, the required radius from target to receive antenna, and the relative strength and timing of target return signals and various error signals that would be detected by the receive antenna. The next step was to quantify the signals received at certain bistatic angles by operating the network analyzer

manually. This ensured that the target returns could be isolated from the error signals and allowed the internal settings of the network analyzer to be set so that the measurement system would do so. Finally, before any bistatic RCS measurements could be performed on test targets to verify system performance, the software that controls the chamber had to be modified to implement the bistatic measurement capability. Both monostatic and bistatic RCS measurements were then performed on relatively simple canonical targets of which RCS predictions had been made for comparison.

#### *Measurement Summary*

This effort developed the foundation required to perform accurate bistatic measurements in the AFIT RCS chamber with future application to both course work and research. The bistatic capability was to include both frequency response measurements and pattern cut measurements. The frequency response measurement provides the RCS in units of dBsm for a target versus frequency for a fixed target aspect angle. The system actually measures the complex return signal, and is thus capable of inverse fourier transforming the data to generate the bandlimited impulse response. The pattern cut measurement provides the RCS in units of dBsm for a target at a fixed frequency versus aspect angle as the target rotates 360 degrees.

The targets selected for the verification phase were a

2.5 inch and 6 inch diameter sphere, a 3.5 inch and 6 inch square flat plate, a 6 inch equilateral triangle flat plate, and a five sided flat plate. The pattern cut RCS measurements were confined to 10 GHz with the targets generally being in the far field of the antennas. RCS pattern cut measurements were performed with a bistatic angle of  $0^\circ$  (monostatic),  $45^\circ$ ,  $90^\circ$ , and  $135^\circ$ ; both antennas were aligned for vertical polarization. The measurements at  $45^\circ$ , for the spheres and square flat plates, were done first with an American Electronic Laboratories (AEL) broadband 2 GHz to 18 GHz antenna and then with a high gain X-band 8 GHz to 12.4 GHz antenna as the transmit antenna. The receive antenna for these measurements was a Flam and Russell 6 GHz to 18 GHz diagonal horn antenna. The bistatic measurements performed at  $90^\circ$  and  $135^\circ$  were done with the X-band antenna only. An additional pattern cut measurement was performed, using the 5 sided flat plate as the target, to verify the system response is independent of which antenna is receiving and which is transmitting.

The frequency response measurements consisted of four measurements. These measurements were noise floor measurements which will be explained in more detail later. Noise floor measurements were taken for the monostatic case as well as for bistatic angles of  $45^\circ$ ,  $90^\circ$ , and  $135^\circ$ . All noise floor measurements were accomplished at a frequency range of 8 GHz to 12.4 GHz using the X-band antenna (for

bistatic) as the transmit antenna and the Flam and Russell antenna as the receive antenna.

#### *Summary of Current Knowledge*

*Theoretical* (8; 15:11-13). With the central focus of radar and radar reflectivity measurements on the monostatic situation, the data available for bistatic measurements is limited, as was noted earlier. Consequently, physical optics approximations were used to develop the monostatic-bistatic equivalence theorem (MBET). This applies to bistatic angles less than 180 degrees, and it predicts bistatic RCS from monostatic data. The theorem states that the bistatic RCS is equal to the monostatic RCS determined at the bisector of the bistatic angle. The theorem assumes that the targets are sufficiently smooth and much larger than the wavelength. This was verified by Crispin et al. for bistatic angles much less than 180 degrees using physical optics approximations.

Kell extended the theorem to a broader class of targets including metallic and dielectric coated ones. His theorem stated that as the bistatic angle approaches zero, the monostatic cross section of a target viewed on the bisector of the bistatic angle ( $\beta$ ) at a frequency reduced by a factor of  $\cos(\beta/2)$  will approximate the bistatic RCS. It is important to remember that Kell's method of predicting bistatic RCS from monostatic data depends upon the individual scattering centers on the target and their phase

differences. Kell's theorem is not applicable to targets in which multiple scattering is important or targets whose cross section has contributions from creeping waves.

*Experimental.* RATSCAT recently completed a report that documents their bistatic measurement capabilities and considerations required to perform accurate measurements. The report notes the fact that "bistatic measurement programs frequently require unique setup approaches" (1:1). As mentioned earlier, the unique setup approaches mentioned in the RATSCAT report are the goal of this research for application to the AFIT RCS measurement range.

Bistatic RCS measurement research (17:85-86) at the WRDC far-field range examined bistatic RCS measurement tradeoffs at their indoor facility. Under the given circumstances, it was determined that CW nulling would be used to obtain the bistatic data. CW nulling is an analog vector subtraction of the background clutter in the chamber. The bistatic measurements were performed with the transmit and receive antennas fixed and the target rotated in the azimuth plane. The research concluded that the MBET prediction technique worked poorly for bistatic angles above 90°.

Additional bistatic research (13; 19) at the WRDC range focused on resonance region scattering from a selected group of targets, and on evaluating the bistatic equivalence theorem for the near and far-field of selected targets. The

research attacked the problems encountered in obtaining bistatic measurements at indoor measurement ranges. The research concluded, as did (17), that much work is needed in the area of bistatic RCS measurement and prediction.

### *Organization*

Chapter II discusses the theory supporting the concept of both monostatic and bistatic RCS. Specific details relating to performing RCS measurements will be investigated as well.

Chapter III will discuss specific details of the AFIT measurement range. The physical layout of the chamber will be provided along with a detailed explanation of the measurement equipment and an overview of the software that controls the measurements. Specific characteristics of the AFIT chamber will then be discussed. Finally, the bistatic measurement approach will be provided in detail.

Chapter IV will discuss the software used for the bistatic measurements and predictions. First, the software written to provide the bistatic capability within the chamber will be explained. This will be followed by a discussion of the software used to transfer data files between computer systems with specific application to the frequency response measurements. In addition, the software used to provide predictions of the targets under test will be discussed.

Chapter V investigates the measurements performed in



the AFIT chamber. The targets measured will be discussed as well as the measurement geometry used to aid in interpreting the data. The measurements will be compared to predictions with specific detail provided on maximum RCS obtained at certain angles. An error analysis will be provided, as well.

The final chapter contains conclusions drawn from this effort. In addition, recommendations for further study will be provided. Three appendices follow the last chapter. Appendix A contains the measurements and predictions performed. Appendix B provides specific steps required to perform bistatic measurements in the AFIT chamber. Appendix C contains four sections with listings of the software code used in this research.

## II. RCS Measurement Theory

### Introduction

This chapter describes the theory supporting the concept of both monostatic and bistatic RCS. Relevant equations will be provided and discussed along with the assumptions required. Several topics related to performing RCS measurements will be investigated as well. These will include a look at the RCS calibration equation along with a discussion of the quiet zone, noise floor measurements, and error signals within the chamber.

### Theory

RCS. The radar cross section (RCS) of a target is a quantity relating the amount of power scattered by the target in some direction to the amount of power incident on the target. The RCS is defined as

$$\sigma = \lim_{R \rightarrow \infty} 4\pi R^2 \frac{|E_s|^2}{|E_i|^2} \quad (1)$$

where  $R$  is the distance from the radar to the target,  $E_s$  is the scattered field, and  $E_i$  is the incident field at the target (4:62).

It is important to note that the RCS is defined so that it is independent of the distance between the radar and the target. This occurs since the scattered field decays as  $1/R$ . The limiting process in the definition ensures that the incident field is a plane wave. In what is called a far-field range, the transmit antenna directly illuminates the target. A large enough  $R$  is needed such that the illuminating field satisfactorily approximates a plane wave. This is related to the far-field spoken of in antenna theory, where a target of a certain size at some distance from an antenna will see a phase variation of no more than  $\pi/8$  radians in the incident field from this antenna. This leads to

$$R > \frac{2 D^2}{\lambda} \quad (2)$$

where

$R$  = range,

$D$  = maximum target dimension, and

$\lambda$  = wavelength.

In the RCS problem, one must ensure that the target sees limited phase and amplitude variation in the incident field (ideally both would be zero, as for a plane wave), and that the receive antenna is effectively in the far zone of the target.

Another assumption inherent to the definition of the

RCS of a target is the requirement that the target be isolated in free space. This condition means that the electromagnetic wave incident at the target and the wave scattered from the target to the receive antenna are solely a function of the antenna and/or the target and nothing else. Other signals present could result in errors in the measurements. Current measurement techniques result in these signals being negligible if the errors are correctly dealt with. The next major section, titled *Measurement Considerations*, will examine this in more detail.

RCS is in units of area, and is often expressed in dB relative to a square meter or a square wavelength. Even though the unit for RCS is area, the radar cross section of an object may be very different from its physical cross section. As noted by Skolnik, "the radar cross section of a target is the (fictional) area intercepting that amount of power, when scattered equally in all directions, produces an echo at the radar equal to that from the target" (18:33).

The RCS of a target depends on parameters related to the target and the radar. The target parameters include its geometry, orientation with respect to the incident wave, and material make-up, while the radar parameters include the operating frequency and waveform along with the polarization of the antennas (5:500).

*Scattering Regions.* Electromagnetic scattering is usually divided into three regions, which are characterized

by the ratio of the target size ( $D$ ) to the wavelength ( $\lambda$ ), or  $D/\lambda$ . The three regions are the Rayleigh region (low frequency), the Mie region (resonance), and the optical region (high frequency). The wavelength and frequency of an electromagnetic field are inversely proportional to each other; that is, as the frequency increases, the wavelength becomes smaller.

In the Rayleigh region the targets are much smaller than the wavelength of the incoming electromagnetic wave. Within the Mie region, the scatterer and the incident wavelength have approximately the same dimension. The shape of the scatterer is important in this region since interactions between points on the scatterer can be significant (9:55). In the optical region the targets are much larger than the incident wavelength. In this region the interactions between points on the scatterer are not significant. The scatterer can be divided into a collection of independent scattering centers that when combined constitute the target's scattered field (9:57). Several techniques exist to determine the solution of the scattered field expected from a scatterer in the high frequency region.

*Scattering Prediction Technique.* One technique utilized in this research to predict the bistatic scattering from square flat plates is the Uniform Theory of Diffraction (UTD). UTD is a high frequency technique that considers

incident, reflected, and various diffracted fields. Figure 2 illustrates edge diffraction, where a line source illuminates a wedge. The incident and reflected field

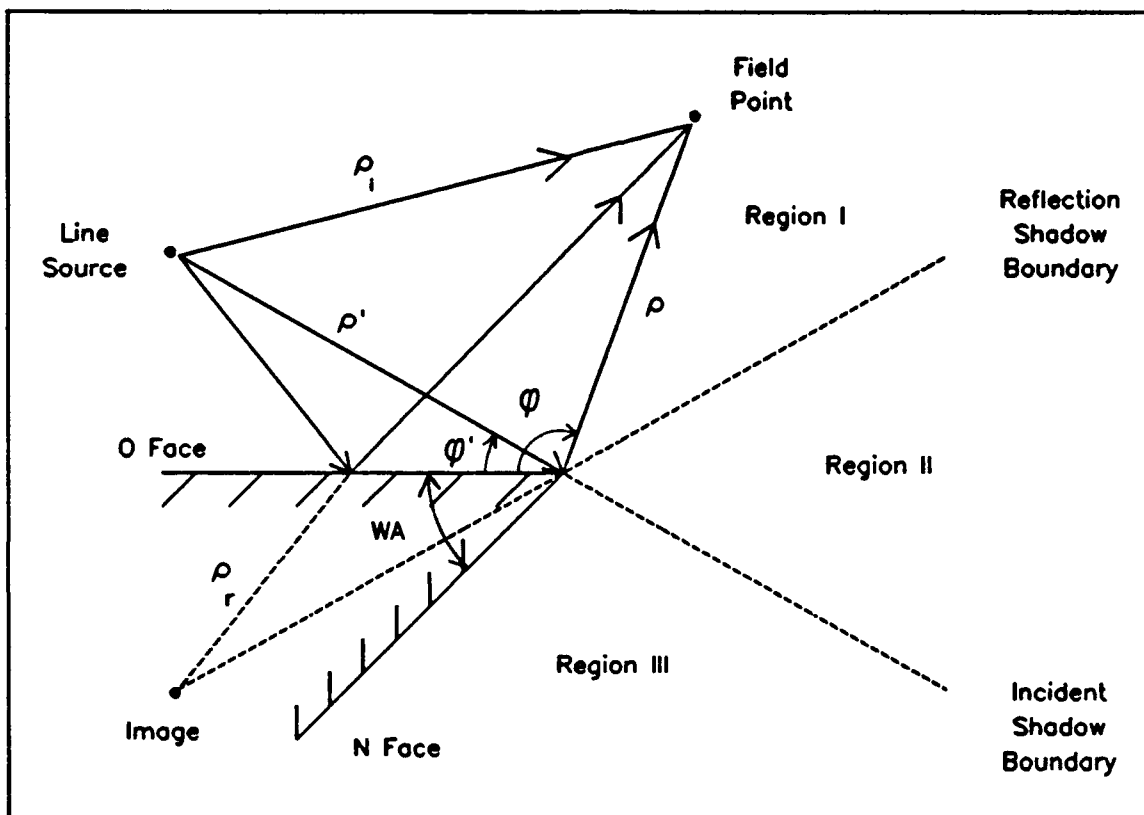


Figure 2. UTD geometry for wedge diffraction (7)

comprise the geometrical optics (GO) solution. GO predicts zero fields in the shadow region and has discontinuities at the reflected and incident field shadow boundaries. UTD adds the diffracted field to the GO result to produce the total field which is continuous across both shadow boundaries.

Using the UTD, a computer code was written that

determined the bistatic scattering from a two dimensional strip considering first order diffractions. The results obtained were then scaled to approximate the RCS for a three dimensional square flat plate. The theoretical derivation for the computer code will be detailed in Chapter IV. The code itself is in Appendix C.

Another code based on the UTD, Radar Cross Section - Basic Scattering Code 2.0 (RCS-BSC2), was used to predict the RCS of the flat plates as well. This code will explained in more detail in Chapter IV.

#### *Measurement Considerations*

When performing RCS measurements, there are many criteria that must be investigated. The fundamental requirements for performing monostatic and bistatic measurements are identical. Currie notes that, "the target return must be extracted, the desired information must be removed from these signals, and the data must be adequately calibrated" (4:148). Several topic areas relating to RCS measurements will be discussed. These will include the equation used to calibrate the RCS, the quiet zone in the chamber, and the error signals that need to be accounted for.

*Calibration Equation.* The RCS of a target is determined by comparing the received signal from the target to the received signal from a known reference target. The received power for any target can be defined using the following

equation and assuming free-space propagation:

$$P_r = \frac{P_t G_t G_r \lambda^2 \sigma}{(4 \pi)^3 R_1^2 R_2^2 L} \quad (3)$$

where

$P_r$  = received power,

$P_t$  = transmitted power,

$G_t$  = transmitting antenna gain,

$G_r$  = receiving antenna gain,

$\lambda$  = wavelength,

$\sigma$  = target radar cross section,

$R_1$  = range from transmitter to target,

$R_2$  = range from target to receiver, and

$L$  = system losses, (4:62-63).

Clearly, there are several parameters involved. Rather than attempt to determine them, a calibration procedure will be developed that eliminates their effect.

A calibration target has an RCS ( $\sigma_0$ ) that is exactly known. While many choices exist for a calibration target, the most common choice is a sphere since its exact RCS can be computed and is independent of orientation. A 5 inch sphere is used for calibration purposes in the AFIT chamber.

It is important to remember that the system does not actually measure the RCS of the target, but measures the received power as suggested by Equation 3. This is a



complex quantity, thus allowing the calculation of  $\sigma$  (magnitude) in dBsm with a phase term used for frequency response measurements.

Assume a calibration sphere ( $\sigma_s$ ) and a target ( $\sigma_T$ ) are in the far-field of the antennas and are measured using the same criteria (identical range, frequency, and transmit power). Solving Equation 3 for the transmitted power for both targets and equating the results will result in the following equation:

$$\frac{P_{rT} (4\pi)^3 R_1^2 R_2^2 L}{\sigma_T \lambda^2 G_t G_r} = \frac{P_{rs} (4\pi)^3 R_1^2 R_2^2 L}{\sigma_s \lambda^2 G_t G_r} \quad (4)$$

which will simplify to

$$\sigma_T = \left( \frac{P_{rT}}{P_{rs}} \right) \sigma_s . \quad (5)$$

The exact RCS of the sphere is used to determine the exact RCS of the target of interest by performing a series of measurements. The RCS is obtained by direct measurement of the 5 inch sphere, the sphere background, the target, and the target's background. The measurement system performs a vector subtraction of the sphere background from the sphere

and the target background from the target, so that

$$P_{rT} = P_{\text{Target}} - P_{\text{Target Background}} \quad (6)$$

and

$$P_{rS} = P_{\text{Sphere}} - P_{\text{Sphere Background}} \quad (7)$$

Upon substitution, the final calibration equation used in the measurement chamber to determine the RCS is

$$\sigma_T = \left( \frac{P_{\text{Target}} - P_{\text{Target Background}}}{P_{\text{Sphere}} - P_{\text{Sphere Background}}} \right) \sigma_S \quad (8)$$

*Target Zone.* The definition for RCS requires plane wave incidence. The plane wave requirement for RCS measurements lead to specifying a target zone in the measurement chamber. Since a true plane wave is impossible to achieve in practice, some deviation from a plane wave must be accepted. Kouyoumjian and Peters (10) discuss this in detail by investigating allowable variations in the amplitude and phase of the incident field, leading to a minimum range between the antenna and target. The extent of these variations in the chamber will define the target zone in which the incident wave is considered "planar".

Acceptable deviation from the plane wave requirement requires the consideration of variations allowed for the downrange amplitude and crossrange phase. Crossrange amplitude variation could be considered as well, but the target zone obtained is not as stringent a requirement as the target zone derived from the crossrange phase variation. By assuming a point source, the downrange amplitude variation and crossrange phase variation can be used to determine the target zone ( $D \times L$ ) within the measurement chamber.

*Downrange Amplitude Variation.* The downrange target zone distance ( $D$ ) can be determined by Equation 9 assuming that antenna and target are separated at such a distance so that the incident field varies as  $R^{-1}$  in the target zone, and that the allowable amplitude variation is 1 dB or less.

$$D \leq \frac{R}{8.2} \quad (9)$$

*Crossrange Phase Variation (7).* The crossrange target extent ( $L$ ), as shown in Figure 3, can be determined by considering the ratio of the field at point 2 to point 1. This is shown in equation 10

$$A e^{-j\theta} = \frac{E^i(\frac{L}{2})}{E^i(0)} \quad (10)$$

where  $A$  is the crossrange amplitude variation and  $\phi$  is the crossrange phase variation as defined below:

$$\phi = \frac{2\pi}{\lambda} (r - R) \quad (11)$$

with

$$r = \left( R^2 + \frac{L^2}{4} \right)^{\frac{1}{2}} . \quad (12)$$

Expanding  $r$  binomially and substituting the first two terms of the expansion into Equation 11 results in Equation 13. This can be used to determine the crossrange extent of the target zone ( $L$ ) given values of  $R$  and  $\phi$ .

$$R = \frac{\pi L^2}{4\phi\lambda} \quad (13)$$

*Error Signals.* Signals other than those directly received from the target cause concern in RCS measurements. These signals, as well as techniques used to counter their corruption in obtaining valid RCS measurements, will be discussed next.

The primary error signals are the scattering from the room, the scattering from the target pedestal, the antenna coupling (direct path from transmit to receive antenna), and

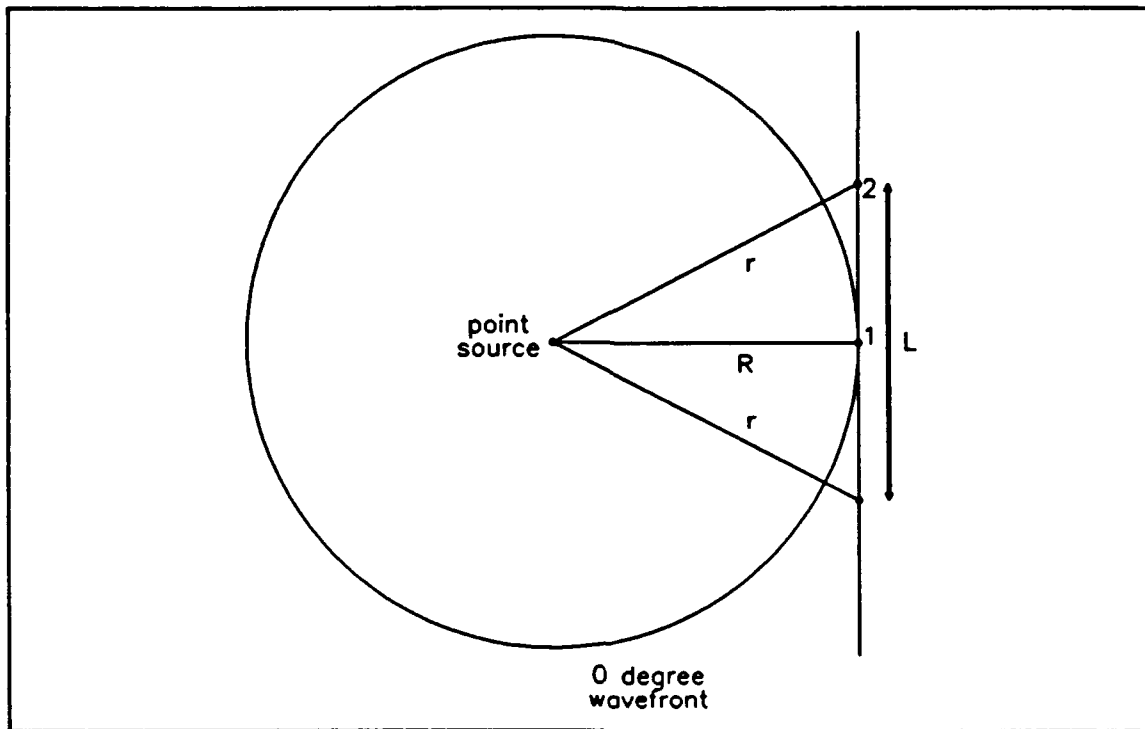


Figure 3. Crossrange phase variation in target zone, modeling transmitter as a point source

the interactions of the target with the background. Even though the measurement chamber is designed to minimize these errors, they still exist. RAM is used in the chamber to attenuate error signals from the room and target pylon. The target pylon is ogive shaped to provide low backscatter, but causes increased concern for bistatic measurements since its RCS increases as the bistatic angle increases and often scatters directly into the second antenna in a bistatic configuration.

An additional technique used to help obtain accurate measurements is background subtraction. In background

subtraction, the target background is measured and vectorially subtracted from the target measurement. While this helps, the target/chamber interactions are not present in the background measurement and are thus not subtracted out.

To minimize the contributions of the error signals even further, a time gate can be applied to the received signal to act as a filter. This means that only the signal received in the time gate will be used by the measurement equipment. This technique is applicable to bistatic measurements except for the situation of forward scattering (bistatic angle approaching  $180^\circ$ ) when the target signal and antenna coupling signal arrive near or at the same time.

### *III. AFIT RCS Measurement System*

#### *Introduction*

This chapter will begin with a description of the AFIT far-field RCS measurement range. The hardware and software involved will be described after a physical description of the chamber is provided. After this, several RCS measurement considerations described in Chapter II will be specifically applied to the AFIT chamber for both monostatic and bistatic measurements. The final part of the chapter will concentrate on the specific bistatic measurement approach for AFIT's RCS measurement chamber.

#### *Chamber Description*

*Physical Layout.* The physical characteristics of AFIT's far-field RCS measurement range are provided in Figures 4 and 5. Figure 4 provides a side aspect view of chamber while Figure 5 shows a view looking down into the chamber from above.

The walls and ceiling are covered with 18 inch pyramidal RAM. The floor has a combination of 18 inch pyramidal and 6 inch wedge RAM. Figure 4 provides detail to show placement of the radar absorbing material in the chamber. The wedge absorber tends to backscatter less as the angles of incidence of incident waves approach grazing

incidence. The wedge absorber on the floor will scatter the incident energy toward the back wall and the bottom portion of the pedestal. Ideally, the wedge RAM would extend to the back wall of the chamber to combat the grazing incidence, but limited quantities dictate present placement.

The pedestal, shown in Figures 4 and 5, has an ogive shaped cross section which results in low backscatter. In addition to the low monostatic RCS of the pedestal, the

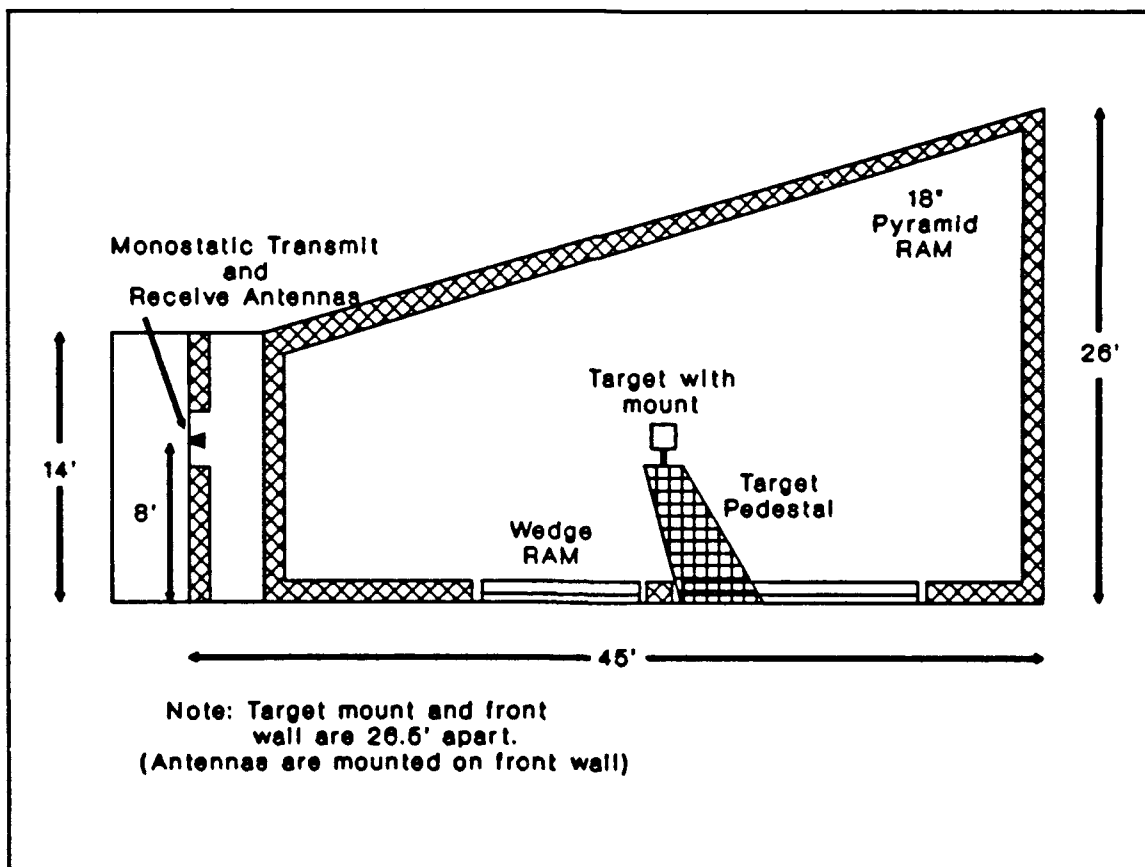


Figure 4. Side view of AFIT far-field RCS chamber



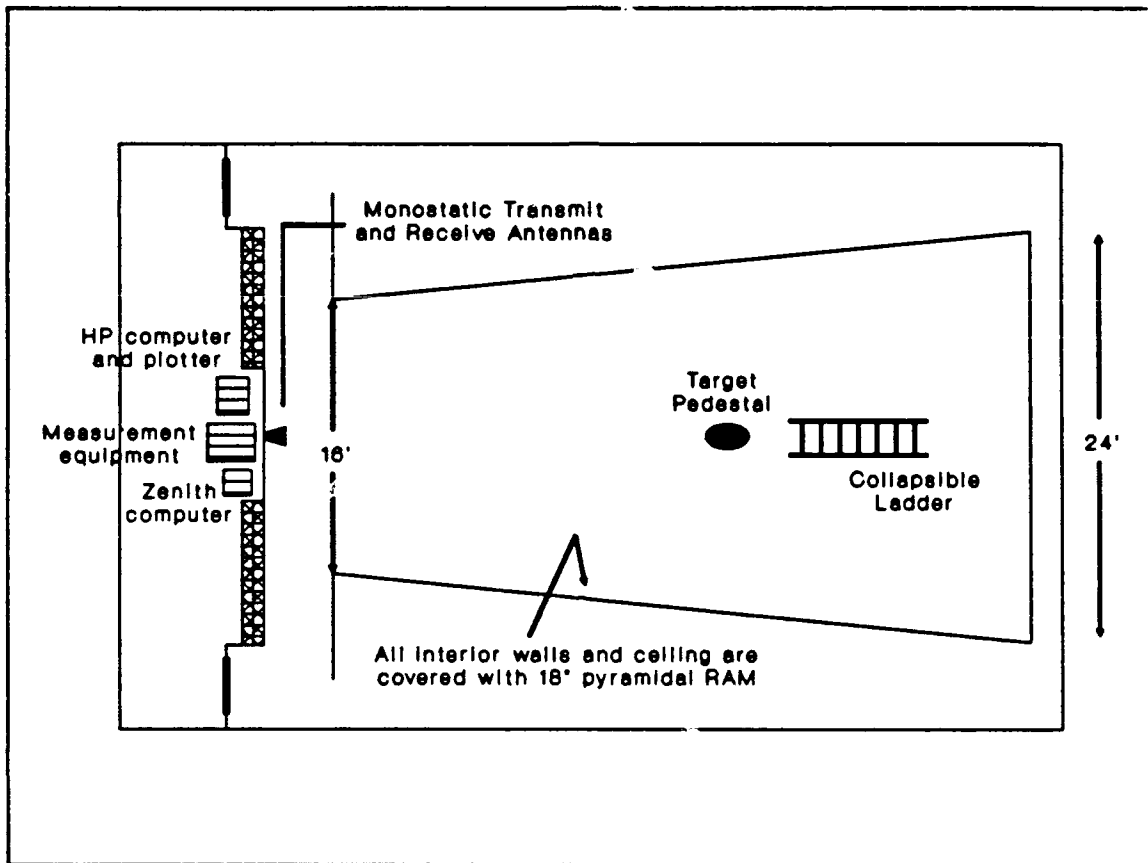


Figure 5. Top view of AFIT far-field RCS chamber

incident energy striking the pedestal is scattered in a cone geometry away from the target zone toward the floor. Since pyramid RAM works better as incident waves approach normal incidence, it was placed at the base of the target pedestal to absorb the edge diffractions from the pylon that propagate down to the floor in front of the pylon. A pedestal cap made of RAM sits on top of the pedestal leaving just enough room for a target mount. The pedestal cap acts

to reduce the pedestals RCS and the interactions occurring between the target and pedestal not accounted for in the background.

*Measurement Equipment.* The radar system used in the AFIT far-field measurement range is a continuous wave (CW) system. Figure 6 provides a block diagram of the current hardware. The AFIT chamber utilizes two antennas for both monostatic and bistatic measurements. Even though there are two antennas separated by a small "bistatic angle" for monostatic measurements, the angle is considered to be zero.

The AFIT measurement system is controlled by an HP 9000 Series 200 Computer. The computer is interconnected into the measurement system via the HP-IB (interconnect bus). A Newport Corporation 855C controller is also connected by the HP-IB to the computer and network analyzer. It can be used for automatic or manual movement of the target on the pedestal or the orientation of the monostatic antennas. The transmit and receive antennas for monostatic measurements are Flam and Russell diagonal horn antennas which operate from 6 to 18 GHz. For bistatic measurements, one Flam and Russell antenna is used along with an X-band antenna (8 to 12.4 GHz) placed in the chamber at the desired bistatic angle.

A CW radar signal is generated by the HP 8340B Synthesized Sweeper. The CW signal generated is sent to a HP 11691B directional coupler. The coupled output signal is

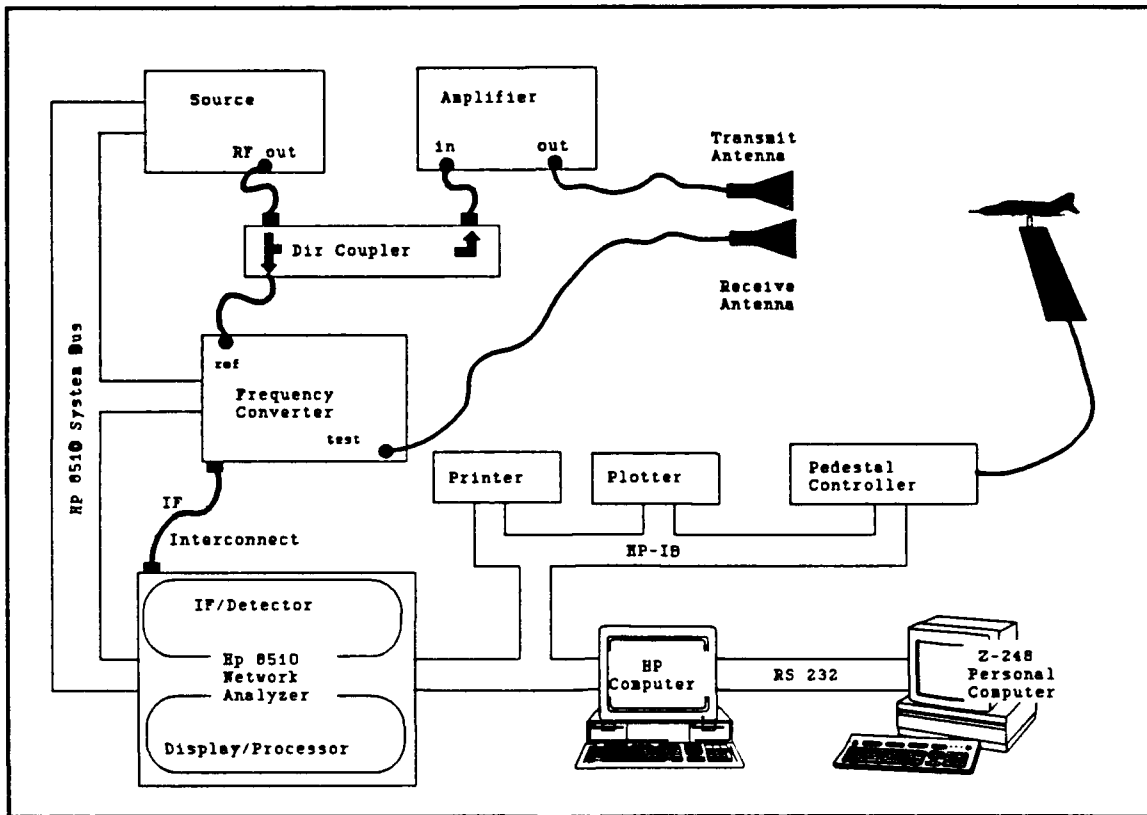


Figure 6. AFIT RCS chamber measurement equipment (16)

routed to the a1 input on the HP 8511A Frequency Converter to be used as a reference. The through output signal from the HP 11691B is amplified to 24 dBm and sent to the transmit antenna. As mentioned earlier, a separate antenna will receive the return test signal sending it to the HP 8511A Frequency Converter b1 input. The frequency converter will convert both the a1 reference signal and b1 test signal

from a radar frequency (RF) to an intermediate frequency (IF) of 20 MHz while maintaining the relative amplitude and phase of the signal. These signals are routed through an IF interconnect to the HP 8510B Network Analyzer for processing. The network analyzer measures the amplitude and phase of the test signal relative to the reference signal.

**Software.** The HP computer controls the automatic operation of RCS measurements using the AFIT RCS measurement software (ARMS). The software provides the capability to perform RCS pattern cuts and frequency responses. In a pattern cut, the RCS of the target is measured during an azimuth angular rotation of  $360^\circ$  at a set frequency. The frequency response is accomplished as the frequency is swept over an established bandwidth with the target's azimuth position fixed. The complex frequency response may be inverse fourier transformed to provide a bandlimited impulse-response.

One important function performed in the software is calibration. The calibration standard used is a 5 inch sphere. The exact solution for the 5 inch sphere, along with the measured RCS of the sphere, is used to calibrate the measured target return. Also, since the target is not in perfect isolation, a background measurement is performed on both the standard and the target. The background is then vectorially subtracted from the RCS measurement of the standard and the target respectively.

### Target Zone

The target zone discussed in Chapter 2 can be determined for AFIT's measurement chamber. Remember, the target zone is an area within the chamber where the incident electromagnetic wave falls within the restrictions placed on it to satisfy the plane wave required in the definition of RCS. Equations 9 and 13 can be used to determine the downrange (D) and crossrange (L) target extent:

$$D \leq \frac{R}{8.2} \quad (9)$$

$$R = \frac{\pi L^2}{4\phi\lambda} \quad (13)$$

Using the generally accepted phase variation ( $\phi$ ) of  $\pi/8$  radians for the incident wave, Equation 13 will reduce to:

$$L = \left( \frac{R \lambda}{2} \right)^{\frac{1}{2}} . \quad (14)$$

Due to different chamber configurations, the target zone will be determined for the monostatic and bistatic RCS

measurement situations separately.

*Monostatic Target Zone.* The target rotator is 26.5 feet from the antennas. Equation 9 produces a downrange target extent of  $D = 3.232$  feet. Since the monostatic RCS measurement antennas operate from 6 to 18 GHz, the crossrange target extent will be determined in this bandwidth. Figure 7 shows  $L$  versus frequency for a range of 26.5 feet. As the frequency increases,  $L$  becomes more restrictive.

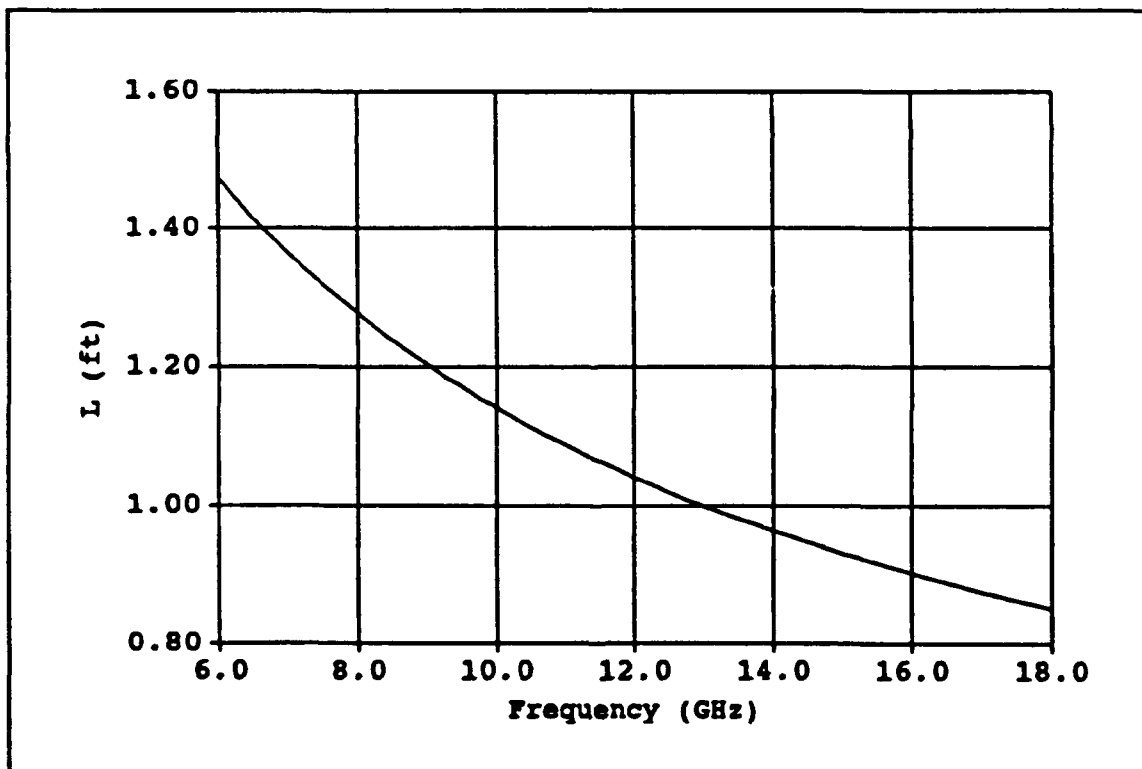


Figure 7. Crossrange extent of target zone versus frequency, monostatic case

*Bistatic Target Zone.* Since bistatic RCS measurements are performed by separating the transmit and receive antennas at a bistatic angle, the limiting factor on the target zone will be the range at which the second antenna can be positioned with respect to the target. In AFIT's chamber, the side wall and pedestal are separated by approximately 9.5 feet, thus limiting the placement of the antenna at a bistatic angle of  $90^\circ$ . Upon placing the second antenna on top of a tripod, the maximum obtainable distance from the target to the antenna was  $R = 8$  feet. This produces a downrange target extent of  $D = 0.976$  feet. Figure 8 shows  $L$  versus frequency for  $R = 8$  feet. The frequency range was limited from 8 to 12.4 GHz, the span of frequency used with the X-band antenna transmitting.

#### *Noise Floor and Calibration*

The RCS of a target is defined with the target residing in free space. As discussed previously (Chapter 2 - Error Signals), there are various techniques used to help simulate free space conditions in the measurement chamber. Even with such techniques, the field illuminating the target also illuminates the target mount, pedestal, and other objects within the chamber. Thus, the scattered field at the receiver is a combination of the desired as well as the undesired signals (3:907).

The noise floor shows the levels of these signals within the chamber. As a result, the noise floor can be used

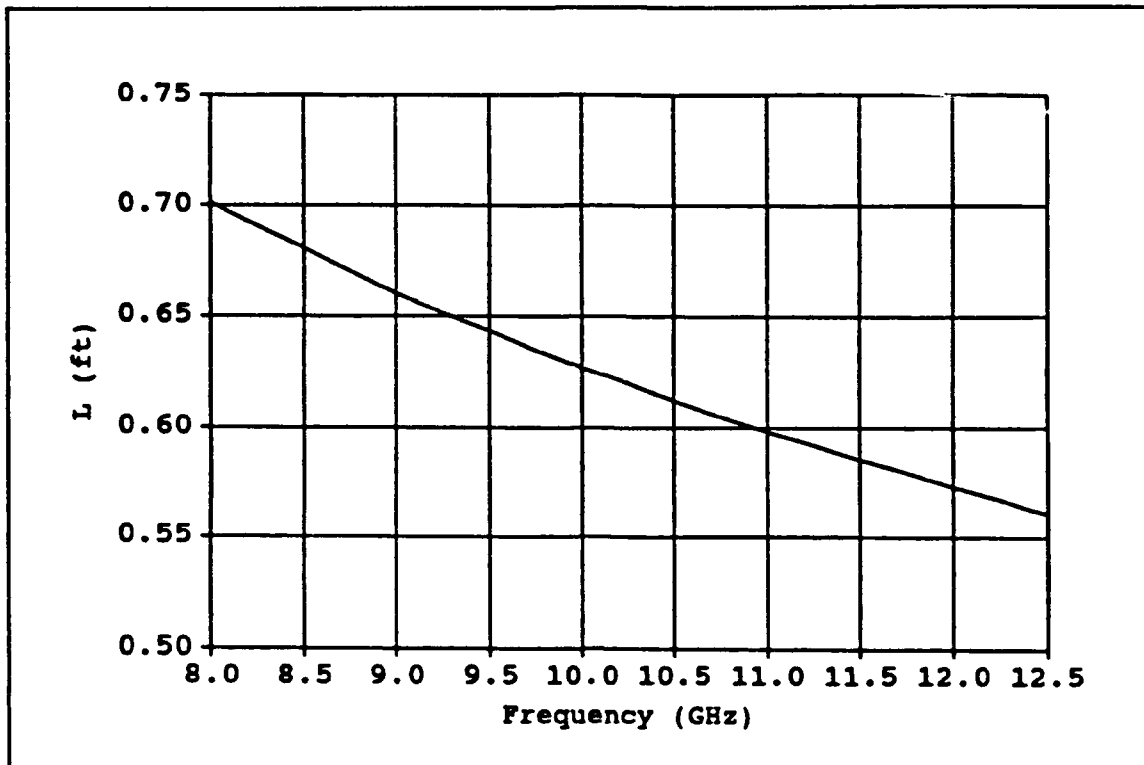


Figure 8. Crossrange extent of target zone versus frequency, bistatic case

to determine the minimum measurable target RCS within the chamber. The noise floor is determined by performing a frequency response RCS measurement with no target in place during the target measurement. Basically, the noise floor is an RCS measurement of the chamber with the chamber acting as the "target". The frequency response is performed utilizing background subtraction and range gating of the signal, along with a certain amount of averaging.

The monostatic noise floor of the chamber for vertical polarization is shown in Figure 9. The monostatic noise floor was accomplished using AFIT's monostatic chamber



configuration with the Flam and Russell antennas. The noise floor varies between -80 to -100 dBsm from 8 to 12.4 GHz.

When bistatic RCS measurements are performed, the noise floor will be different for each bistatic angle since the chamber clutter varies as the separation angle between the antennas change. Each time the bistatic angle is changed, the signals received change as well. The bistatic noise floor of AFIT's chamber for vertical polarization is provided in Figures 10, 11, and 12 for bistatic angles of 45°, 90°, and 135°. For each measurement, the transmit antenna was an 8 to 12.4 GHz X-band antenna and the receive antenna was one of the stationary Flam and Russell antennas.

When a frequency response RCS measurement is performed, an exact sphere data file is required by the software for calibration purposes. As the bistatic angle between the antennas change, the exact sphere solution changes as well. The exact sphere solution needed for frequency response RCS measurements using the HP 8510B network analyzer consists of the real and imaginary parts of the scattered field at the desired bistatic angle. The HP based system requires the real and imaginary field for the desired bandwidth divided into 800 equal intervals or 801 data pairs.

A computer program that provides the exact monostatic and bistatic scattering from a sphere was used to obtain the necessary data files for bistatic angles of 45°, 90°, and 135°. The code is used at the Wright Research and

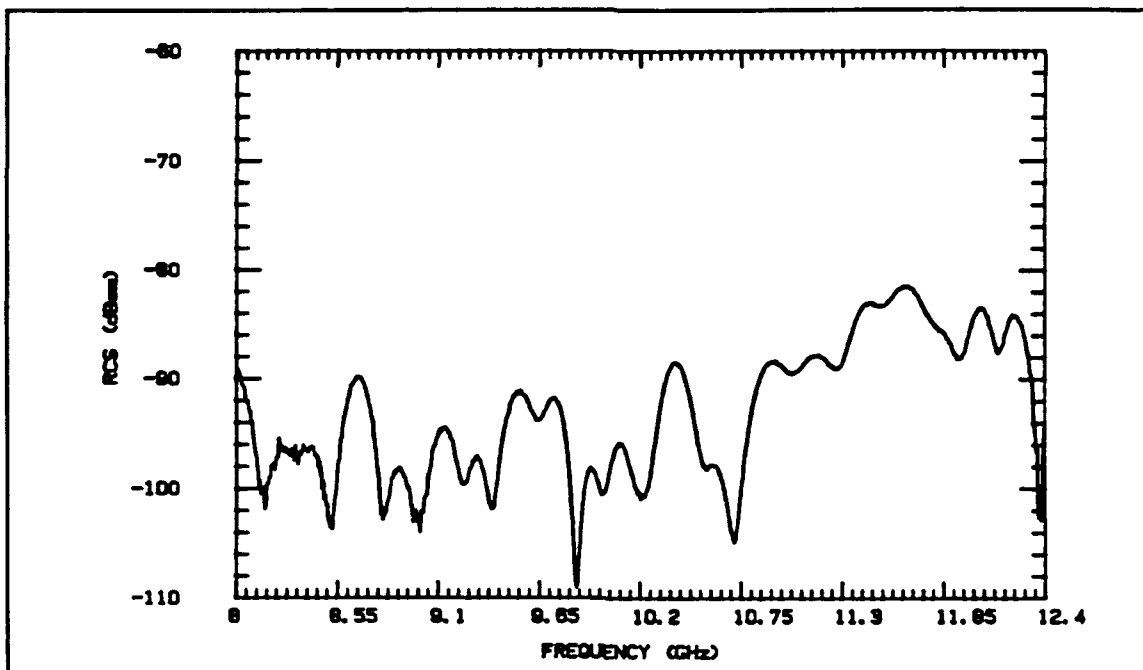


Figure 9. Monostatic noise floor; range gate of 7 nsec, vertical polarization, and averaging factor of 32

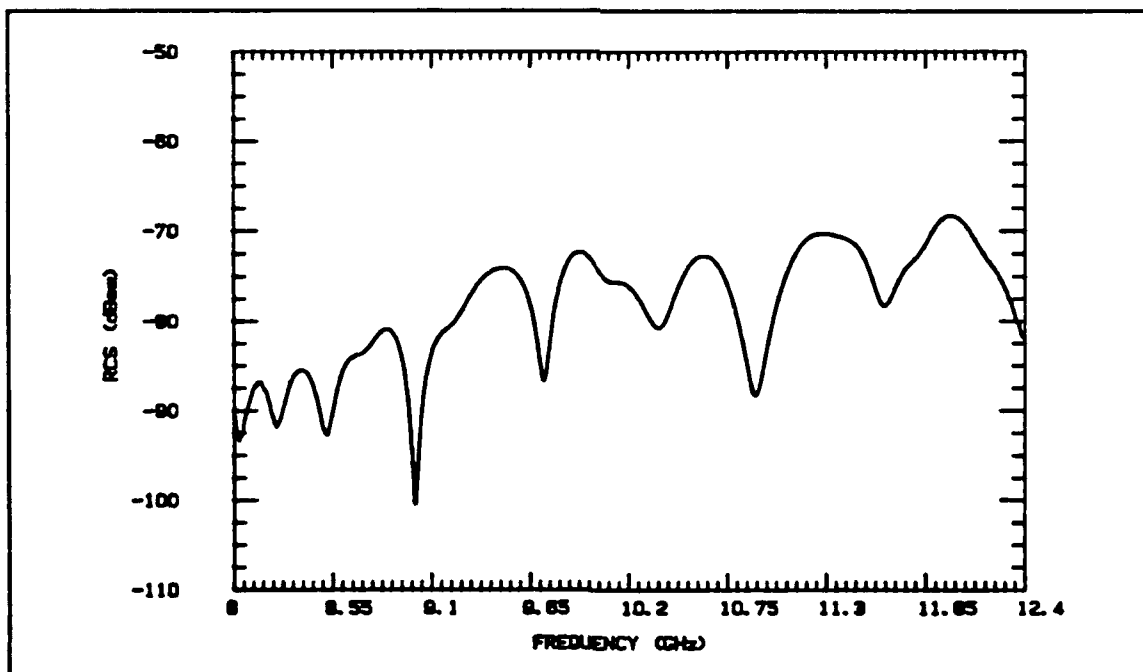


Figure 10. Bistatic noise floor; bistatic angle of 45 degrees, range gate of 7 nsec, and averaging factor of 32

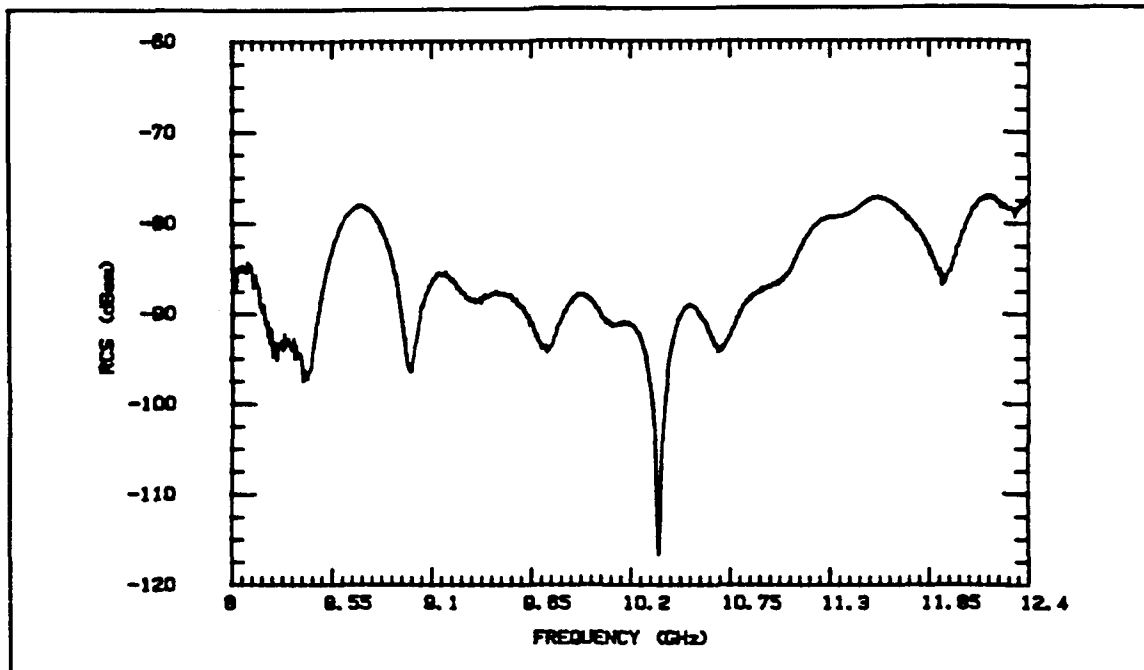


Figure 11. Bistatic noise floor; bistatic angle of 90 degrees, range gate of 7 ns, and averaging factor of 32

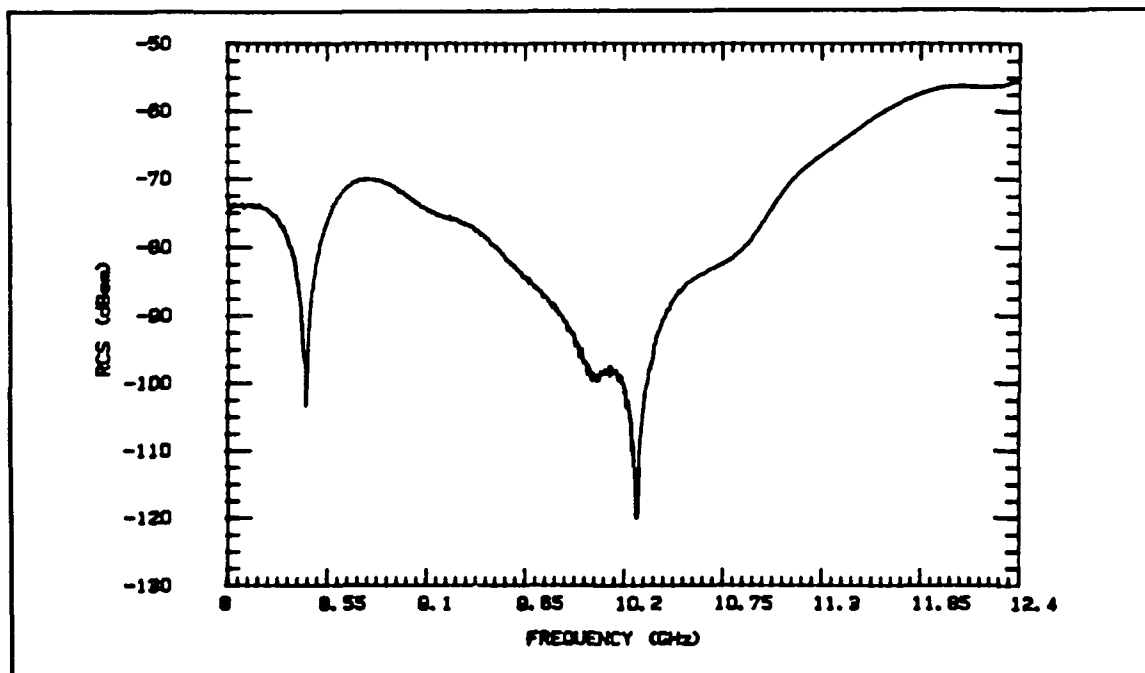


Figure 12. Bistatic noise floor; bistatic angle of 135 degrees, range gate of 7 ns, and averaging factor of 32

Development Centers (WRDC) far-field and compact RCS measurement ranges at Wright-Patterson Air Force Base to calculate the exact sphere solution for RCS calibration. The computer code was developed at The Ohio State University in 1978 and has been modified since then. The code is based on a Mie series solution. An infinite series of Legendre functions are weighted based on the electrical size of the sphere to determine the number of terms required for the series to converge (13:25).

A listing of the code is provided in Appendix C. The code was modified slightly, depending on the exact solution needed for the RCS measurements. The RCS pattern cut measurement require an exact sphere solution in magnitude (dBsm) at the desired frequency, while the RCS frequency response measurement requires 801 real and imaginary exact numbers for the desired bandwidth.

#### *Bistatic RCS Measurement Approach*

To obtain accurate bistatic measurements in AFIT's chamber, it was necessary to characterize the signals in the chamber at the various bistatic angles. Before this could be accomplished, though, several preliminary steps had to be performed.

Since the AFIT chamber had been used only for monostatic measurements, there was no established method of knowing exactly where the antenna at the bistatic angle should be placed. The chamber floor was marked for vertical

polarization using a transit to determine the exact separation angle between the two antennas. The transit was mounted on top of the pedestal and the centerline of the Flam and Russell diagonal antennas was used as a reference of zero degrees.

Second, an antenna mount was needed to hold the antenna at the desired height. It was determined that a simple tripod met the necessary criteria to mount the antenna upon. The tripod was used to hold the antenna at a fixed height of 8 feet.

*Characterizing the Chamber.* The scattered signals in the chamber change when bistatic measurements are performed. In fact, the signals vary as the bistatic angle changes. The scattered signals in the chamber have to be investigated to determine the effect they will have on the RCS measurements. The characterization is necessary for each antenna configuration and/or bistatic angle desired to ensure accurate measurements. The dominant RCS returns received within the chamber were analyzed by operating the network analyzer manually and viewing the signal in the time domain. The numbers obtained on the measurements are relative (uncalibrated). Chamber characterization is necessary since an attempt will be made to use software gating to capture the desired target signal and reject all other signals to obtain the bistatic RCS. This is possible since the scattered signals arrive at different times,

except for bistatic measurements approaching forward scatter.

*Monostatic time domain.* To establish a starting point, the signals present in the chamber for monostatic RCS measurements were obtained. A bandwidth of 4.4 GHz (8 to 12.4 GHz) was used for each measurement with the antennas oriented for vertical polarization. An empty chamber (no target on pedestal) was evaluated. Figure 13 shows the signals present in the chamber in the time domain. The dominant signals expected were from the direct coupling between the two antennas, the target pedestal and the back wall. As shown, the largest return is caused by the direct coupling between the antennas. The next largest return is from the target pedestal. Even though the walls are lined with radar absorbing material (RAM), the RAM is a significant scatterer as well in the chamber. This is verified by the large return received from the chamber rear wall.

*Bistatic time domain.* The bistatic time domain characteristic measurements are shown in Figures 14 to 19. These measurements were needed to prove that the target zone could be isolated from error signals, and to determine the time gate parameters to do so. Table 1 provides the variety of chamber configurations that were considered.

A bandwidth of 4.4 GHz (8 to 12.4 GHz) was used for each bistatic time domain measurement. All antennas were

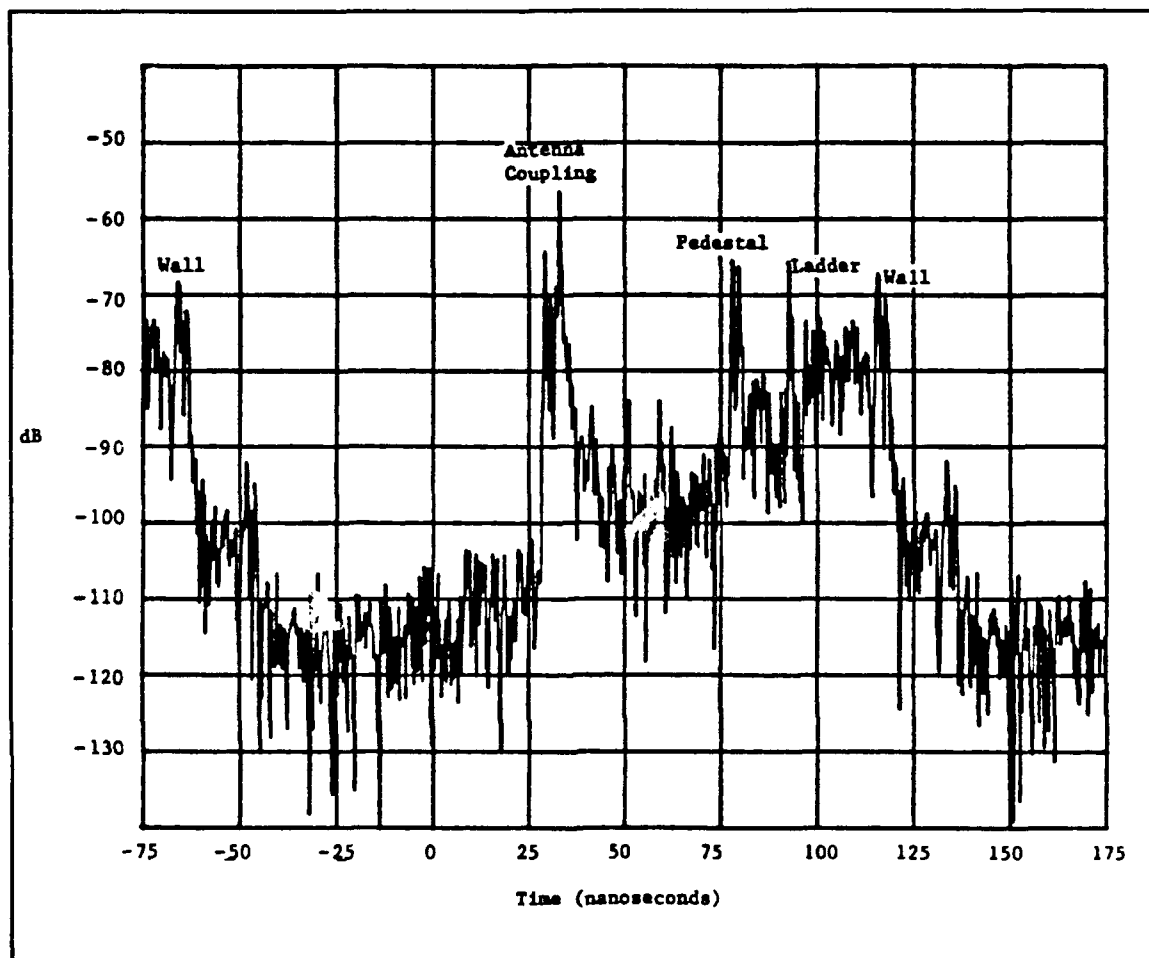


Figure 13. Time domain measurement, monostatic case

oriented for vertical polarization.

Figures 14, 17, and 18 show the bistatic time domain characteristic measurements of the chamber for bistatic angles ( $\beta$ ) equal to  $45^\circ$ ,  $90^\circ$ , and  $135^\circ$  respectively. For all three cases, the transmit antenna is the X-band antenna placed along an arc approximately 8 feet from the target at

the appropriate bistatic angle. The receive antenna is the Flam and Russell antenna mounted permanently on the front wall of the chamber 26.5 feet from the target.

Figure 18 shows the antenna coupling and target signal arriving at almost the same time for  $\beta = 135^\circ$ . Figure 19 shows this portion of the measurement with the time scale expanded. Expanding the scale provides the timing detail required to set the initial instrument state of the HP 8510 network analyzer.

Figures 15 and 16 are bistatic time domain characteristic measurements of the chamber for  $\beta = 45^\circ$ . Figure 15 results from a broadband AEL antenna transmitting at approximately 8 feet from the target with the Flam and Russell antenna receiving at 26.5 feet. Several bistatic RCS measurements were performed at  $45^\circ$  with this configuration to determine the effect the broadband antenna had on the bistatic measurements performed with this configuration. Figure 16 is a time domain measurement with the Flam and Russell antenna transmitting from its fixed position of 26.5 feet from the target with the X-band antenna receiving at approximately 8 feet (just the opposite of the configuration used in Figure 14). This characterization was necessary to show that the RCS obtained for a target is independent of which antenna receives and which antenna transmits.

The level of the signals obtained in the two



measurements with the antennas interchanged (Figures 14 and 16) are similar in magnitude. The time that the signals appear differ since the target to receive antenna distance varies (26.5 feet versus 8 feet).

When the AEL broadband antenna (Figure 15) is used to transmit, the antenna coupling signal increases approximately 15 dB - 20 dB over that obtained for the measurements in Figures 14 and 16. This results since the AEL antenna has a much wider main beam than the other two antennas (X-band, Flam and Russell) used. A direct consequence of this is noted by the signal received from the pedestal. It is approximately 6 dB lower with the AEL antenna transmitting than the signal received in the other configurations (Figures 14 & 16) at  $\beta = 45^\circ$ . The X-band antenna and the Flam and Russell antenna have narrow main beams (with same output power as AEL antenna), thus illuminating the pedestal at a higher energy level.

As the bistatic angle increases, the antenna coupling moves toward the pedestal (target) signal and increases in magnitude. This occurs since the distance the wave travels from the transmit antenna directly to the receive antenna coupling path approaches the distance the wave travels from the transmit antenna to the target to the receive antenna as the bistatic angle increases. By using these distances, along with the fact that the speed of light is 11.8 inches per nanosecond, the separation distances expected in the

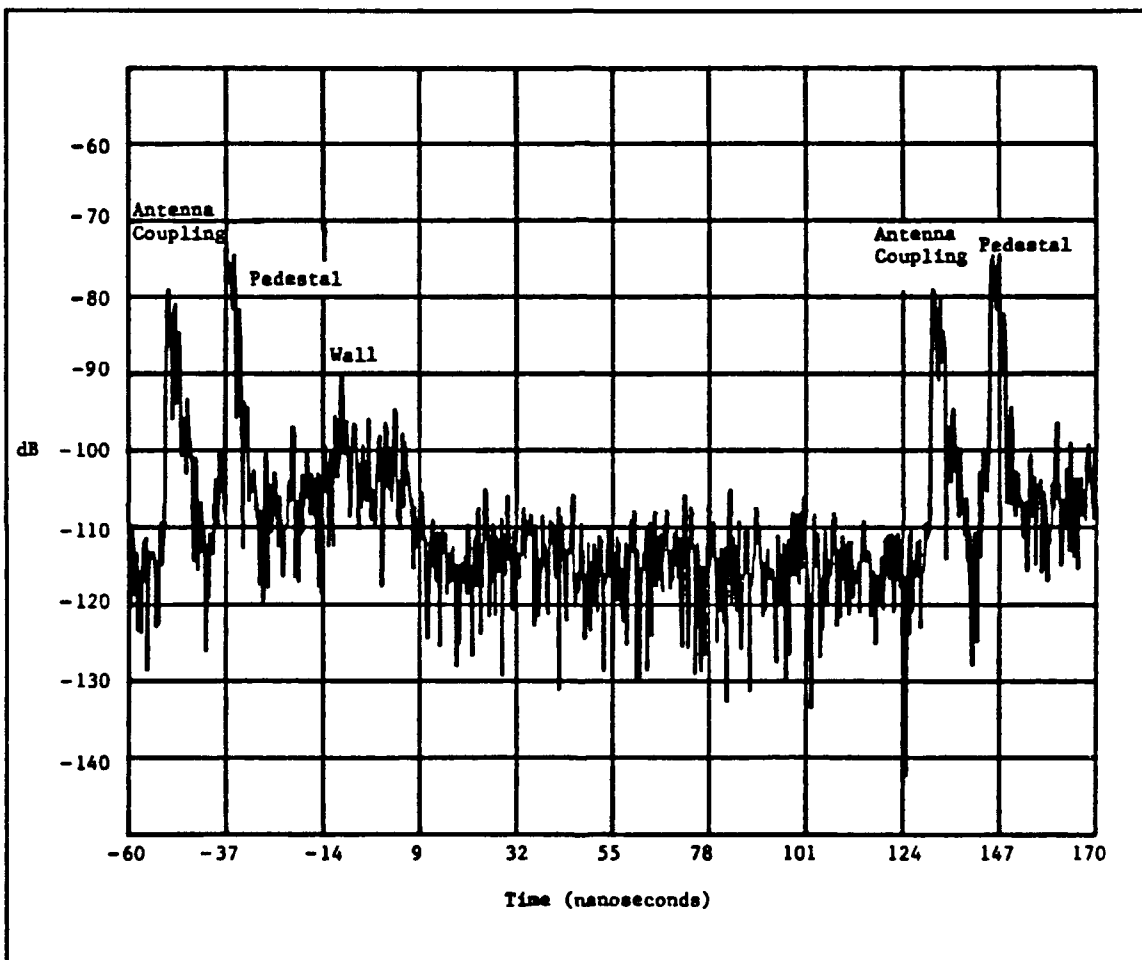


Figure 14. Time domain measurement for bistatic angle of 45 degrees, X-band antenna transmitting

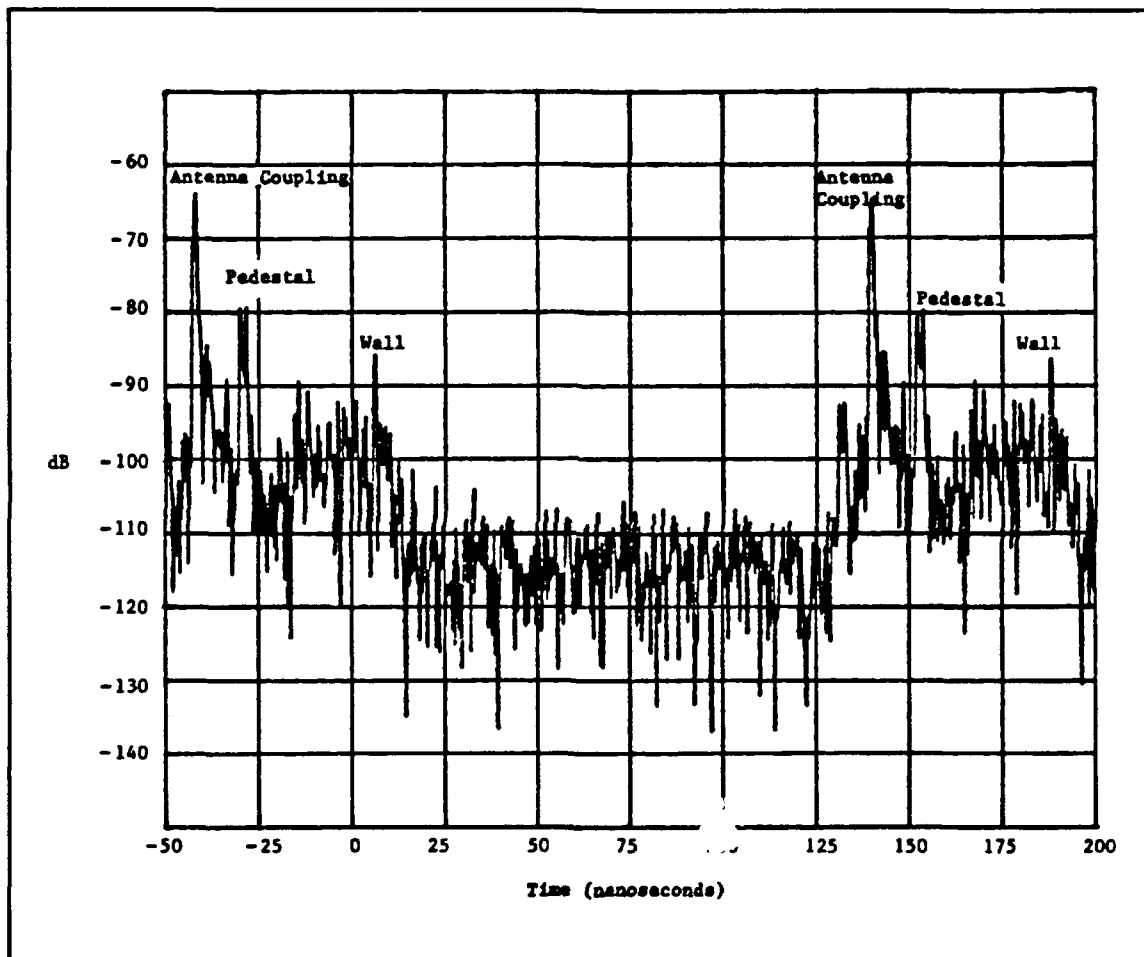


Figure 15. Time domain measurement for bistatic angle of 45 degrees, AEL antenna transmitting

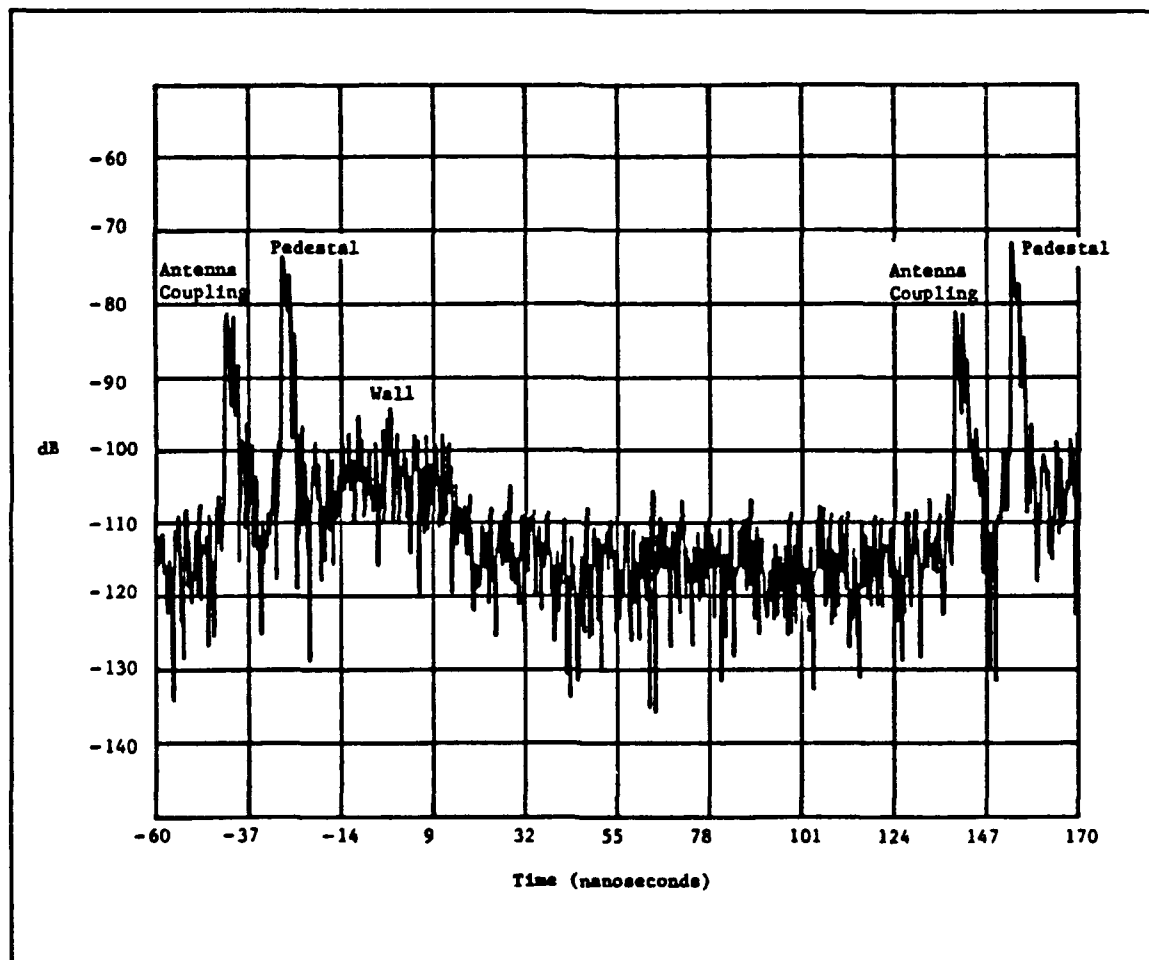


Figure 16. Time domain measurement for bistatic angle of 45 degrees, Flam and Russell antenna transmitting

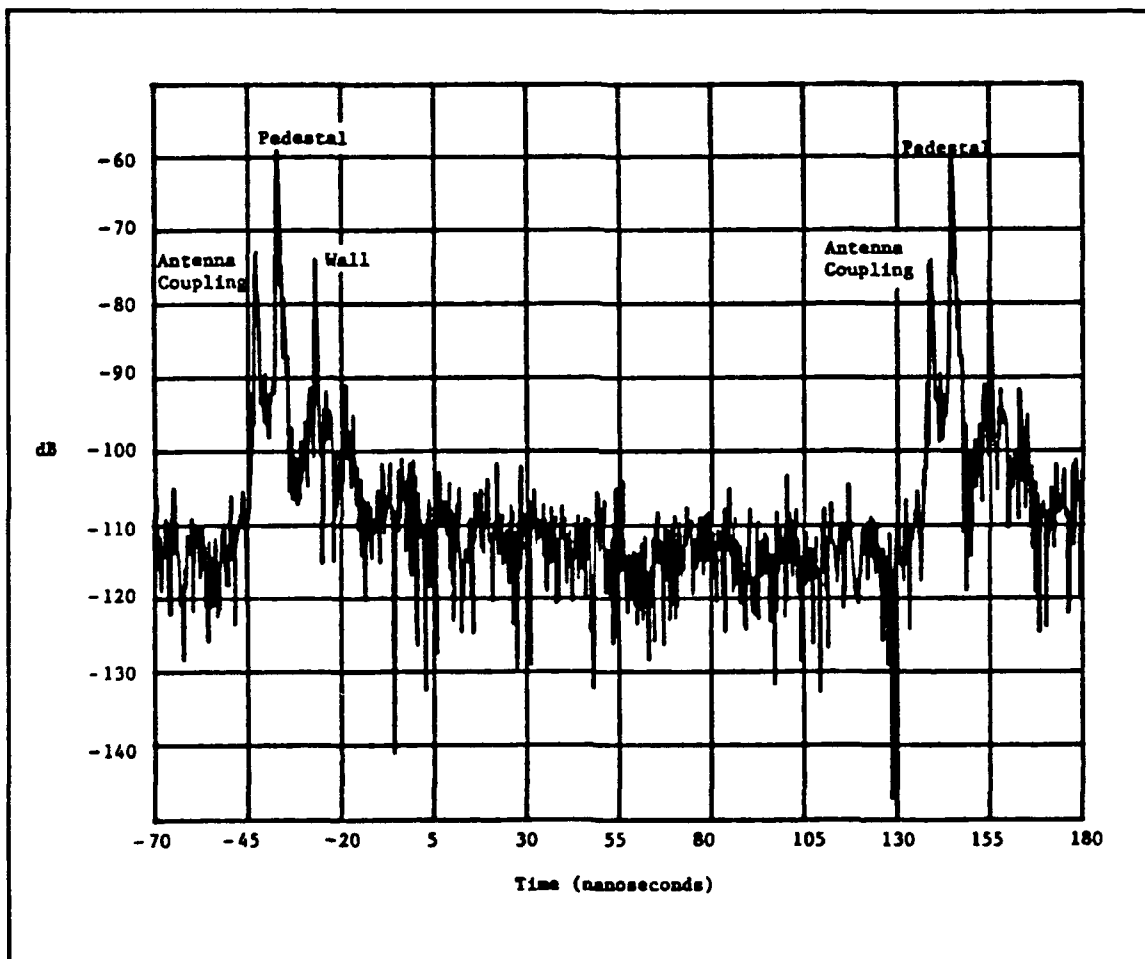


Figure 17. Time domain measurement for bistatic angle of 90 degrees, X-band antenna transmitting

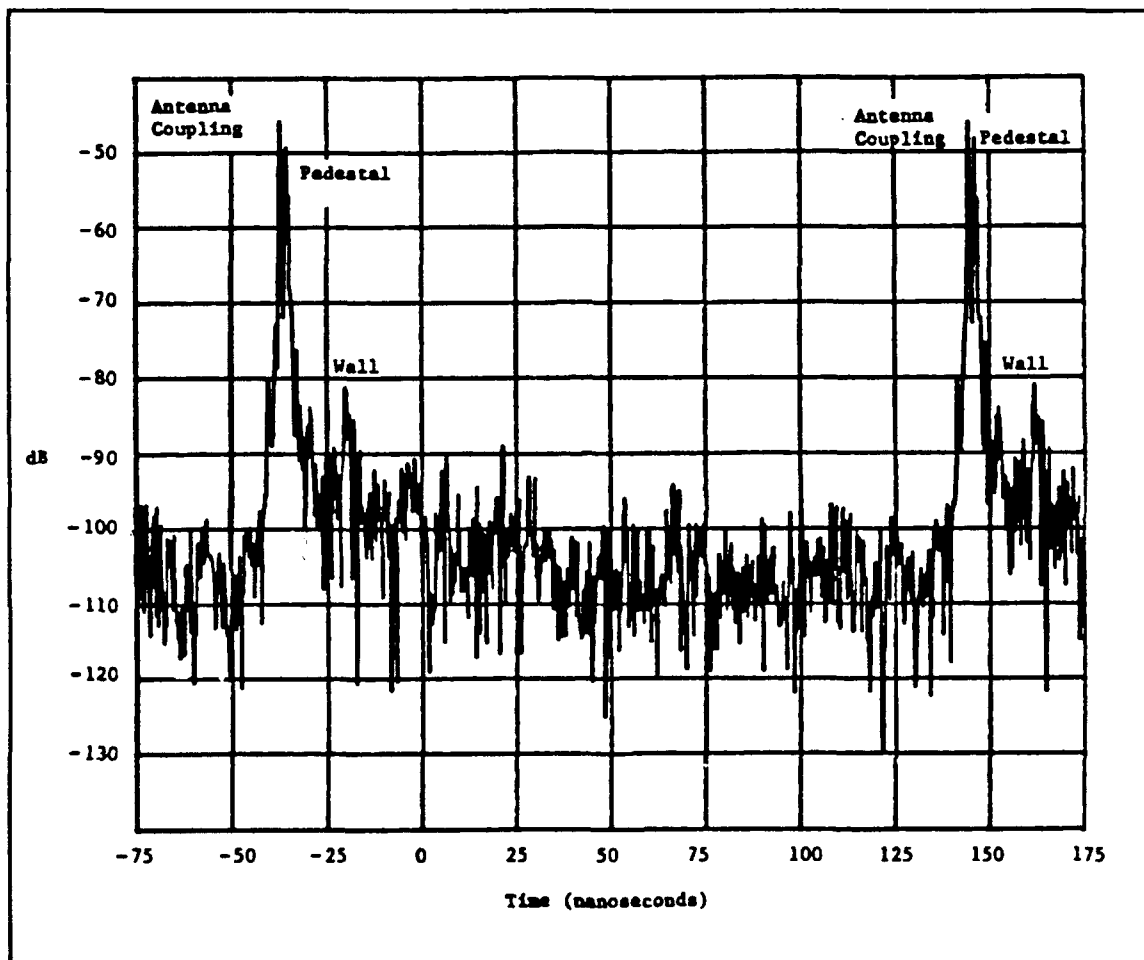


Figure 18. Time domain measurement for bistatic angle of 135 degrees, X-band antenna transmitting

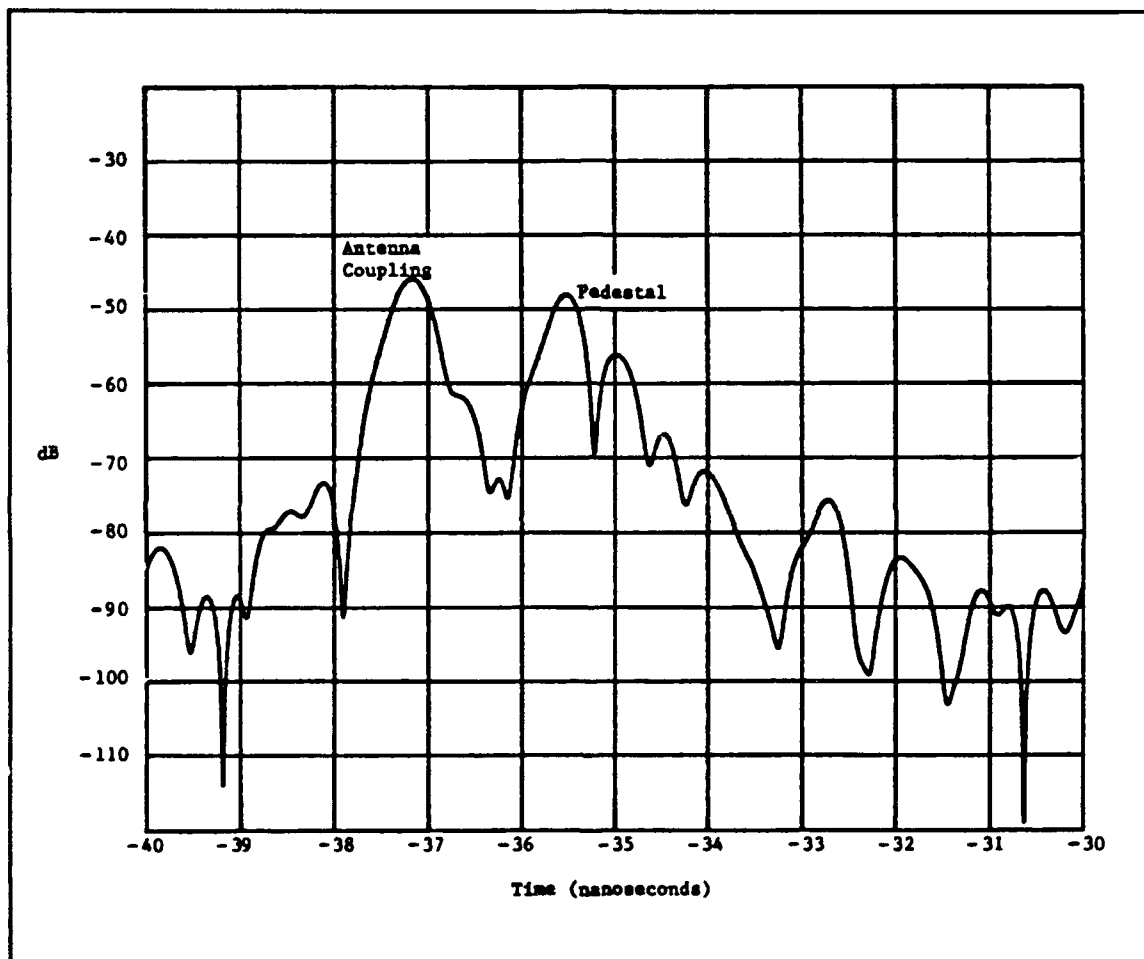


Figure 19. Time domain measurement with time scale expanded for bistatic angle of 135 degrees

measurements in nanoseconds between the pedestal and antenna coupling can be determined. For instance, at a bistatic angle of  $135^\circ$ , the distance the target signal travels is 34.5 feet while the direct signal travels 32.65 feet. This equates to a 1.85 nanosecond separation of the signals in time. This compares well with the measurements in Figures 18 and 19 which indicate a 1.8 nanosecond ( $-37.3\text{ns} - (-35.5\text{ns})$ ) separation.

As the bistatic angle approaches  $180^\circ$ , the bistatic RCS measurement approach used in this research breaks down due to the arrival of the target signal and antenna coupling at the same time. Note also that as the bistatic angle increases, the RCS of the pedestal (without target) also increases. In prior research at the WRDC RCS far-field range, it was determined that the scattering due to the low RCS monostatically designed pedestal in bistatic RCS measurements above  $90^\circ$  could be controlled somewhat by rotating the pedestal so that the radar signal striking it was scattered away from the receive antenna (for more information see references 13 and 17). Additional research occurring in AFIT's chamber concurrently prevented this approach from being investigated.

The automatic software controlling the RCS measurements uses a software gate which is preset in the HP 8510 to surround the target signal for use in determining the RCS. After correctly identifying the origin of the signals in the



chamber for each measurement situation, the signals occurrence in time had to be evaluated so the initial instrument settings of the HP 8510B network analyzer could be adjusted. Table 1 contains the gate span and gate center for the different bistatic configurations used for RCS measurements. The network analyzer uses instrument state 8 on initial start up. Since the AFIT chamber is primarily used for monostatic measurements, state 8 has been set accordingly and the software (ARMS) that controls the monostatic measurements refer to that instrument setting. The ARMS subroutines (Appendix C) that were rewritten for bistatic measurements contain commands that reset the network analyzer to instrument state 2 when a bistatic RCS measurement is desired. Since the time domain response (Figures 13 to 19) changes as the setup parameters change, state 2 must be set accordingly for each different bistatic system configuration.

The HP 8510 had several common instrument state settings that existed for all the measurements performed (including monostatic). These include the selection of the  $S_{11}$  log scale, the frequency range being 8 to 12.4 GHz, a reference value of -50 dB with 10 dB/div, and the Gate set on.

Note that the values in Table 1 for the bistatic measurements with the antenna placed in the chamber transmitting are very close in value. This occurs since the

bistatic antenna placed in the chamber is approximately the same distance (8 feet) from the pedestal for all four cases. The gate center changes considerably at  $\beta = 45^\circ$  when the antennas exchange transmitting and receiving roles. Although the overall path length remains the same, the shift in time occurs because the path length between the target and receive antenna changes from 26.5 feet to approximately 8 feet.

The gate widths for the monostatic and bistatic ( $45^\circ$  &  $90^\circ$ ) measurements are the same allowing the entire target signal to be used for the RCS. This gate permits the minimum signal received in the gate to be down to at least -100 dB which is approaching the minimum signal levels received. The shorter gate width at  $135^\circ$  results from the antenna coupling being very close in time to the target signal. Figure 19 shows that with a gate width of 2.5 nsec the minimum target signal received is only down to -80 dB. It is important to remember that the numbers from the time domain measurements (Figures 13 - 19) are relative (uncalibrated) values.

Table 1. Initial instrument states of HP 8510 network analyzer for RCS measurements

	Gate	
	Center (ns)	Span (ns)
<b>0°</b>		
Flam and Russell (F&R) antennas transmit and receive	79.375	5
<b>45°</b>		
X-band antenna transmit, F&R antenna receive	-34.7	5
AEL antenna transmit, F&R antenna receive	-28.125	5
F&R antenna transmit, X-band antenna receive	-27.5	5
<b>90°</b>		
X-band antenna transmit, F&R antenna receive	-34.5	5
<b>135°</b>		
X-band antenna transmit, F&R antenna receive	-34.75	2.5

#### *IV. Relevant Software*

The bistatic RCS measurements and predictions that were performed depended on software to a large extent. This chapter will explain the software required by the measurement system to perform automatic bistatic measurements, the software required to transfer data from the Zenith to the HP computers, the software that made the RCS predictions of the various targets measured, and the theory used for the first order RCS prediction code.

##### *Measurement Software*

The AFIT RCS measurement software (ARMS) program is the software that controls the automatic RCS measurements in the AFIT chamber. As previously mentioned, the software requires the exact solution of a reference target (5 inch sphere). The exact solution is provided as a magnitude in dBsm for pattern cut RCS measurements, while for frequency response RCS measurements, the exact solution is provided in the real and imaginary components. As the bistatic angle changes, the exact solution of the sphere also changes. Appendix C contains a listing of the BISPH code that was used to provide the exact solution for a 5 inch sphere at the desired bistatic angle.

Two subroutines (frequency response and pattern cut) of

the ARMS were rewritten to provide the capability of either performing monostatic or bistatic measurements automatically. A listing of the code for the two subroutines is provided in Appendix C.

The frequency response measurement subroutine requires a separate data file for the 5 inch sphere which the measurement software automatically calls into the program. The data file for the 5 inch sphere contains 801 real and imaginary pairs for each bistatic angle corresponding to a particular bandwidth (if bandwidth changes, exact sphere file will change). Since this research was performed at 3 bistatic angles, 3 representative data files were required for bistatic angles of  $45^\circ$ ,  $90^\circ$ , and  $135^\circ$ . The 801 points are equally spaced between 8 and 12.4 GHz. The software uses the exact sphere solution in the calibration equation given in Chapter 2. The data files reside in the software.

The pattern cut RCS measurement requires an exact reference as well. The RCS magnitude is entered via the screen. The exact solution for pattern cuts is required in magnitude (dBsm) only. It depends on sphere size, frequency, polarization and bistatic angle.

An example of data obtained from BISPH is provided in Table 2 for a 5 inch sphere. Note that the output provided is in magnitude and phase angle. These numbers can easily be converted to the corresponding real and imaginary pairs required for the frequency response measurements.

**Table 2. Exact sphere data from BISPH at 10 GHz**

<b><i>Horizontal Polarization</i></b>				
<b><i>Sphere Size (inches)</i></b>	<b><i>Bistatic Angle (degrees)</i></b>	<b><i>Frequency (GHz)</i></b>	<b><i>RCS Magnitude (dBsm)</i></b>	<b><i>Phase (degrees)</i></b>
5.00	0	10	-18.612	-95.05
5.00	45	10	-18.962	149.73
5.00	90	10	-18.863	178.58
5.00	135	10	-17.577	39.25
<b><i>Vertical Polarization</i></b>				
5.00	0	10	-18.612	-95.05
5.00	45	10	-18.692	149.54
5.00	90	10	-19.914	177.82
5.00	135	10	-19.274	29.06

### *Data Transfer Software*

The frequency response measurement program requires a Hewlett-Packard binary data (BDAT) format exact sphere calibration file. This caused some problems since the BISPH programs runs on an Ultrex based computer. A method was established to transfer the data from Ultrex to HP ending with a BDAT format exact sphere file containing 801 real and imaginary pairs equally divided in the desired bandwidth.

First the BISPH program was changed to output only the real and imaginary components onto a TK-50 tape. These files were then transferred to DOS ASCII format. The ASCII files were edited resulting in a file which had the 801 real components followed by the 801 imaginary components in a single column as required by the HP software. These files were then transferred across the RS-232 cable between the Zenith DOS computer and the HP computer.

A computer program (Appendix C) had to be written to transfer the data between the computers. It was used along with a communications package, SMARTCOM, to obtain the exact sphere files required by the software for the frequency response measurements.

### *Prediction Software.*

Three software programs were used to provide RCS predictions of the targets measured. The first program (BISPH) predicted the exact scattering from spheres, while the other two (UTD Single Diffraction & RCS-BSC2) programs

predicted the RCS of the flat plates.

The computer code used for the spheres was developed at The Ohio State University in 1978. The code is based on a Mie series solution. An infinite series of Legendre functions are weighted based on the electrical size of the sphere to determine the number of terms required for the series to converge (13:25).

A listing of the code is provided in Appendix C and has previously been discussed in Chapter 3. The code was modified slightly, depending on the exact solution needed for the RCS measurements. The RCS pattern cut measurement require an exact sphere solution in magnitude (dBsm) at the desired frequency, while the RCS frequency response measurement requires 801 real and imaginary exact numbers for the desired bandwidth.

The second code used was a first order approximation obtained using the Uniform Theory of Diffraction (UTD) to determine the scattering from a two dimensional strip geometry, with application to square or rectangular flat plates. The theory behind the code will be provided later in this chapter with a listing of the code in Appendix C.

A more sophisticated RCS approximation of the targets measured was obtained using Radar Cross Section - Basic Scattering Code 2.0 (RCS-BSC2). This code was developed at The Ohio State University using UTD techniques as well. The code considers the diffracted fields at the corners and



edges, the second order diffractions on a plate to include double diffracted fields and edge wave effects, second and third order interaction terms between multiple plates, and first order terms with caustic corrections for cylinder geometries for monostatic and bistatic situations. RCS-BSC2 can be used for flat plates, cylinders, cone frustums, and finite ellipsoids (12:1-3). For sample predictions and more information, see (12).

The next chapter will compare the predictions obtained with the measurements. BISPH was used for all sphere RCS predictions. The other two programs, UTD Single Diffraction (UTDSD) and RCS-BSC2, were both used for the square flat plates. The RCS predictions for the triangle and 5 sided flat plate were obtained from RCS-BSC2 only.

#### *First Order UTD Analysis of 2D Strip (11)*

The geometry for this UTD analysis is provided in Figure 20. The strip is of finite width  $d$  (meters) with a phase reference in the middle. The geometry is set up so that the angle of incidence ( $\theta^i$ ) and angle of scattering ( $\theta^s$ ) is arbitrary from the normal to the strip geometry. The distance from the source and the receiver to the phase reference is  $R$ . The distance from the source and receiver to points 1 and 2 on the strip depend on the incident and scattered field angle respectively. Using trigonometry, the distance from the source to points 1 and 2 ( $\rho'$ ) on the strip

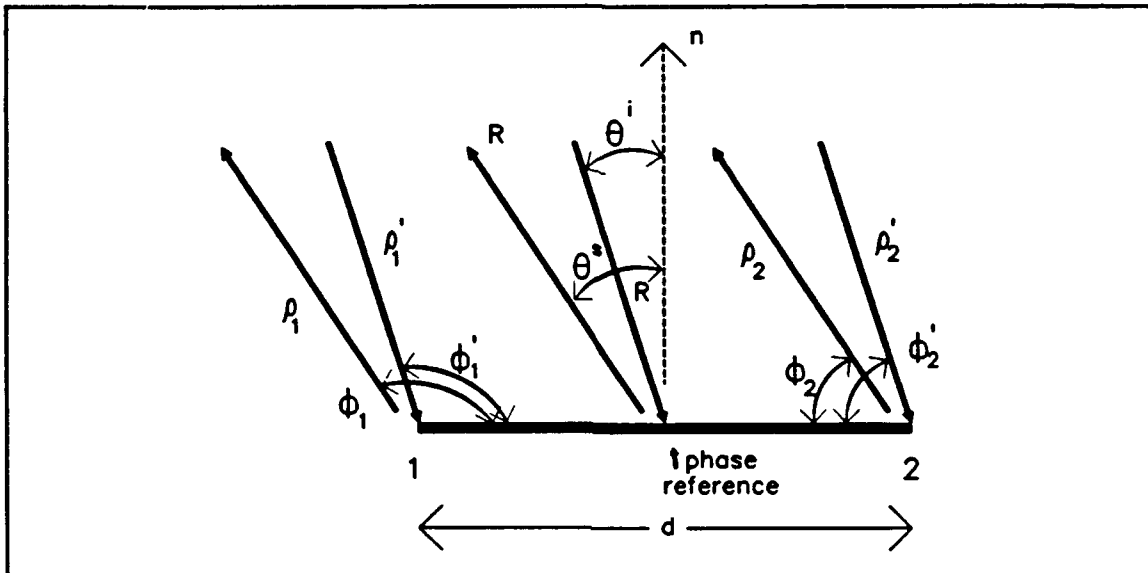


Figure 20. Definition of strip geometry used in UTD analysis

and from points 1 and 2 to the receiver ( $\rho$ ) are related by  $\theta^{i,s}$  as given in the equations below:

$$\begin{aligned}
 \rho_1' &= R - \frac{d}{2} \sin(\theta^i) \\
 \rho_2' &= R + \frac{d}{2} \sin(\theta^i) \\
 \rho_1 &= R - \frac{d}{2} \sin(\theta^s) \\
 \rho_2 &= R + \frac{d}{2} \sin(\theta^s)
 \end{aligned}
 \tag{15}$$

The half plane geometry for each edge of the strip is a special case of the wedge shown in Figure 2, where the wedge angle (WA) equals  $0^\circ$  and  $n = 2$  since  $n$  is defined as:  $n = 2 - (WA/\pi)$ . The incident and scattered wave angles are measured counterclockwise from the surface normal, and have the following limits:  $0^\circ \leq \theta^i, \theta^s \leq 360^\circ$ . The angular position of the source and the receiver with respect to each edge is represented by  $\phi'$  and  $\phi$ , respectively, where  $0^\circ \leq \phi', \phi \leq n\pi$ . The angles  $\phi$ ,  $\phi'$  for edges 1 and 2 are related to  $\theta^i$  and  $\theta^s$  as shown in the following set of equations:

$$\begin{aligned}
 \phi'_1 &= \begin{cases} 90^\circ + \theta^i & ; \quad 0^\circ \leq \theta^i \leq 270^\circ \\ \theta^i - 270^\circ & ; \quad 270^\circ < \theta^i \leq 360^\circ \end{cases} \\
 \phi_1 &= \begin{cases} 90^\circ + \theta^s & ; \quad 0^\circ \leq \theta^s \leq 270^\circ \\ \theta^s - 270^\circ & ; \quad 270^\circ < \theta^s \leq 360^\circ \end{cases} \\
 \phi'_2 &= \begin{cases} 270^\circ + \theta^i & ; \quad 0^\circ \leq \theta^i \leq 90^\circ \\ \theta^i - 90^\circ & ; \quad 90^\circ < \theta^i \leq 360^\circ \end{cases} \\
 \phi_2 &= \begin{cases} 270^\circ + \theta^s & ; \quad 0^\circ \leq \theta^s \leq 90^\circ \\ \theta^s - 90^\circ & ; \quad 90^\circ < \theta^s \leq 360^\circ \end{cases}
 \end{aligned} \tag{16}$$

The diffracted field from either edge is defined by Equation 17. The variable  $u$  represents an electric or magnetic field for the case of an electric or magnetic line source, respectively. The diffracted field is the product of the incident field at the edge, a diffraction coefficient  $D_{s,h}$  (s for electric line source, h for magnetic line source), and a term that accounts for phase change and amplitude decay after diffraction.

$$u^d = u^i(Q_E) D_{s,h}(\phi', \phi, L) \frac{e^{-jk\rho}}{\sqrt{\rho}} \quad (17)$$

The incident field at points 1 and 2 on the strip is defined as

$$u_1^i = e^{jk \frac{d}{2} \sin(\theta')}$$

$$u_2^i = e^{-jk \frac{d}{2} \sin(\theta')} \quad (18)$$

respectively. The source can reside in any of the 4 standard quadrants related to the strip geometry. The diffraction coefficient term is

$$D_{s,h}(\phi', \phi, L) = \frac{-e^{-j\frac{\pi}{4}}}{2\sqrt{2\pi k}} \left( \frac{F[kLa(\phi - \phi')]}{\cos(\frac{\phi - \phi'}{2})} + \frac{F[kLa(\phi + \phi')]}{\cos(\frac{\phi + \phi'}{2})} \right) \quad (19)$$

where the function  $F$  is called the transition function and is defined by (11) as

$$F(x) = 2j\sqrt{x} e^{ix} \int_{x^2}^{\infty} e^{-j\tau^2} d\tau . \quad (20)$$

The coefficient  $L$ , within the transition function, is a distance parameter relating the distances from the strip to the source and receiver as (11)

$$L = \frac{\rho' \rho}{\rho' + \rho} . \quad (21)$$

When considering only single diffractions from the strip, with the source and receiver in the far-field, the transition function is approximately unity since  $L \rightarrow \infty$ . This will reduce Equation 19 for single diffractions to

$$D_{\frac{\pi}{h}}(\phi', \phi, L) = \frac{-e^{-j\frac{\pi}{4}}}{2\sqrt{2\pi k}} \left[ \frac{1}{\cos\left(\frac{\phi - \phi'}{2}\right)} + \frac{1}{\cos\left(\frac{\phi + \phi'}{2}\right)} \right] . \quad (22)$$

Upon making substitutions into Equation 14 and assuming a magnetic line source, the diffracted field at the receiver from points 1 and 2 on the strip are

$$H_1^d = e^{jk\frac{d}{2}\sin(\theta')} \left\{ \frac{-e^{-j\frac{\pi}{4}}}{2\sqrt{2\pi k}} \left( \frac{1}{\cos\left(\frac{\phi_1 - \phi'_1}{2}\right)} + \frac{1}{\cos\left(\frac{\phi_1 + \phi'_1}{2}\right)} \right) \right\} \left\{ \frac{e^{-jk(R - \frac{d}{2}\sin\theta')}}{\sqrt{R}} \right\} \quad (23)$$

$$H_2^d = e^{-jk\frac{d}{2}\sin(\theta')} \left\{ \frac{-e^{-j\frac{\pi}{4}}}{2\sqrt{2\pi k}} \left( \frac{1}{\cos\left(\frac{\phi_2 - \phi'_2}{2}\right)} + \frac{1}{\cos\left(\frac{\phi_2 + \phi'_2}{2}\right)} \right) \right\} \left\{ \frac{e^{-jk(R + \frac{d}{2}\sin\theta')}}{\sqrt{R}} \right\}$$

respectively. The total diffracted field at the receiver ( $H_{Total}$ ) is the summation of the individual ( $H_1$  and  $H_2$ ) diffracted fields from each point.

The two dimensional RCS for the strip is defined as

$$\sigma_{2dim} = \lim_{R \rightarrow \infty} 2\pi R \frac{|H_s|^2}{|H_i|^2} \quad (24)$$

with  $H_s$  representing the total magnetic field obtained above.

The 2D RCS of the strip was investigated since it

models the principal plane scattering from a 3D rectangular plate, and can be used to estimate the 3D RCS of such a plate. A conversion factor is necessary, and is given by

$$\sigma_{3\text{dim}} \approx \sigma_{2\text{dim}} \frac{2l^2}{\lambda} \quad (25)$$

where  $l$  is the length of the plate (in the third dimension) and  $\lambda$  is the illuminating wavelength (2:578).

The equations above were incorporated into the Fortran program included in Appendix C. The program outputs the flat plate RCS in dBsm versus the angle theta in degrees.

## V. Data Analysis and Validation

The predictions and measurements performed in this research effort are contained in Appendix A. All the measurements were performed in the AFIT anechoic chamber. The measurements and predictions were done using the geometry shown in Figure 21. The transmit and receive

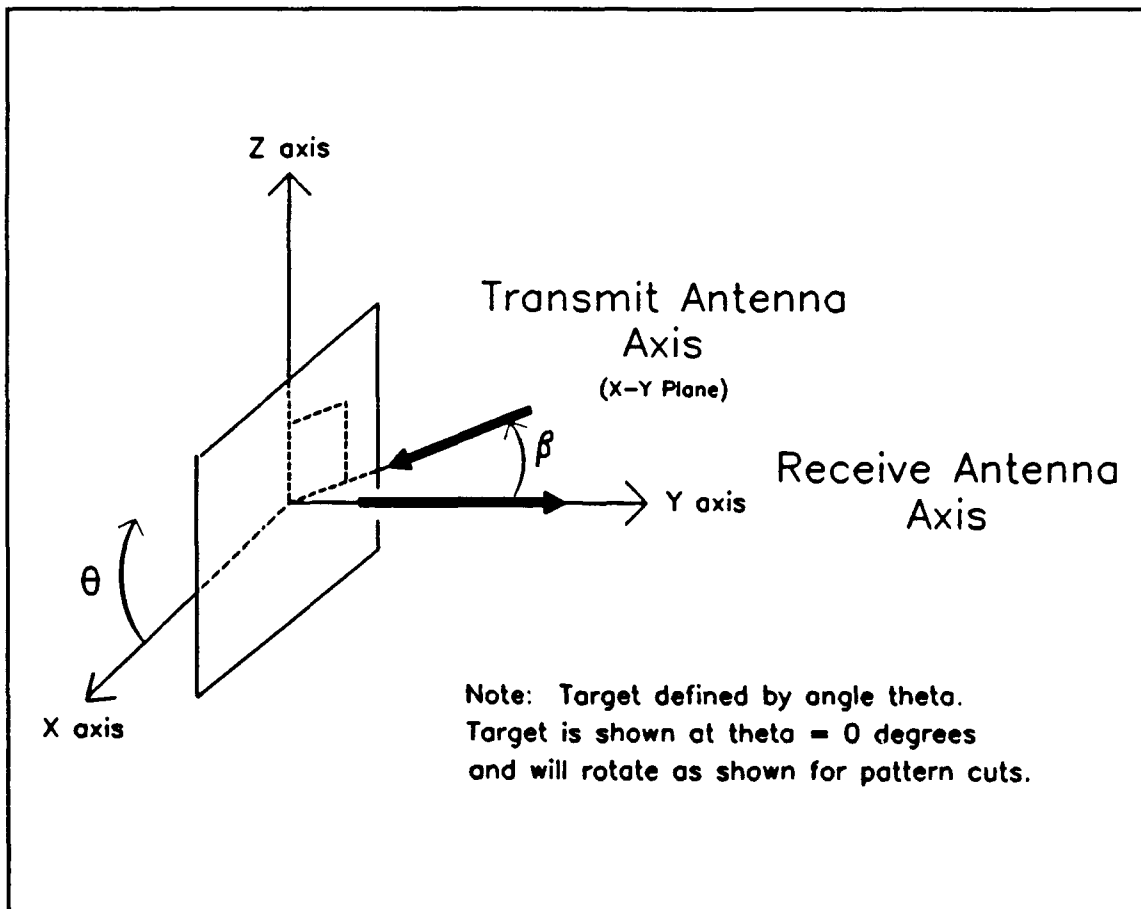


Figure 21. Target geometry used for RCS predictions and measurements



antennas are in the X-Y plane while the targets are perpendicular to the X-Y plane. The positive X axis and Y axis correspond to  $\theta = 0^\circ$  and  $270^\circ$  respectively. To provide further understanding of the geometry used, the bistatic angles ( $\beta$ ) of  $45^\circ$ ,  $90^\circ$ , and  $135^\circ$  represent  $\theta = 225^\circ$ ,  $180^\circ$ , and  $135^\circ$  respectively.

The targets predicted and measured are shown in Figure 22. The targets were selected since their RCS could be

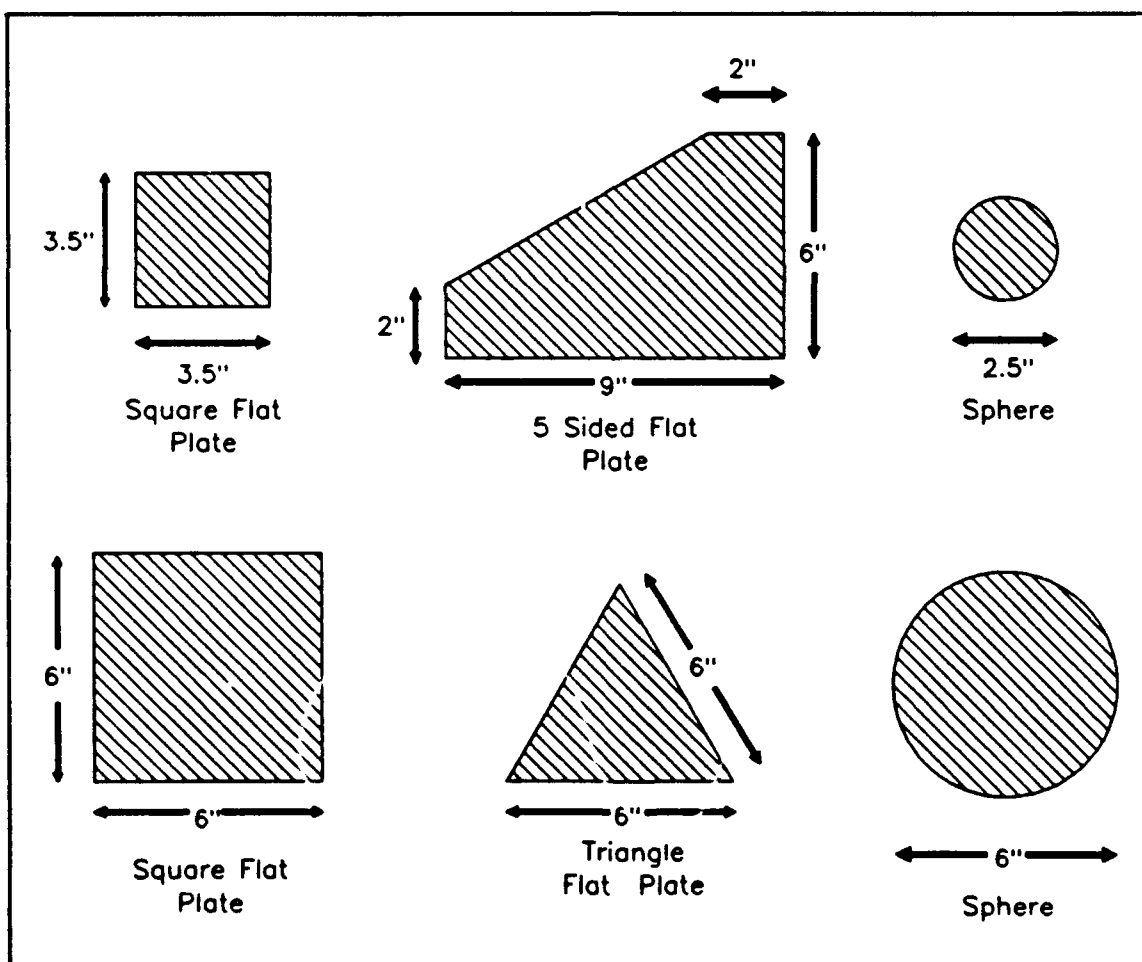


Figure 22. Targets used

predicted.

First, the predictions and pattern cut measurements for the targets will be compared using the data obtained at vertical polarization and 10 GHz with the X-band antenna transmitting and the Flam and Russell antenna receiving. Next, two measurements obtained for the five sided flat plate with the antennas interchanged will be compared. This will be followed by a comparison of the pattern cut measurements obtained at  $\beta = 45^\circ$  using two different transmit antennas, an AEL and an X-band. After this, the frequency response relating to the noise floor will be investigated. Finally, an analysis will be provided on antenna placement with respect to measurement calibration.

### *Spheres*

As previously mentioned, the computer program BISPH was used to obtain the exact RCS of the spheres. The values obtained from BISPH for the two spheres measured are provided in Table 3.

The measured RCS patterns for the 2.5 inch and 6 inch sphere are included in Figures 23 through 32 in Appendix A. As measured, the RCS of a sphere should remain constant as theta is rotated 360°. The variation obtained in the measurements is due to slight measurement errors. The average measured RCS is listed in Tables 4 and 5 for the 2.5" and 6" spheres, respectively.

The data detailed in the tables indicate that the

monostatic RCS is quite accurate. As the bistatic angle between the antennas increases the magnitude of the

Table 3. Exact sphere data from BISPH at 10 GHz and vertical polarization

<i>Sphere Size (inches)</i>	<i>Bistatic Angle (degrees)</i>	<i>RCS Magnitude (dBsm)</i>
2.5	0	-26.001
2.5	45	-25.881
2.5	90	-24.368
2.5	135	-26.352
6.0	0	-17.436
6.0	45	-17.190
6.0	90	-17.907
6.0	135	-14.890

difference (delta) between the predicted and measured also increases.

The data obtained from BISPH indicates the RCS for a sphere is highly dependant on the bistatic angle. That is, for a 1 degree error in the position of the antenna at a bistatic angle at 135 degrees for a sphere at 10 GHz and vertically polarized, the RCS varies from -25.027 dBsm at  $\beta = 134^\circ$  to -28.079 dBsm at  $\beta = 136^\circ$  for the 2.5 inch sphere,

and from -14.798 dBsm at  $\beta = 134^\circ$  to -15.58 dBsm at  $\beta = 136^\circ$  for the 6 inch sphere. This will be discussed more near the end of the chapter.

Table 4. RCS for 2.5 inch Sphere (10 GHz, Ver Pol)

$\beta$ (deg)	<i>Predicted RCS</i> (dBsm)	<i>Measured RCS</i> (dBsm)	<i>Delta</i> (dBsm)
0	-26.001	-25.70	0.301
45	-25.881	-25.06	0.821
90	-24.368	-25.70	1.332
135	-26.352	-24.22	2.132

Table 5. RCS for 6 inch Sphere (10 GHz, Ver Pol)

$\beta$ (deg)	<i>Predicted RCS</i> (dBsm)	<i>Measured RCS</i> (dBsm)	<i>Delta</i> (dBsm)
0	-17.436	-17.06	0.376
45	-17.19	-17.0	0.19
90	-17.907	-18.05	0.143
135	-14.89	-17.95	3.06

### *Square Flat Plates*

Figures 33 through 50 of Appendix A contain the predicted and measured monostatic and bistatic RCS patterns for the 3.5 inch and 6 inch square flat plates. The predicted RCS values were obtained from two sources, as discussed previously. The first code used for the predictions was RCS-BSC2 (12). The second code, UTD Single Diffraction, was written for this research. The two predictions were placed in the same figure for comparison purposes.

In comparing the predictions from the two codes used (Figures 33, 35, 38, 40, 42, 44, 47 & 49), the main lobe and all side lobes match very well in magnitude, width, and position of all lobe peaks along the theta axis. With the antennas in vertical polarization, the monostatic predictions (Figures 33 & 42) indicate an RCS at  $\theta = 90^\circ$  and  $270^\circ$  from the plate edge since the incident electric field aligns along the vertical edge of the plate. While the code does predict an RCS at  $\theta = 90^\circ$  and  $270^\circ$  in the monostatic predictions, it does not predict the two lobes (Figures 34 & 43) measured at these positions. This results since the prediction code uses a flat plate with no thickness (knife edge). The lobe on the two measurements result from the diffraction from the finite width plate edge. The prediction code based on single diffractions adequately predicts the bistatic scattering from square flat plate

geometries in vertical polarization as verified by the comparison with RCS-BSC2.

The measurements were performed at 10 GHz. This means that the targets were 2.96 and 5.08 wavelengths on a side, respectively. As the dimensions of a flat plate increase in wavelengths, the number of lobes in the pattern cut increases, as shown in the predictions and measurements.

As a comparison, the main lobe peaks from the flat plates are compared in Tables 6 and 7. Using the target geometry defined in Figure 19, the main lobe peak returns for bistatic angles ( $\beta$ ) of  $45^\circ$ ,  $90^\circ$ , and  $135^\circ$  were expected to occur at the angles determined by

$$\theta_{\max}^\circ = 360^\circ - \frac{(\beta)^\circ}{2} \quad (26)$$

and since the target is symmetrical also at  $\theta_{\max}^\circ - 180^\circ$ . Using the equation, the maximum RCS should occur at  $\theta = 157.5^\circ$  and  $337.5^\circ$  for  $\beta = 45^\circ$ ,  $135^\circ$  and  $315^\circ$  for  $\beta = 90^\circ$ , and  $112.5^\circ$  and  $292.5^\circ$  for  $\beta = 135^\circ$ . The measurements and predictions agreed on the positions of the peak signals.

The predictions and measurements compare well with the physical optics approximation for broadside monostatic RCS

$$\sigma = \frac{4\pi(A)^2}{\lambda^2} \quad (27)$$

which uses the area of the plate and the wavelength of operation. The physical optic approximation provides an RCS of -0.594 dBsm (3.5 inch flat plate) and 8.769 dBsm (6 inch flat plate) for backscatter.

As the bistatic angle between the antennas increase, the magnitude of the difference ( $\Delta$ ) between the predicted and measured main lobe peaks increases as well. The side lobes from the measurements and predictions match in quantity, placement, and width. In general, the peaks of all the sidelobes have approximately the same  $\Delta$  difference in magnitude (as noted in Tables 6 & 7 for main lobe) between prediction and measurement.

Table 6. Main Lobe Peak RCS for 3.5 inch Square Flat Plate (10 GHz, Ver Pol)

$\beta$ (deg)	Predicted RCS (dBsm)		Measured RCS (dBsm)	Delta (dBsm)
	RCSBSC	UTDSD		
0	-0.59	-0.26	-0.3	0.29, 0.04
45	-1.19	-1.26	-2.0	0.81, 0.74
90	-3.60	-3.56	-5.01	1.41, 1.45
135	-8.77	-8.35	-10.61	1.84, 2.26

Table 7. Main Lobe Peak RCS for 6 inch Square Flat Plate (10 GHz, Ver Pol)

$\beta$ (deg)	<i>Predicted RCS</i> (dBsm)		<i>Measured RCS</i> (dBsm)	<i>Delta</i> (dBsm)
	<i>RCSBSC</i>	<i>UTDSD</i>		
0	8.774	8.88	8.66	0.114, 0.22
45	8.12	8.08	6.68	1.44, 1.40
90	5.76	5.77	4.08	1.68, 1.69
135	0.491	0.607	-1.98	2.47, 2.59

### *Triangle Flat Plates*

Figures 51 through 58 of Appendix A contain the predicted and measured monostatic and bistatic radar cross section patterns for the 6 inch equilateral triangle flat plate.

The predictions for these flat plates were done using RCS-BSC2. The main lobe peaks for the RCS will occur at the same angles as for the square flat plates. The difference between the predicted and measured RCS patterns increases as the bistatic angle increases. This is verified by the values of RCS contained in Table 8 for the main lobe RCS peaks from the plates.

In general, the placement of the peaks of the main lobe



and the side lobes match. In all the measurements, the

Table 8. Main Lobe Peak RCS for Triangle Flat Plate (10 GHz, Ver Pol)

$\beta$ (deg)	<i>Predicted RCS</i> (dBsm)	<i>Measured RCS</i> (dBsm)	<i>Delta</i> (dBsm)
0	2.69	2.22	0.47
45	0.84	0	0.84
90	-1.49	-2.86	1.37
135	-6.24	-8.46	2.22

main lobe is wider than the one predicted. The null between the main lobe and first side lobe is not as deep, though, resulting in the position of the peaks of the first side lobe (on each side of main lobe) to match the predictions. Half way between the two main peaks on the plots, the measurements and predictions do not agree as well. This is due, in part, to the triangle plate measured having a finite width which scatters, while the RCS predicted is from a single knife edge (infinitesimal) scattering.

#### *Five Sided Flat Plates*

Figures 59 through 67 of Appendix A contain the predicted and measured monostatic and bistatic radar cross

section patterns for the five sided flat plate.

The predictions for this flat plate were done using RCS-BSC2. The main lobe peaks for the RCS will occur at the same angles as the other flat plates. Table 9 contains the peak RCS for the main lobes. As before, the difference between the predicted and measured RCS patterns increases as the bistatic angle increases. This is verified in Table 9; as  $\beta$  increases, delta increases. In fact, the delta between the predicted and measured RCS values at each bistatic angle are close to the numbers obtained for the 3.5 inch and 6 inch square flat plate in Tables 6 and 7.

The diffraction from the side edges (different lengths) cause the RCS pattern to differ on both sides of the main lobe peak. The lobing is similar to the square flat plates, with the diffractions from both sides adding in and out of phase. The lower values of RCS on the plots between  $\theta = 0^\circ$  and the first main lobe are attributed to the short side edge (2 inch) dominating the signal, while the higher RCS obtained between the two main peaks on the plots results from the domination of the diffracted field from the longer side edge (6 inch).

The quantity, width, and position of the lobes match well. Once again, the predictions are lower than the measurements throughout the entire  $360^\circ$  by approximately the delta level in Table 9.

Table 9. Main Lobe Peak RCS for 5 sided Flat Plate (10 GHz, Ver Pol)

$\beta$ (deg)	Predicted RCS (dBsm)	Measured RCS (dBsm)	Delta (dBsm)
0	9.69	9.72	0.03
45	9.01	(X-band TX) 7.9 (F&R TX) 7.9	1.11 1.11
90	6.71	5.18	1.53
135	1.39	-1.07	2.46

### Reciprocity

Two measurements were performed on the five sided flat plate to verify that the measured RCS is independent of transmit and receive antenna using the bistatic RCS measurement approach in this research.

Figures 14 and 16 show the time response measurement of the empty chamber at  $\beta = 45^\circ$ . These measurements were necessary since the background in the chamber changes significantly as the antennas change. The chamber characterization was used to establish the criteria needed to set the initial instrument state of the HP 8510 network analyzer so that the system would use the target signal for

the RCS.

Figures 62 and 63 are the measurements obtained. The measurement setup for the RCS in Figure 62 has the X-band antenna transmitting and the Flam and Russell antenna receiving, while just the opposite is true for the RCS measurement in Figure 63.

As expected, the patterns match extremely well over the entire 360° azimuth pattern cut.

#### *Bistatic Measurements Using Different Transmit Antennas*

A broadband 2 to 18 GHz AEL antenna and a high gain X-band antenna were used to transmit at a bistatic angle of 45° to determine the effect the different antennas had on the RCS measurements. The receive antenna was the Flam and Russell antenna for both cases. The measurements are provided in Figures 24, 25, 29, 30, 36, 37, 45, and 46 of Appendix A.

Figures 14 and 15 provide the time response of the empty chamber signals at  $\beta = 45^\circ$  for the two antennas. This characterization was required to set the initial instrument state of the network analyzer. The antenna coupling signal is 20 dB larger for the AEL antenna versus the X-band antenna. This results since the AEL has a much broader main beam than the X-band antenna. A direct consequence of this is noted by the signal received from the pedestal. The narrow beam high gain X-band antenna illuminates the pedestal at a higher energy level resulting in the pedestal

return appearing 6 dB higher than for the AEL antenna.

Table 10 contains the peak RCS from the spheres and square flat plates using the two different antennas. While the values measured from the two antennas do differ, there is no major difference or discrepancy between the patterns obtained. The patterns match fairly well.

Table 10. Peak RCS from the spheres and square flat plates at  $\beta = 45^\circ$  using different transmit antennas (10 GHz, Ver Pol)

Target	Predicted RCS (dBsm)	Measured RCS (dBsm)		Delta (dBsm)
		X-band	AEL	
2.5" sphere	-25.881	-25.06	-24.53	0.82, 1.35
6" sphere	-17.19	-17.0	-16.92	0.19, 0.27
3.5" FP	-1.19	-2.0	-2.0	0.81, 0.81
6" FP	8.12	6.68	6.27	1.44, 1.85

#### Noise Floor Measurements

Figures 9 - 12 provide the noise floor (a frequency response) measurements of the empty chamber from 8 to 12.4 GHz. As the frequency changes, the signal level measured in the chamber varies. As the bistatic angle increases, the pattern tends to smooth out and increase in magnitude resulting in a higher noise floor. The noise floor should

be as low as possible with the measurement configuration.

### *Error Analysis*

The measurements performed relied on many variables. One problem encountered in the bistatic measurement approach was the positioning the transmit antenna properly. While the bistatic angles in the chamber were accurately marked using a transit, aligning the antenna sitting on top of the 8 foot high tripod proved difficult.

As discussed earlier, as the bistatic angle increased, the differences between the measured and predicted RCS values increased as well, with the largest differences appearing at 135°. An investigation of the calibration RCS in dBsm of a 5 inch sphere near a bistatic angle of 135 degrees, as in Table 11, shows that the bistatic RCS is very dependent on the correct bistatic angle. Since the measured RCS depends on the calibration data input into the software for the bistatic pattern cuts, the antenna position must be correct.

For example, if the true bistatic placement of the antenna was 134.4° instead of 135°, an error of 1.28 dB  $(-19.27 - (-20.55))$  would be added into the measurement simply due to the incorrect calibration RCS provided the measurement software.

While this does not mean that this is the sole contributor for the larger differences in RCS magnitude obtained as the bistatic angle increased, it is simply meant

to show that something as simple as correctly placing the antenna can really have an adverse effect on the data.

As shown in Table 11, this is more critical at some bistatic angles. For the bistatic angles selected in this research effort, Table 11 indicates that incorrect placement of the antenna at  $\beta = 135^\circ$  could really alter the RCS obtained.

Table 11. RCS of 5 inch sphere at 10 GHz and Vertical Polarization

$\beta$	RCS	$\beta$	RCS	$\beta$	RCS
(deg)	(dBsm)	(deg)	(dBsm)	(deg)	(dBsm)
44.0	-18.76	89.0	-20.13	134.0	-21.52
44.2	-18.75	89.2	-20.11	134.2	-21.03
44.4	-18.73	89.4	-20.07	134.4	-20.55
44.6	-18.72	89.6	-20.03	134.6	-20.10
44.8	-18.70	89.8	-19.97	134.8	-19.68
45.0	-18.69	90.0	-19.91	135.0	-19.27
45.2	-18.68	90.2	-19.85	135.2	-18.90
45.4	-18.67	90.4	-19.78	135.4	-18.54
45.6	-18.66	90.6	-19.70	135.6	-18.21
45.8	-18.66	90.8	-19.62	135.8	-17.90
46.0	-18.65	91.0	-19.53	136.0	-17.61

## *Conclusions and Recommendations*

### *Summary*

The purpose of this research was to expand the measurement capability of the AFIT far-field RCS range. The objective was to establish the capability to perform accurate bistatic radar cross section measurements using AFIT's far-field range.

The capability was established to perform pattern cut and frequency response RCS measurements. Accurate bistatic RCS measurements were obtained by characterizing the signals within the chamber and using this information to establish the initial instrument settings of the network analyzer so that the correct signal would be used to determine the RCS. Several computer codes (RCS-BSC2, UTD Single Diffraction, & BISPH) were used to validate the measured data. To automate the measurements, the software (ARMS) controlling the RCS measurements had to be changed to incorporate the bistatic capability.

### *Conclusions*

The conclusions drawn from this research effort are:

1. The approach used to obtain bistatic RCS data proved valid for the AFIT RCS measurement chamber. The measurements and predictions were close for almost all of



the measurement configurations. The RCS measurement capability of the AFIT chamber now includes the bistatic situation.

2. The approach provided reasonable results independent of the antennas used or their configuration (i.e. transmit or receive).

3. The separation of the transmit and receive antenna for bistatic measurements adds additional measurement complexities that must be considered. This is in addition to those already existing for monostatic measurements.

4. The bistatic measurement technique used tends to break down as the bistatic angle approaches  $180^\circ$ , since the antenna coupling and target signal arrive at the same time.

5. Correct calibration of the relative RCS measurements of the targets used to obtain the exact target RCS is necessary to obtain valid measurements.

6. The available detail on bistatic RCS measurements and bistatic measurement considerations is minimal. Additional bistatic research needs to be performed and documented.

### *Recommendations*

The capability of the AFIT chamber has been expanded to include bistatic RCS measurements. The present research should be expanded upon to include different frequencies (much lower and higher), horizontal polarization, and cross-polarization measurements.

The measurements performed used the ramp mode of operation for the network analyzer. Another mode of operation, the step mode, should be implemented in the ARMS software. The step mode will increase the repeatability of the frequencies synthesized which will improve calibration and background subtraction in the RCS measurements. The step mode should increase the validity of the data received.

An exact sphere calibration program needs to be incorporated into the ARMS software that controls the RCS measurements so that the sphere files could be accessed directly. It could be used for monostatic and bistatic measurements. This would increase the frequency response capability to all bistatic angles.

A technique should be developed to ensure that the second antenna in the bistatic configuration is correctly positioned. For starters, a metal track and antenna cart could be considered.

The feasibility of incorporating a bistatic continuous sweep measurement capability needs to be investigated. If implemented, this would allow the bistatic data to be obtained for a particular target orientation as the transmit or receive antenna rotates through the azimuth plane for any range of bistatic angles. The calibration of this configuration could prove difficult.

## *Appendix A. Predicted and Measured RCS of Targets*

This appendix contains the data used in this research. The sphere measurements are first. These are followed by the flat plates (first the square flat plates, then the triangle and five sided flat plates). For the flat plates, each measurement is preceded by the prediction. The square flat plates have two predictions (RCSBSC-2 and UTD single Diffraction) for each situation, while the triangle and five sided flat plate predictions are from RCS-BSC2 only. Each plot is labeled with the prediction or measurement criteria.

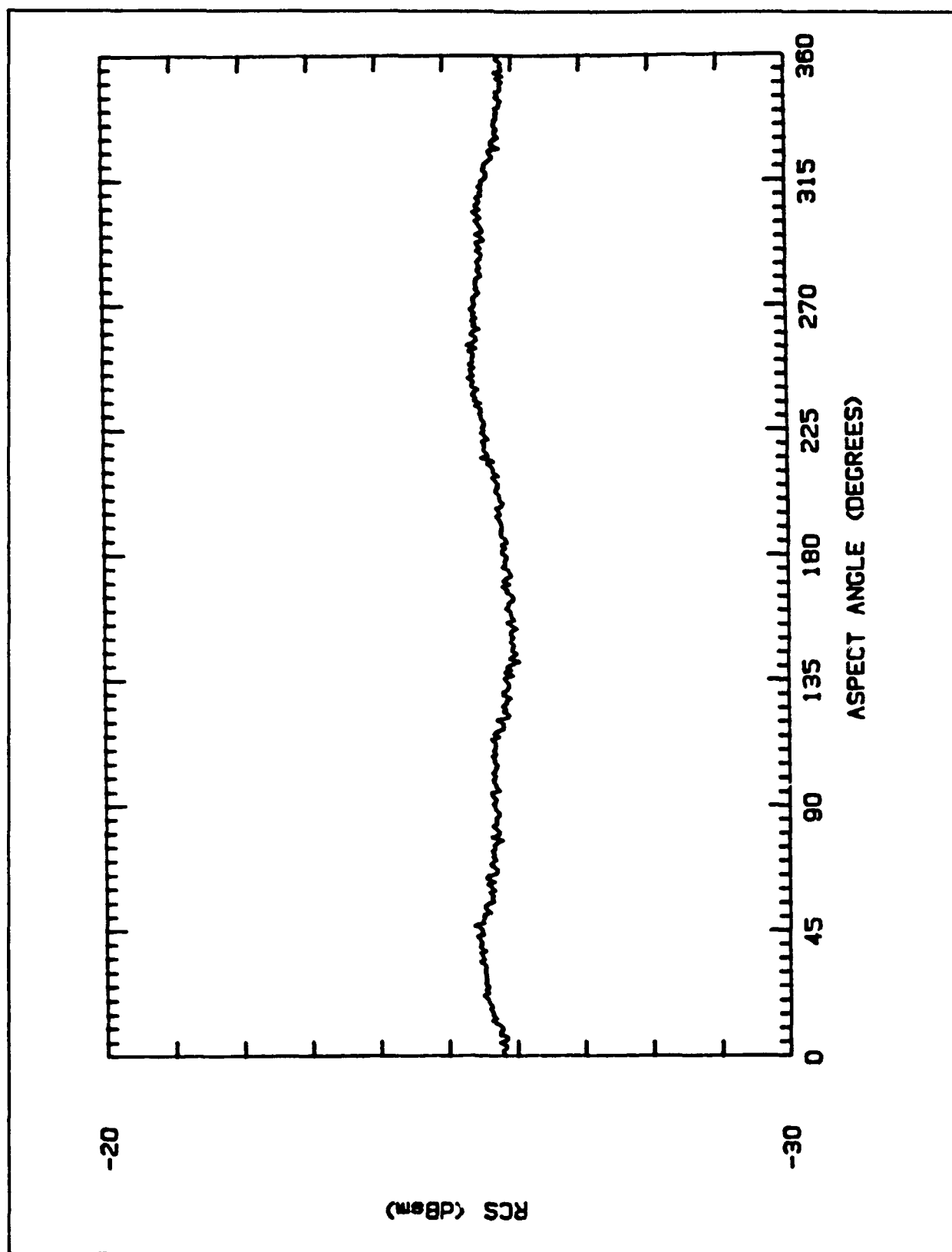


Figure 23. Measured RCS: 2.5 inch sphere, monostatic, 10 GHz, Vertical Polarization

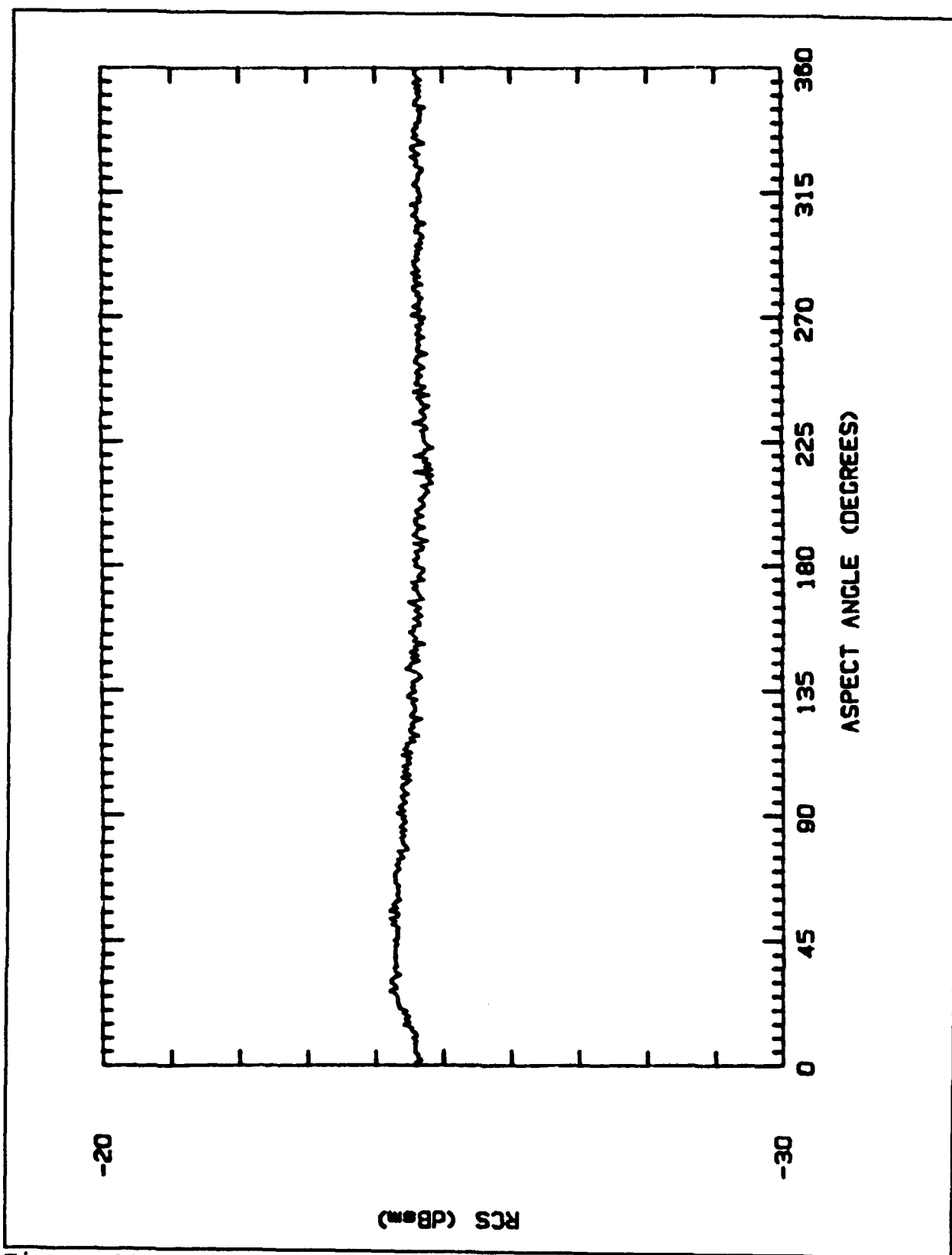


Figure 24. Measured RCS: 2.5 inch sphere,  $\beta = 45^\circ$ , 10 GHz, Vertical Polarization, AEL antenna transmitting

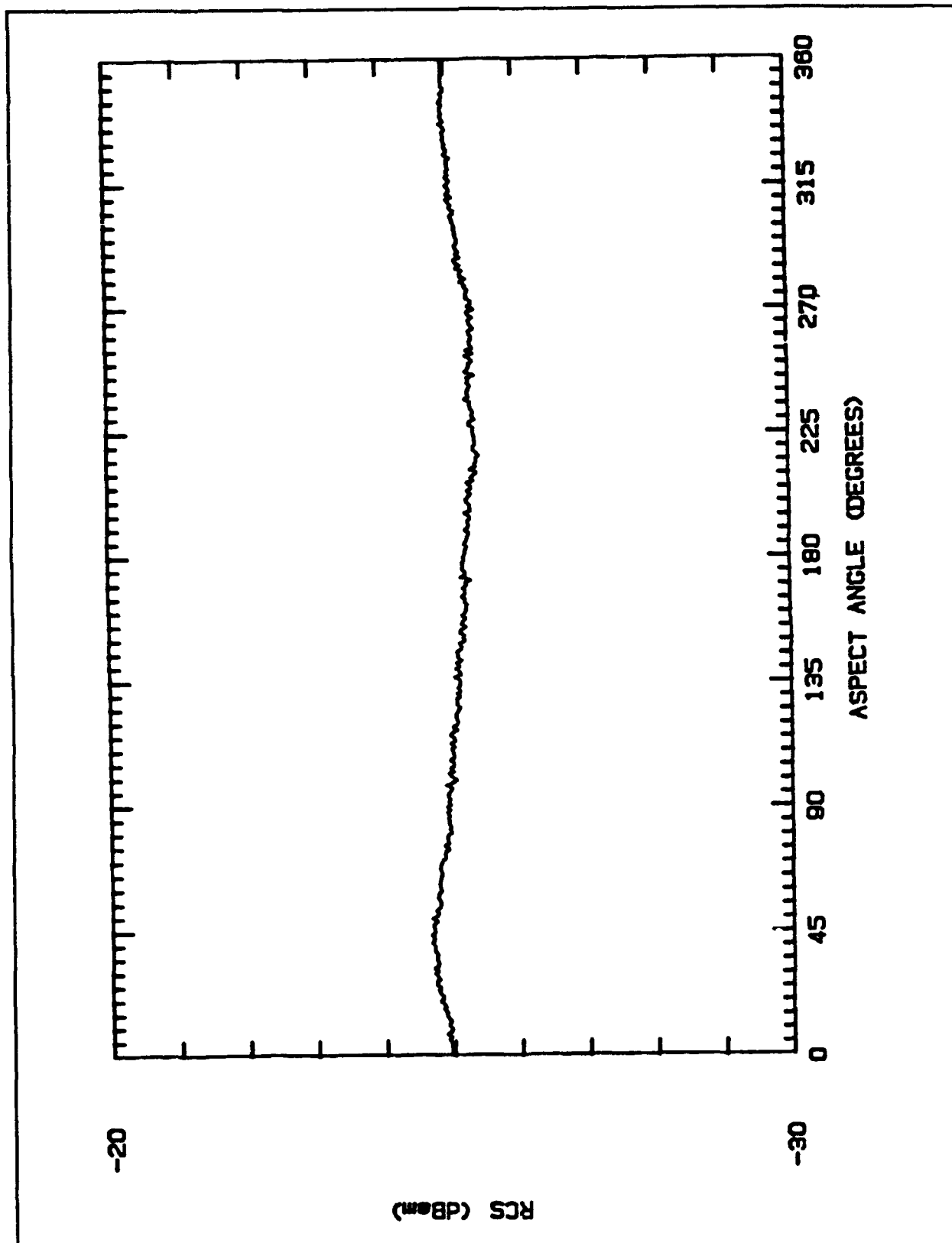


Figure 25. Measured RCS: 2.5 inch sphere,  $\beta = 45^\circ$ , 10 GHz, Vertical Polarization, X-band antenna transmitting

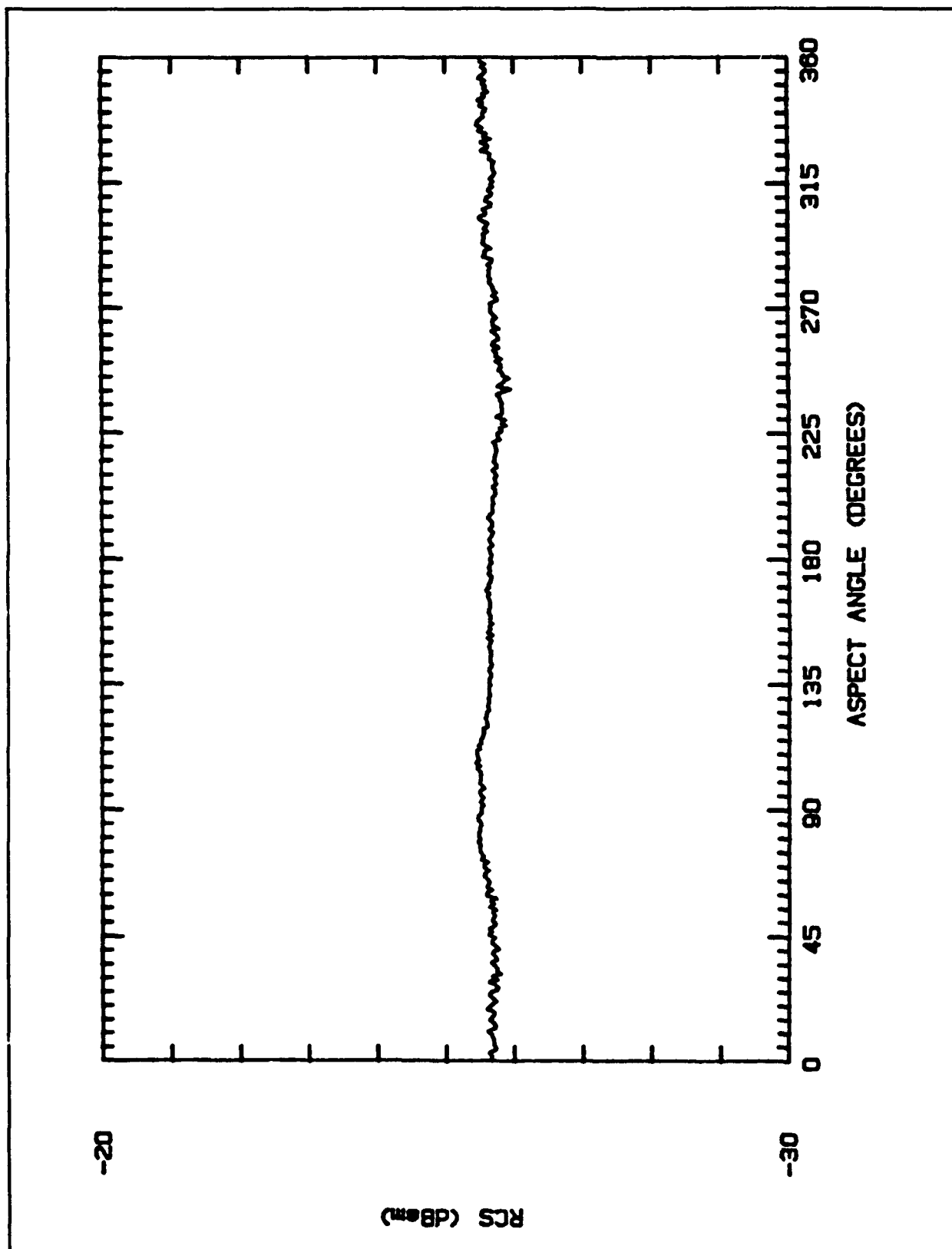


Figure 26. Measured RCS: 2.5 inch sphere,  $\beta = 90^\circ$ , 10 GHz, Vertical Polarization

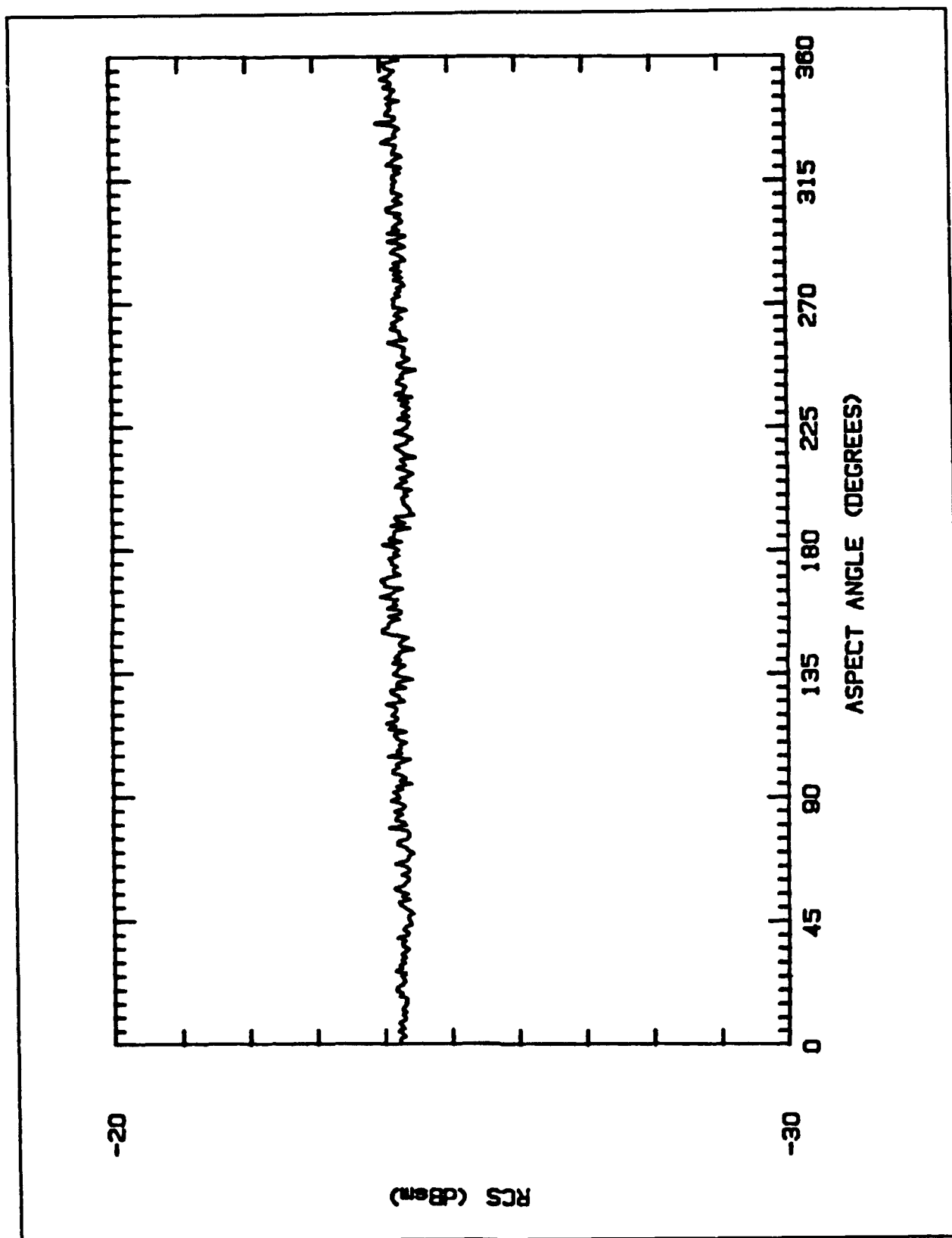


Figure 27. Measured RCS: 2.5 inch sphere,  $\beta = 135^\circ$ , 10 GHz, Vertical Polarization



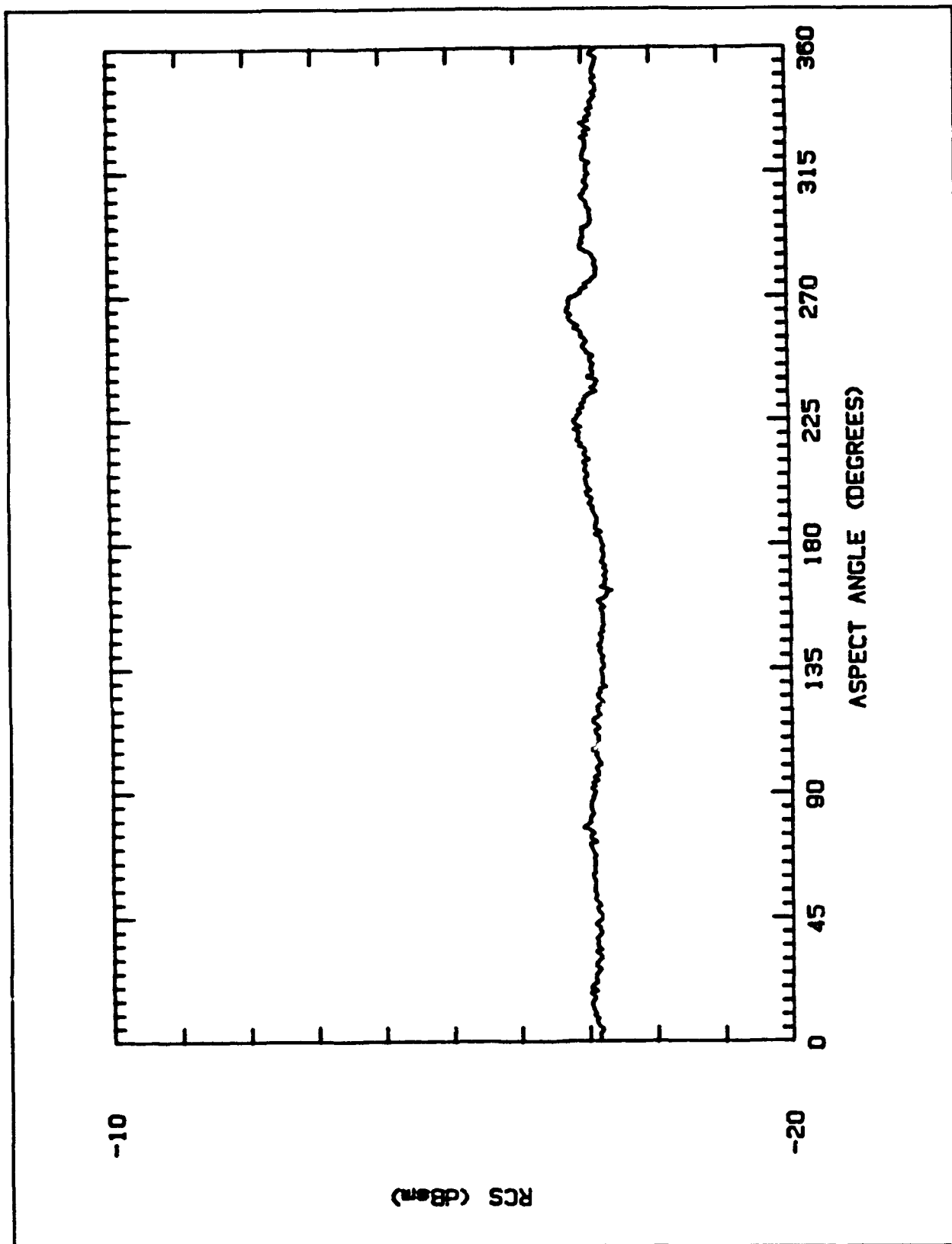


Figure 28. Measured RCS: 6 inch sphere, monostatic, 10 GHz, Vertical Polarization

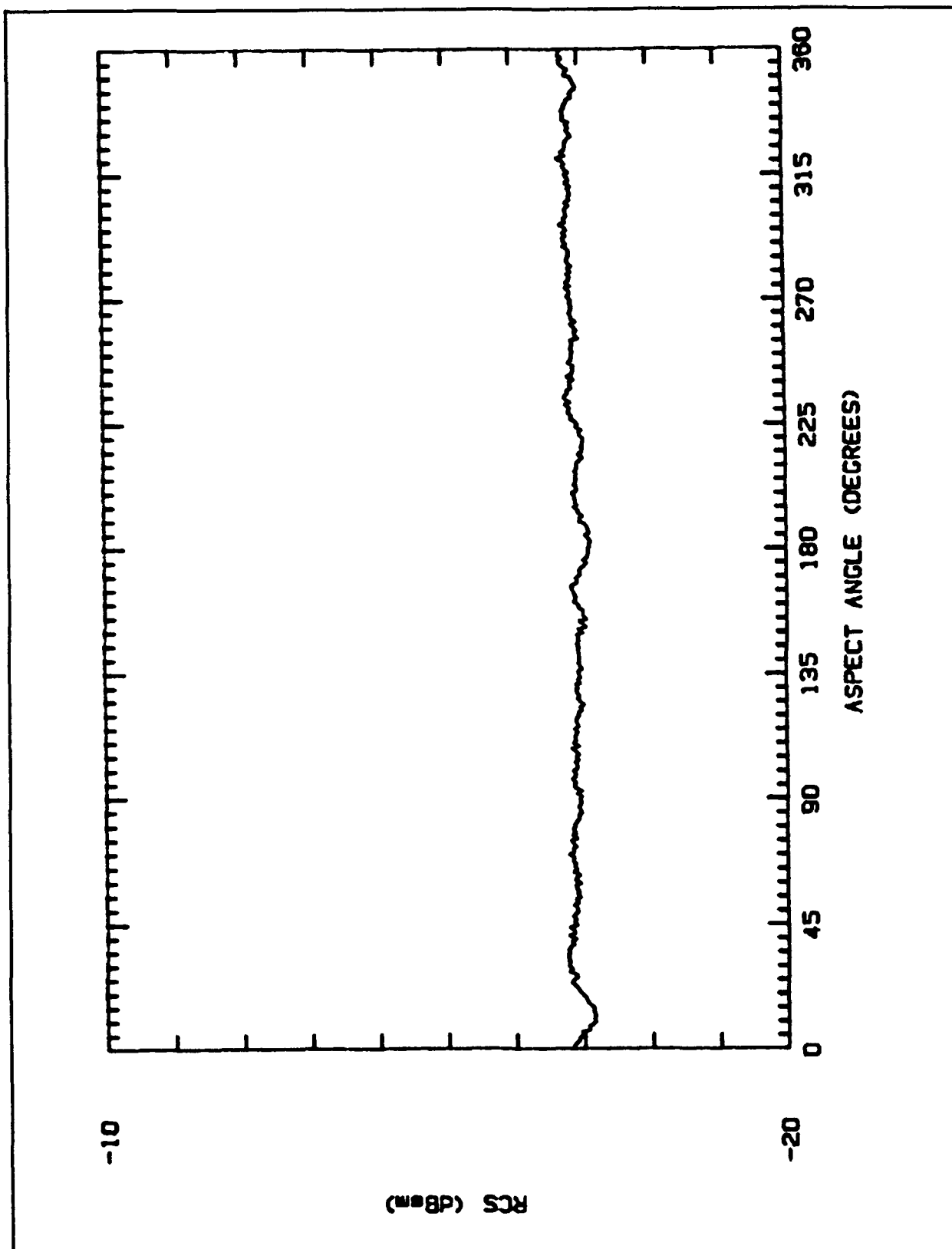


Figure 29. Measured RCS: 6 inch sphere,  $\beta = 45^\circ$ , 10 GHz, Vertical Polarization, AEL antenna transmitting

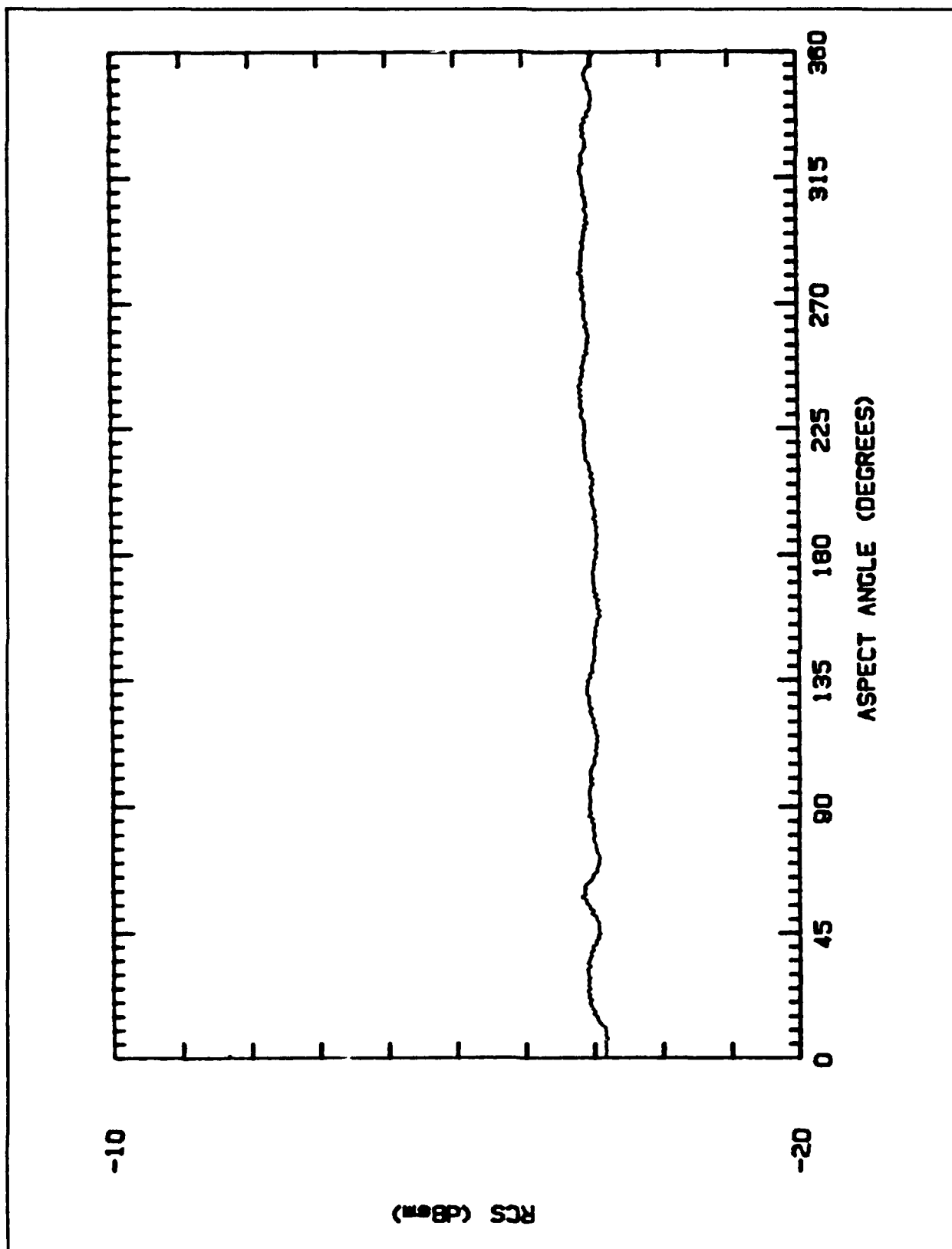


Figure 30. Measured RCS: 6 inch sphere,  $\beta = 45^\circ$ , 10 GHz, Vertical Polarization, X-band antenna transmitting

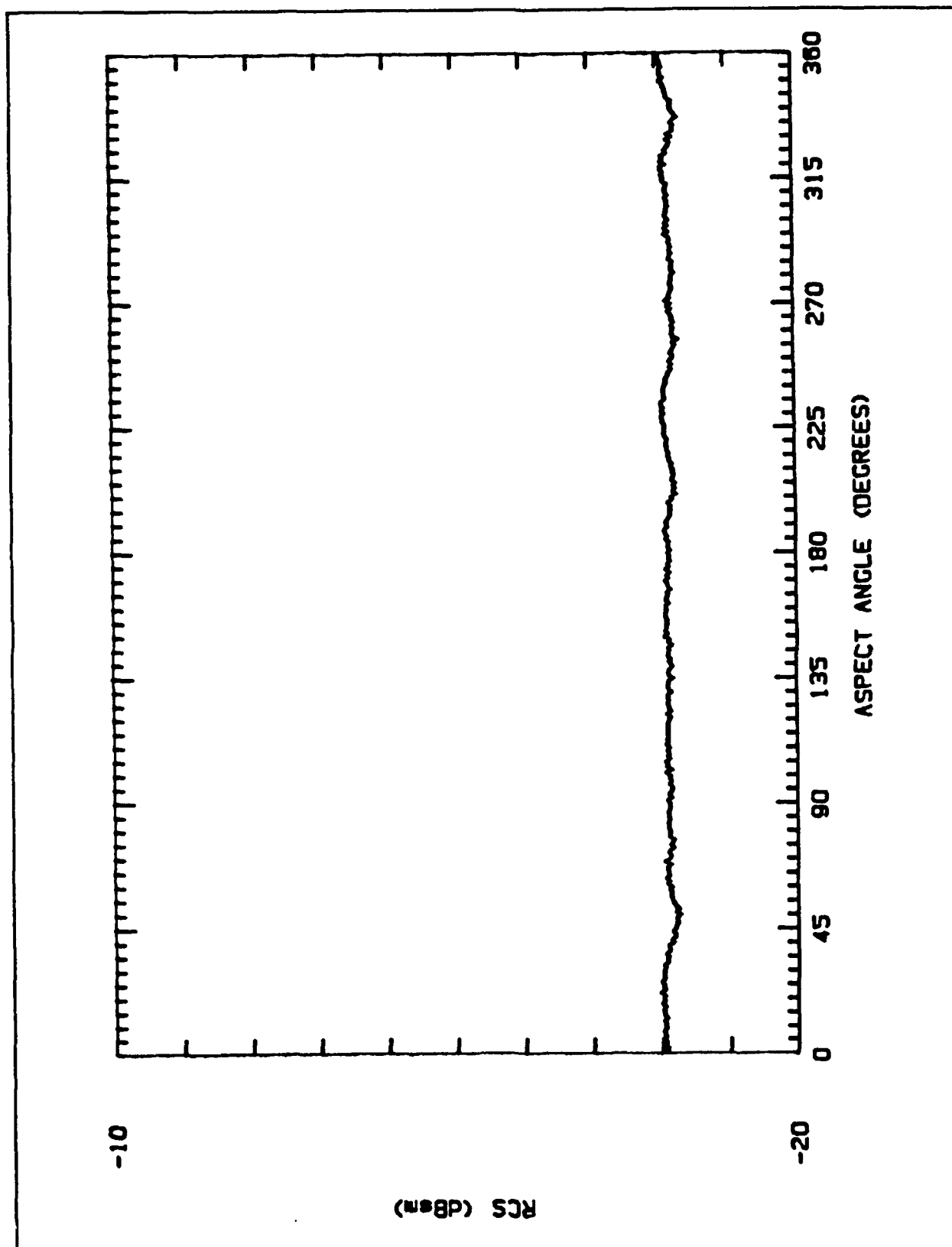


Figure 31. Measured RCS: 6 inch sphere,  $\beta = 90^\circ$ , 10 GHz, Vertical Polarization

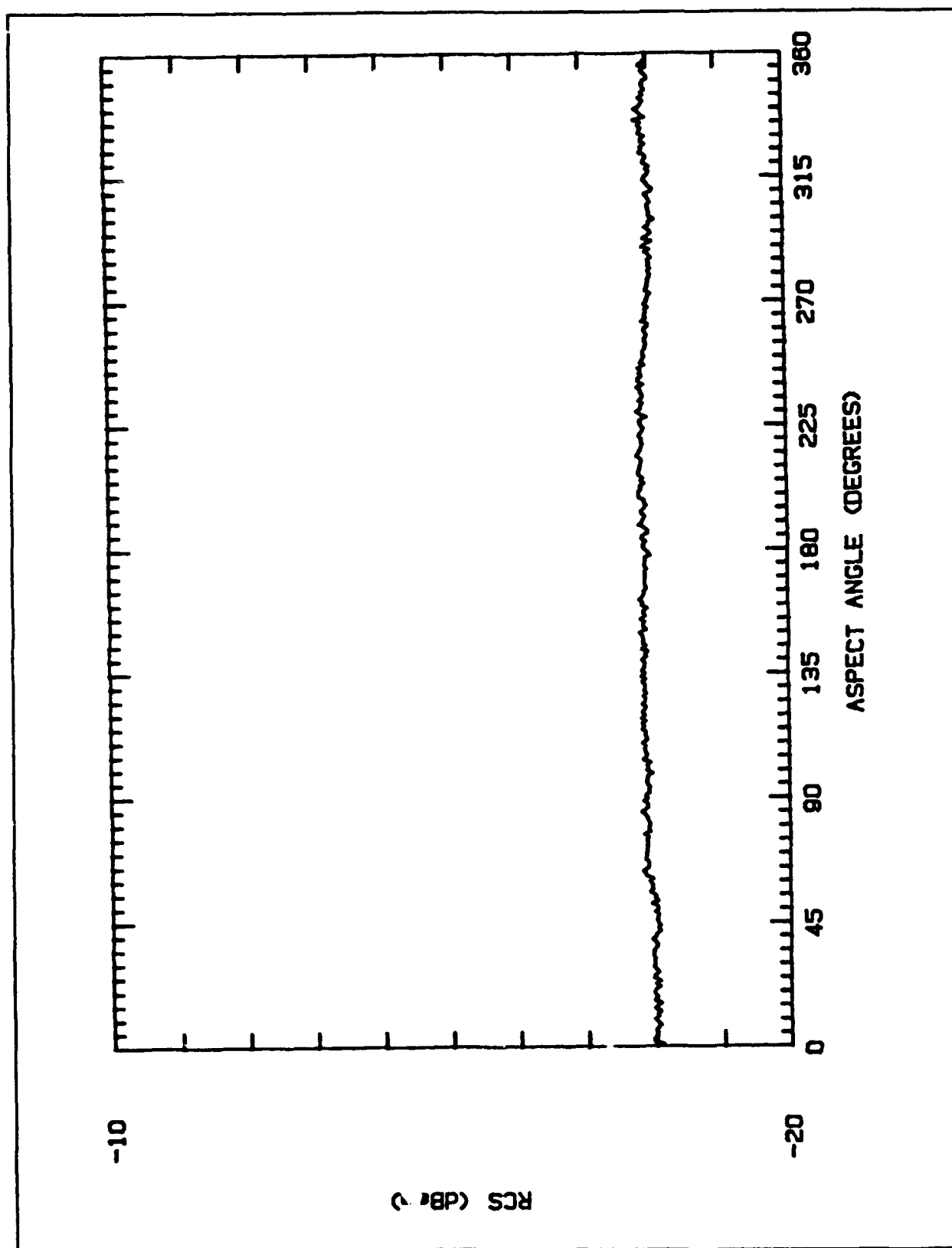


Figure 32. Measured RCS: 6 inch sphere,  $\beta = 135^\circ$ , 10 GHz, Vertical Polarization

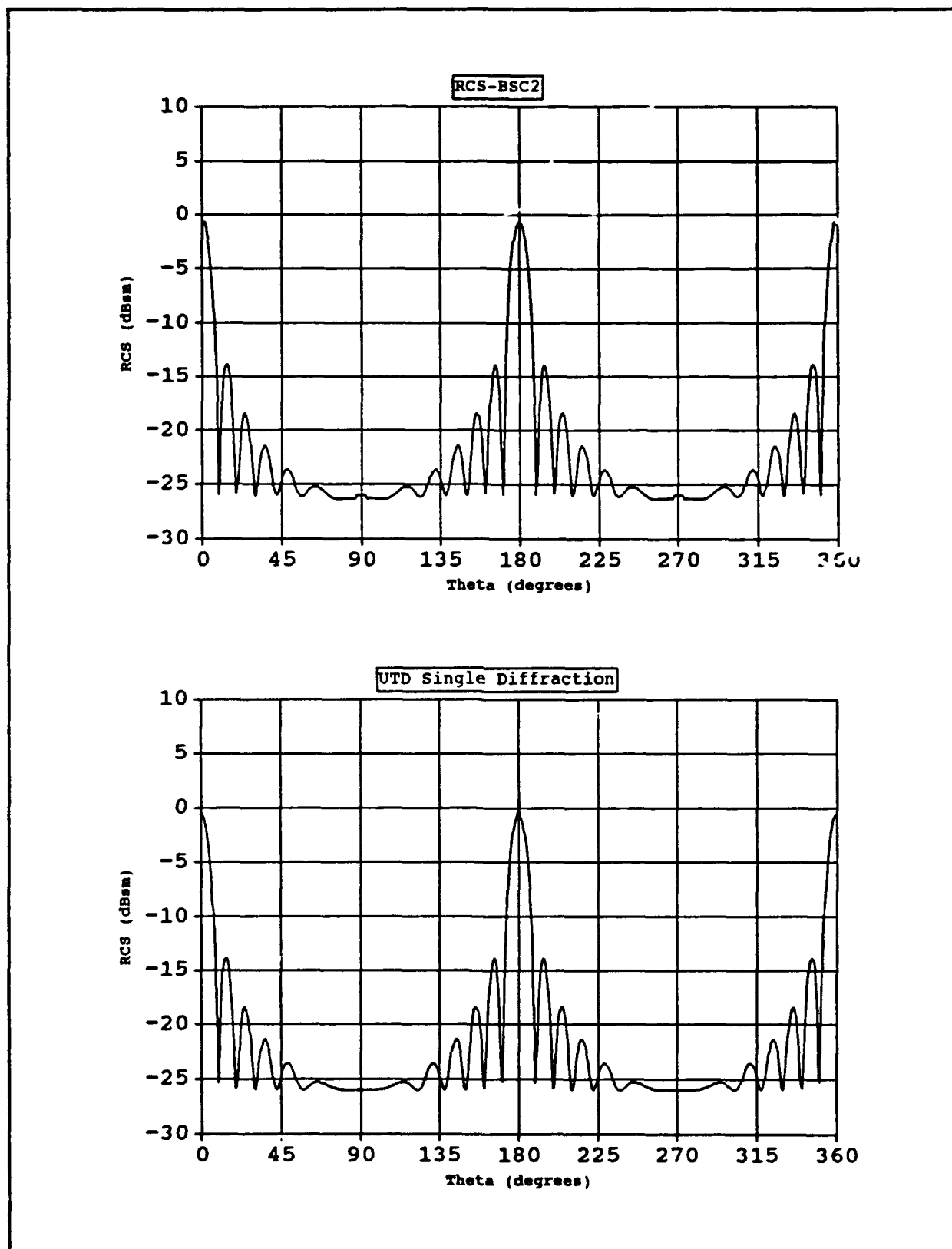


Figure 33. Comparison of monostatic RCS predictions: 3.5 inch square flat plate, 10 GHz, Vertical Polarization

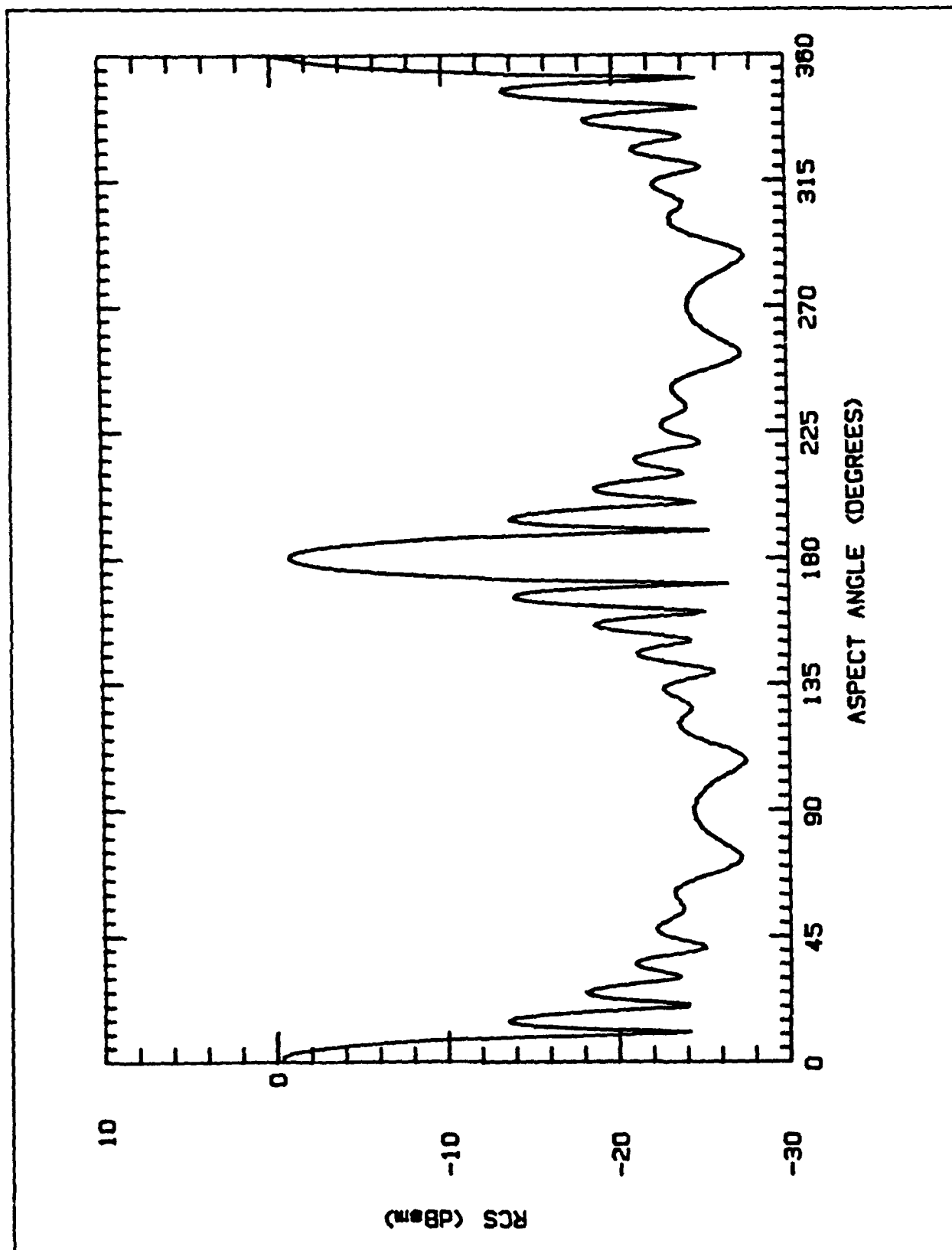


Figure 34. Measured RCS: 3.5 inch square flat plate, monostatic, 10 GHz, Vertical Polarization

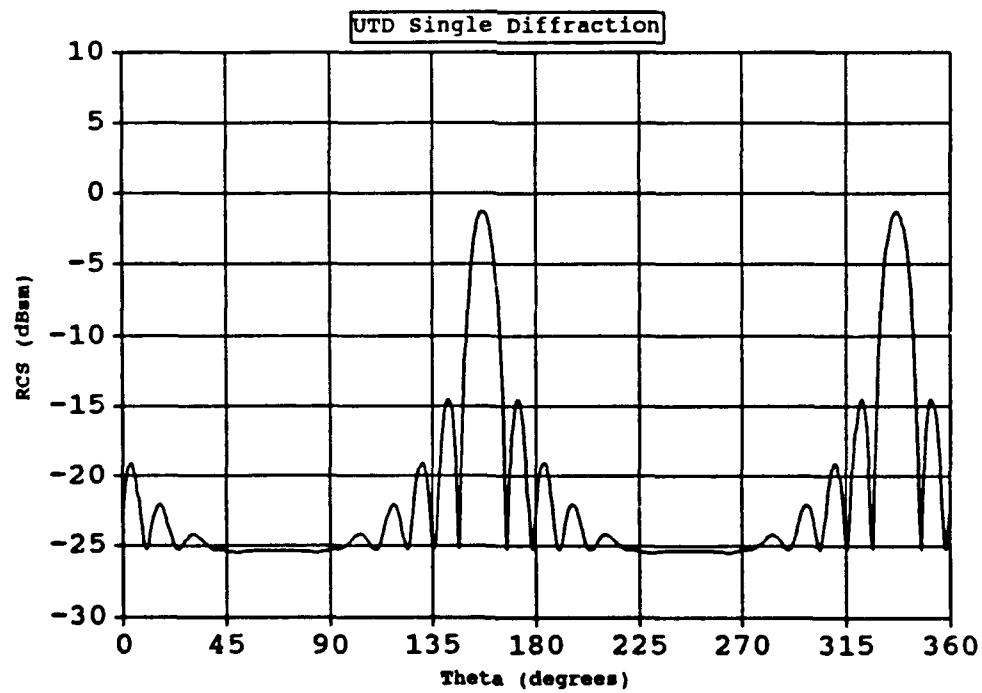
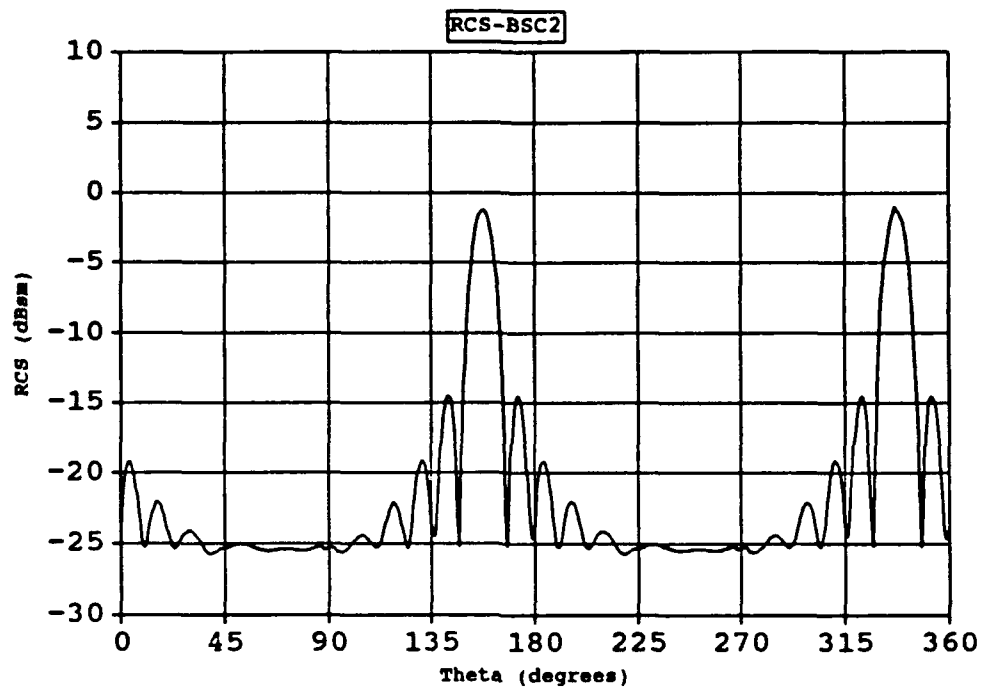


Figure 35. Comparison of bistatic RCS predictions: 3.5 inch square flat plate,  $\beta = 45^\circ$ , 10 GHz, Vertical Polarization



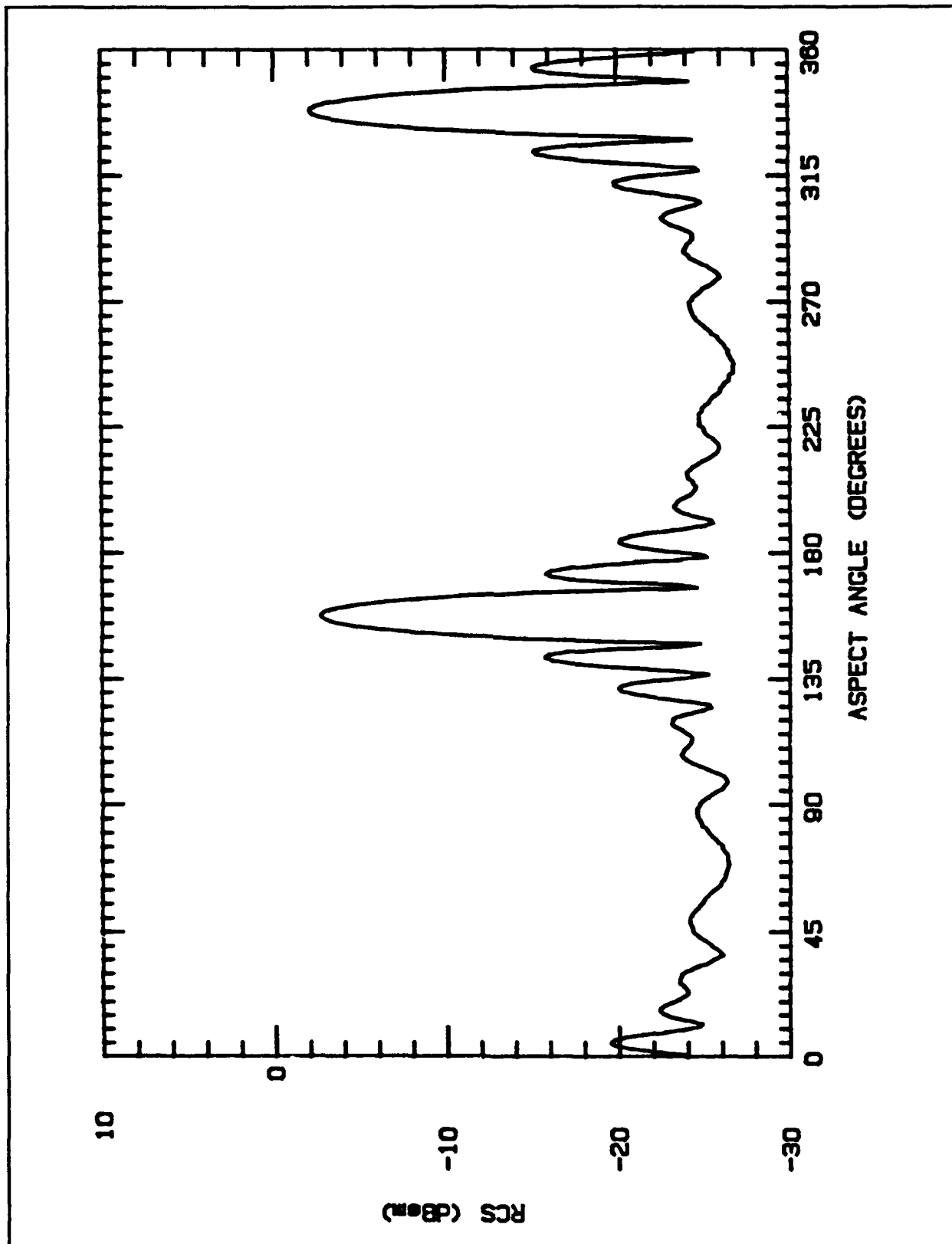


Figure 36. Measured RCS: 3.5 inch square flat plate,  $\beta = 45^\circ$ , 10 GHz, Vertical Polarization, AEL antenna transmitting

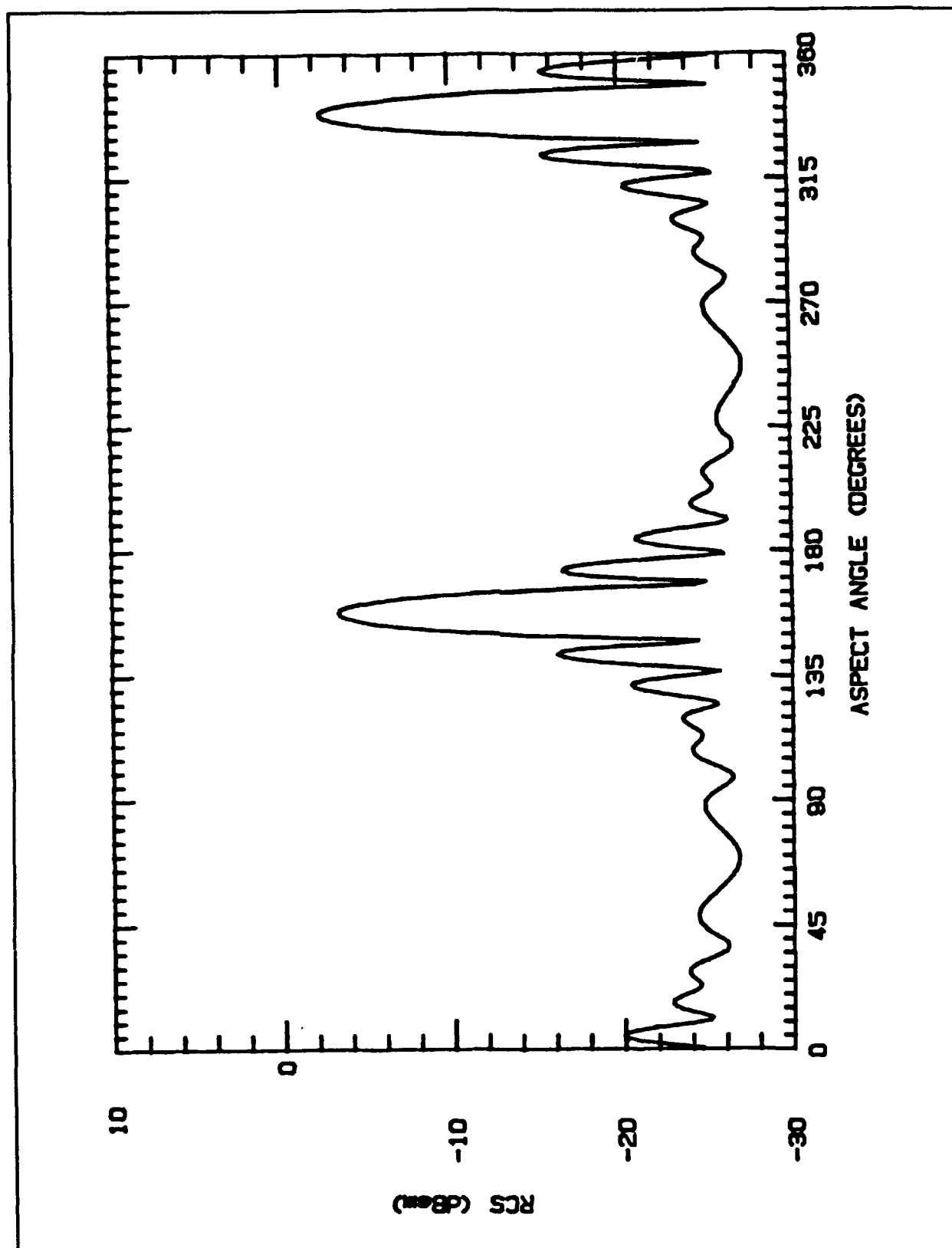


Figure 37. Measured RCS: 3.5 inch square flat plate,  $\beta = 45^\circ$ , 10 GHz, Vertical Polarization, X-band antenna transmitting

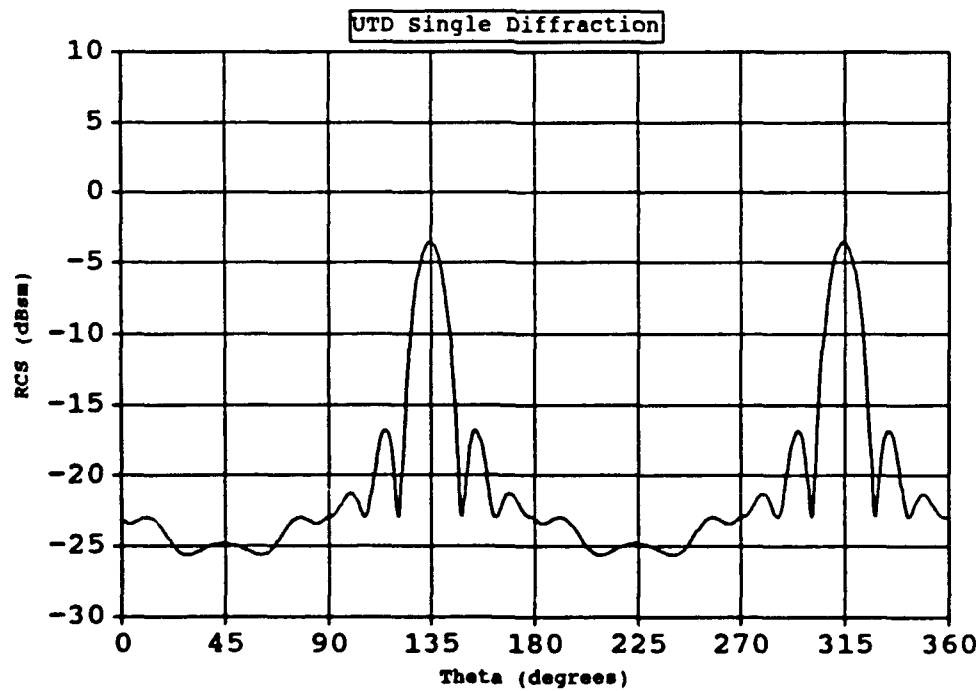
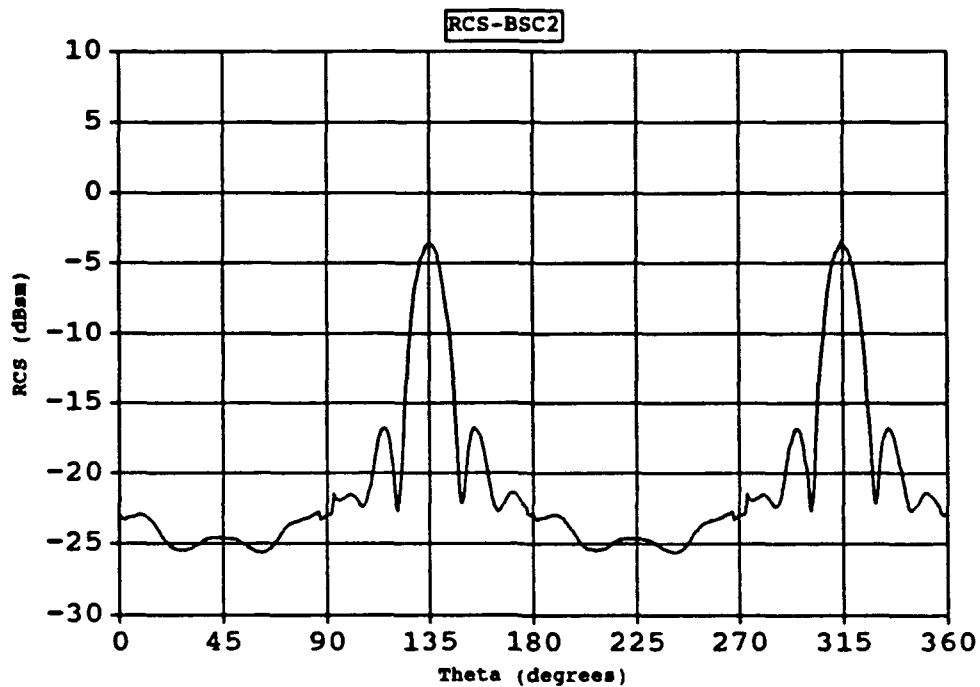


Figure 38. Comparison of bistatic RCS predictions: 3.5 inch square flat plate,  $\beta = 90^\circ$ , 10 GHz, Vertical Polarization

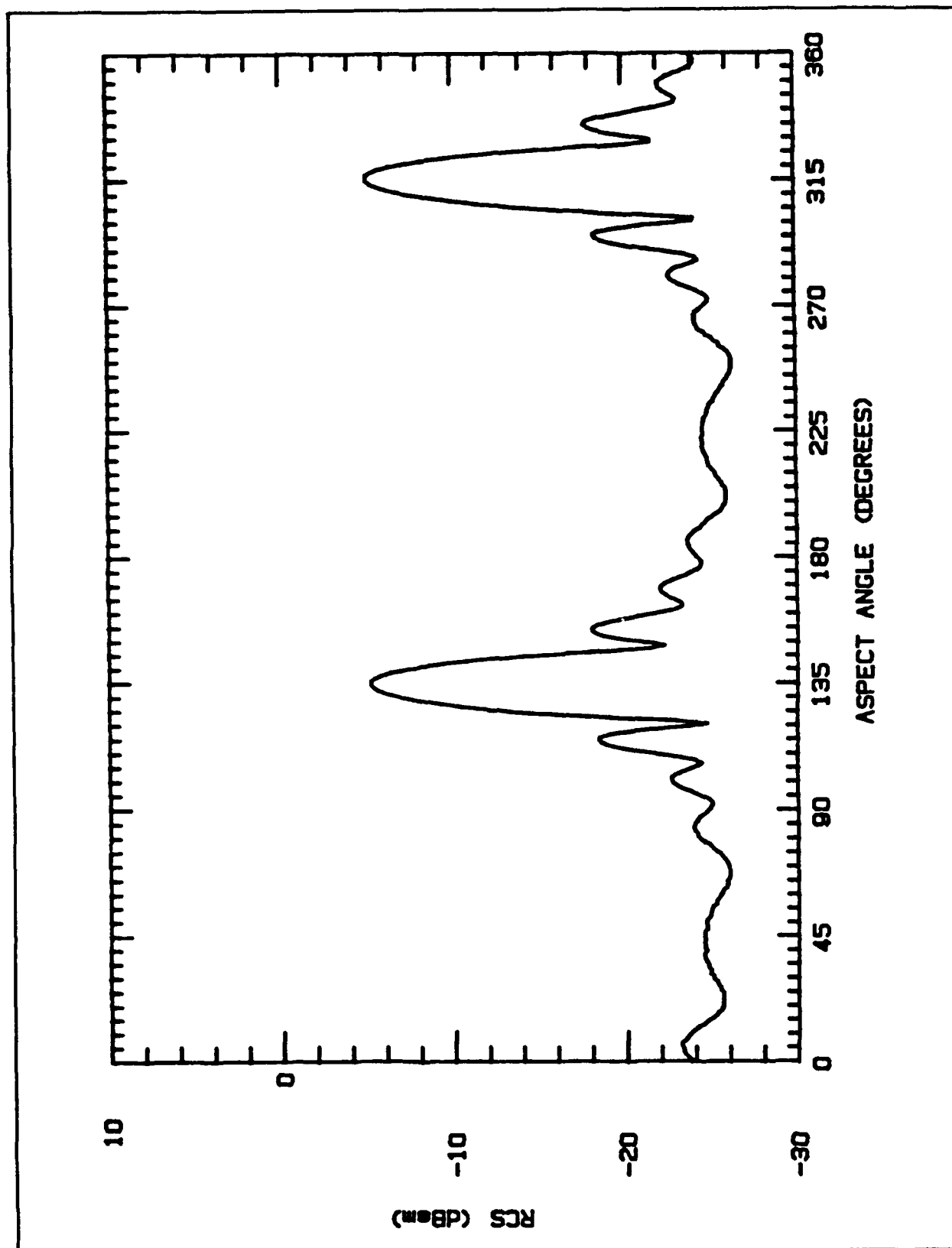


Figure 39. Measured RCS: 3.5 inch square flat plate,  $\beta = 90^\circ$ , 10 GHz, Vertical Polarization

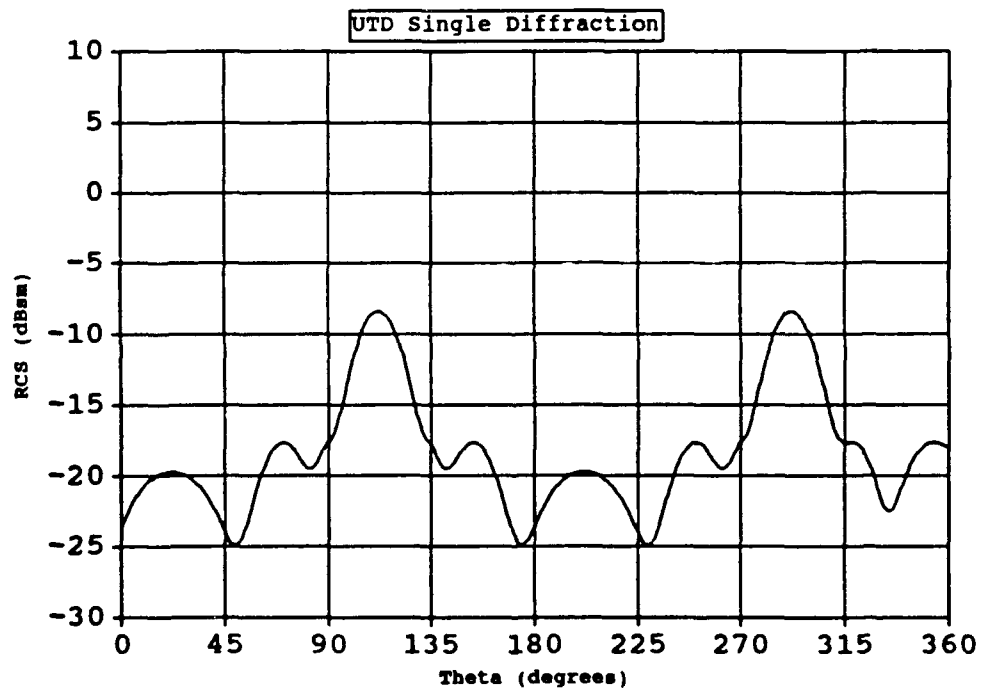
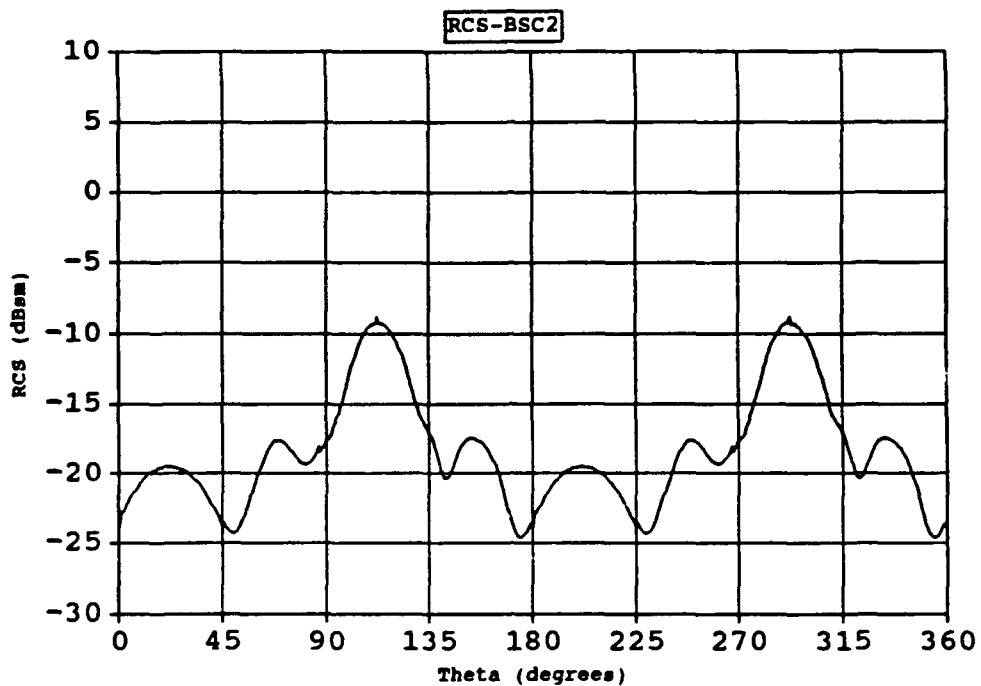


Figure 40. Comparison of bistatic RCS predictions: 3.5 inch square flat plate,  $\beta = 135^\circ$ , 10 GHz, Vertical Polarization

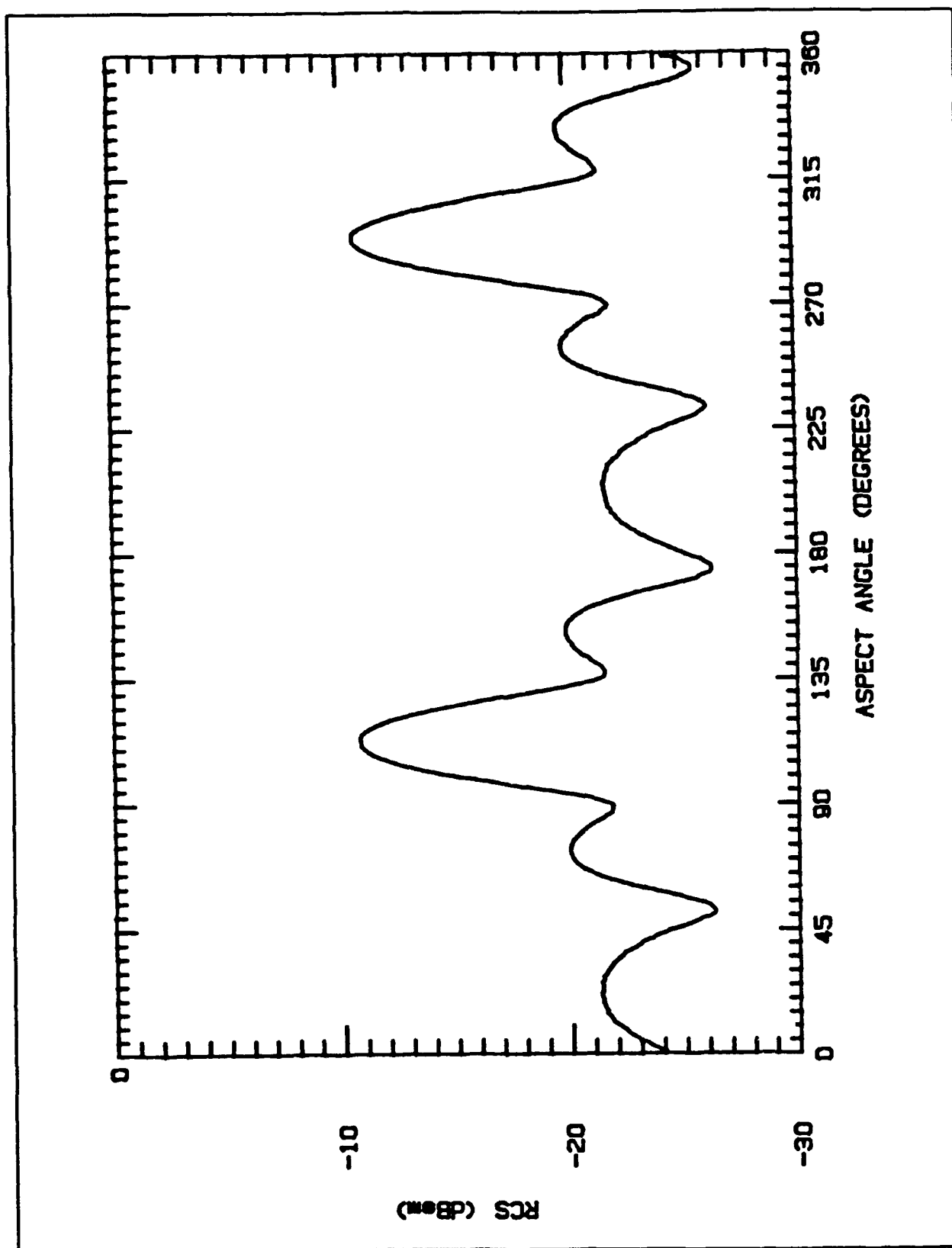


Figure 41. Measured RCS: 3.5 inch square flat plate,  $\beta = 135^\circ$ , 10 GHz, Vertical Polarization

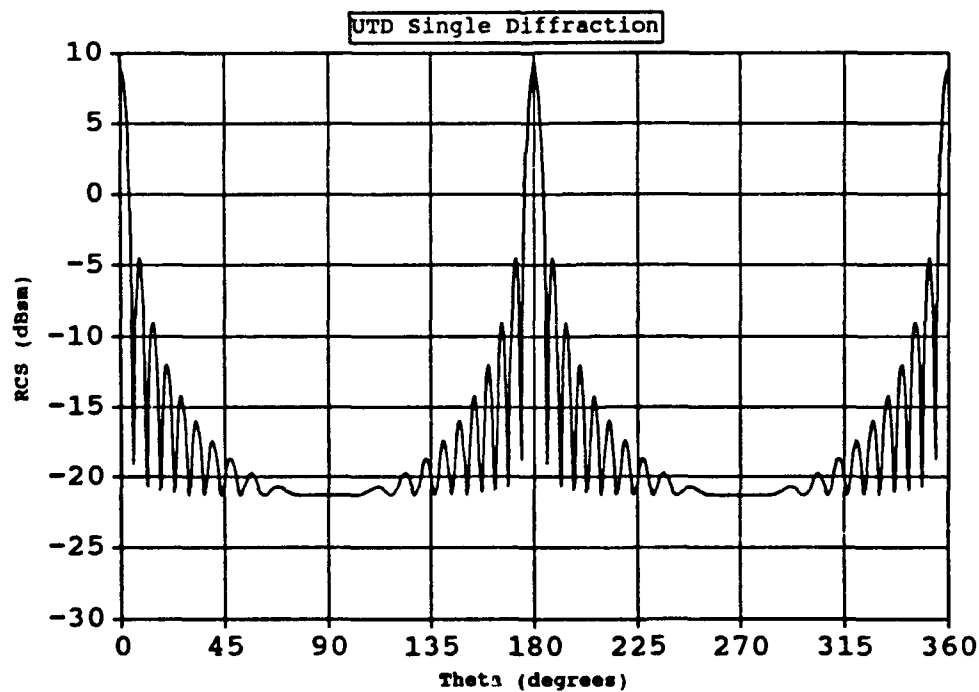
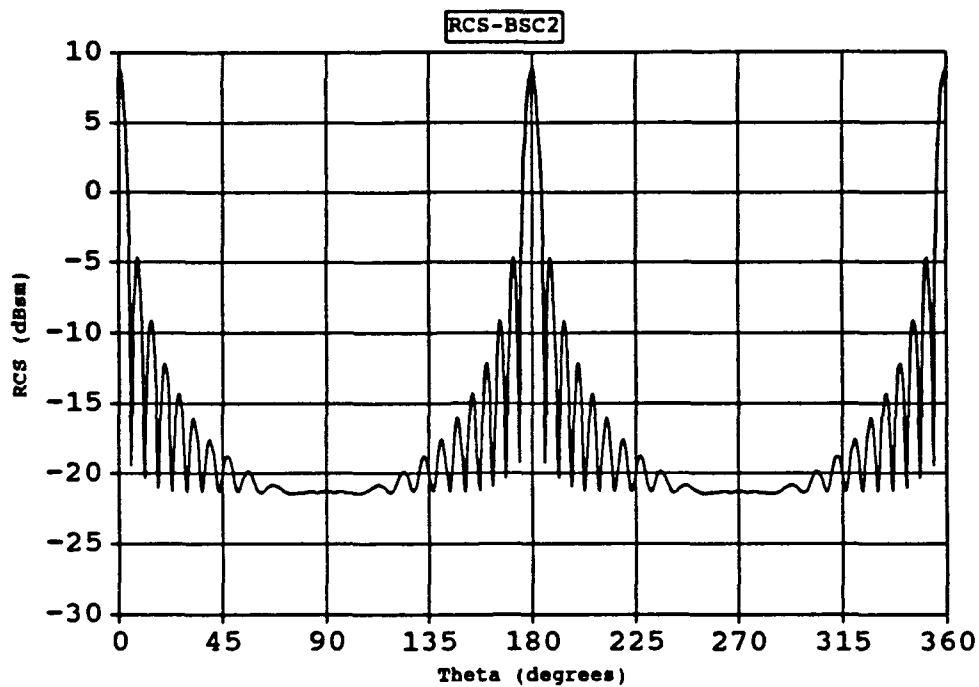


Figure 42. Comparison of monostatic RCS predictions: 6 inch square flat plate, 10 GHz, Vertical Polarization

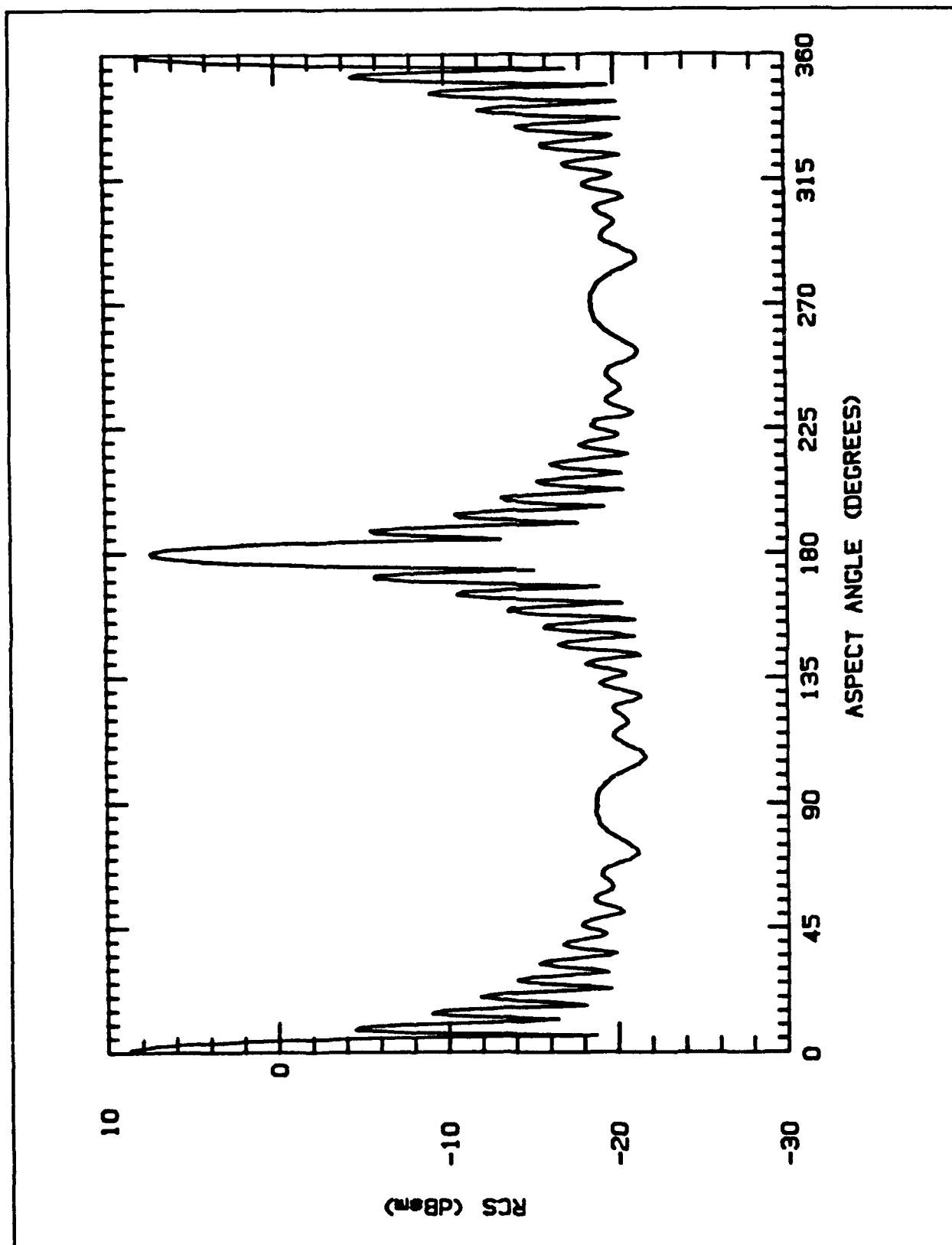


Figure 43. Measured RCS: 6 inch square flat plate, monostatic, 10 GHz, Vertical Polarization



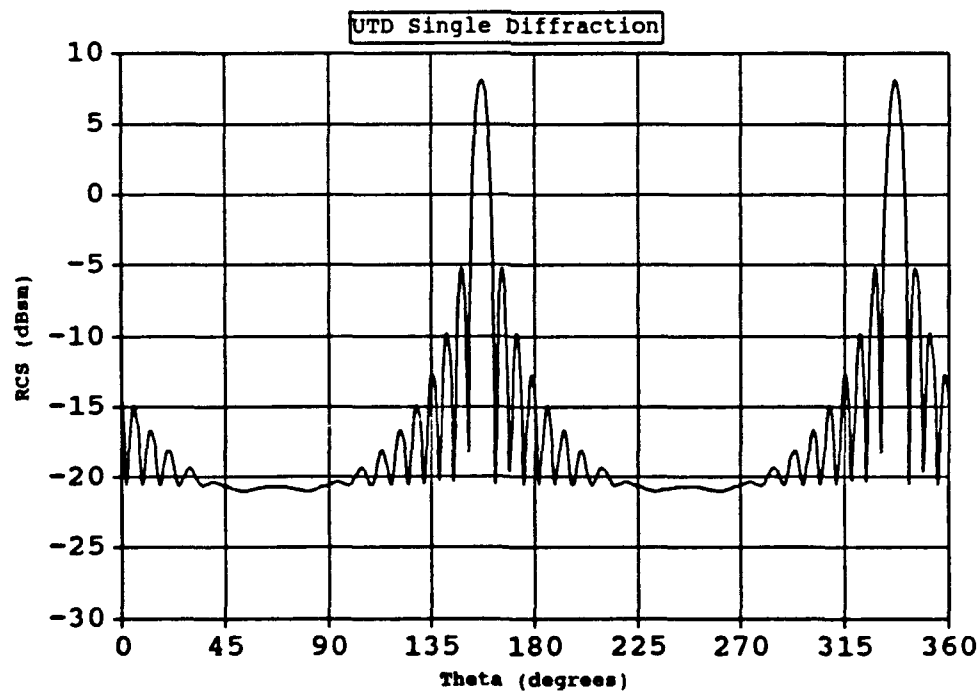
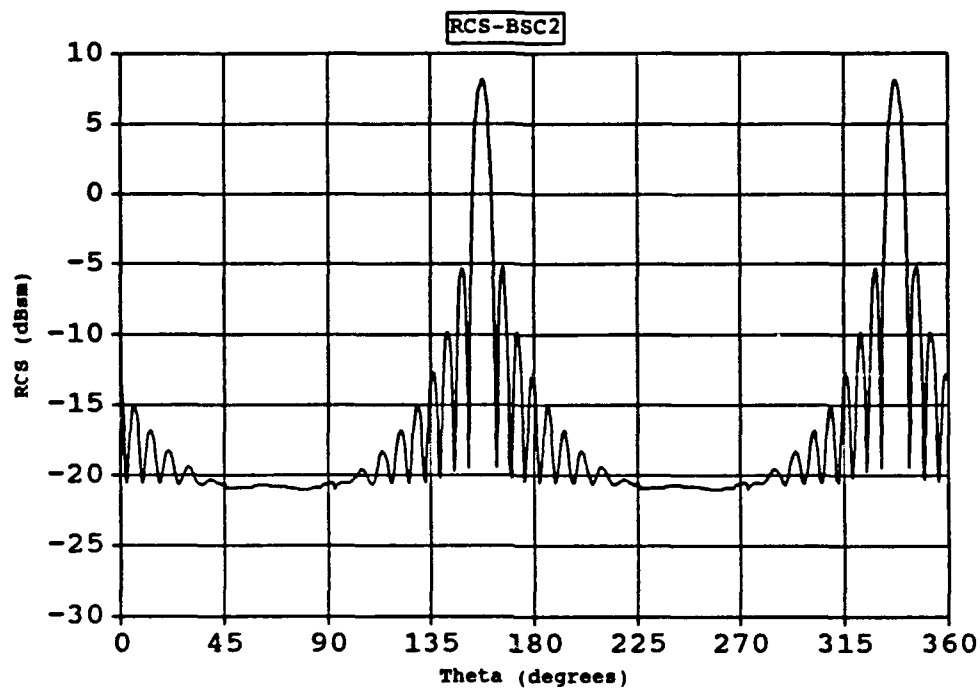


Figure 44. Comparison of bistatic RCS predictions: 6 inch square flat plate,  $\beta = 45^\circ$ , 10 GHz, Vertical Polarization

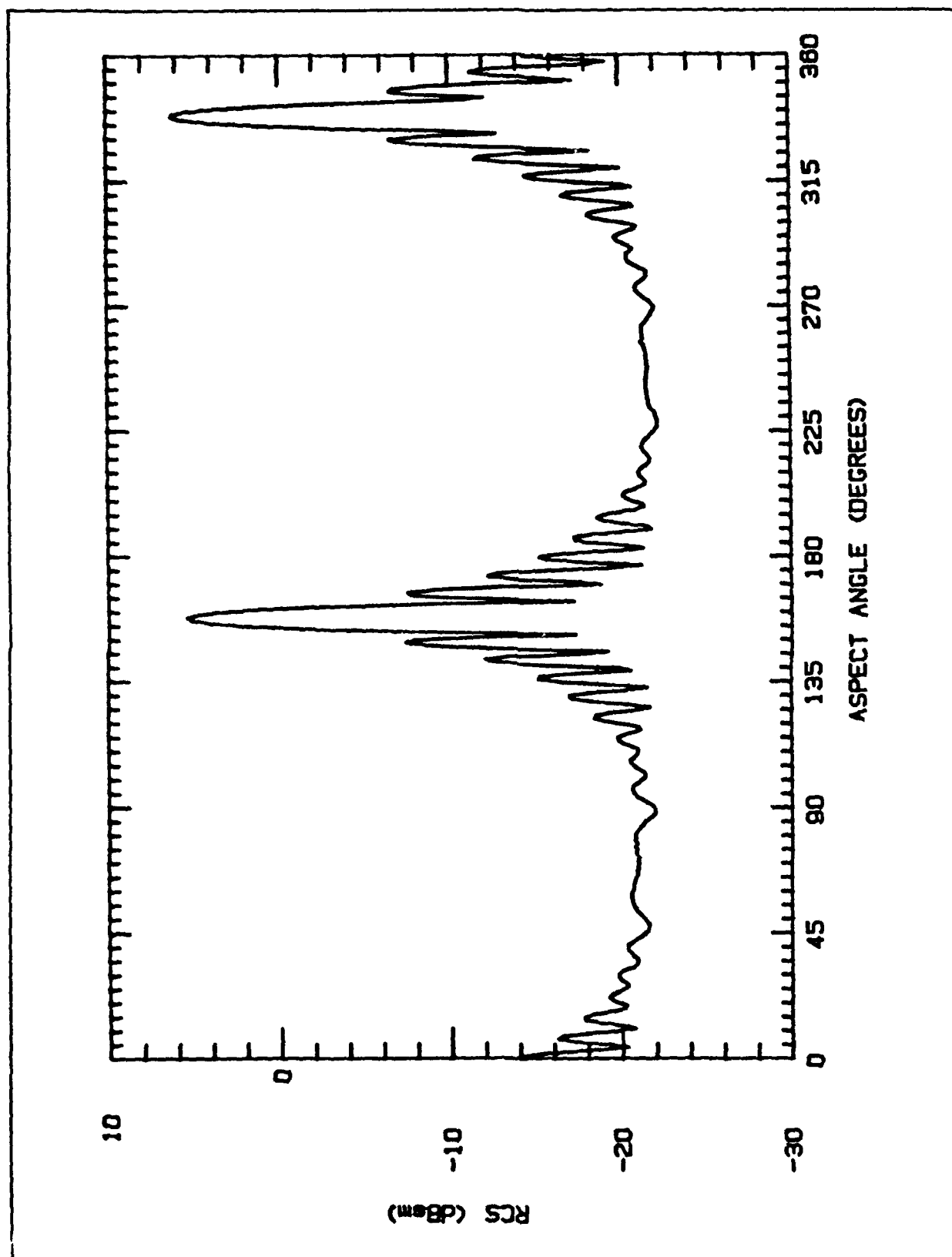


Figure 45. Measured RCS: 6 inch square flat plate,  $\beta = 45^\circ$ , 10 GHz, Vertical Polarization, AEL antenna transmitting

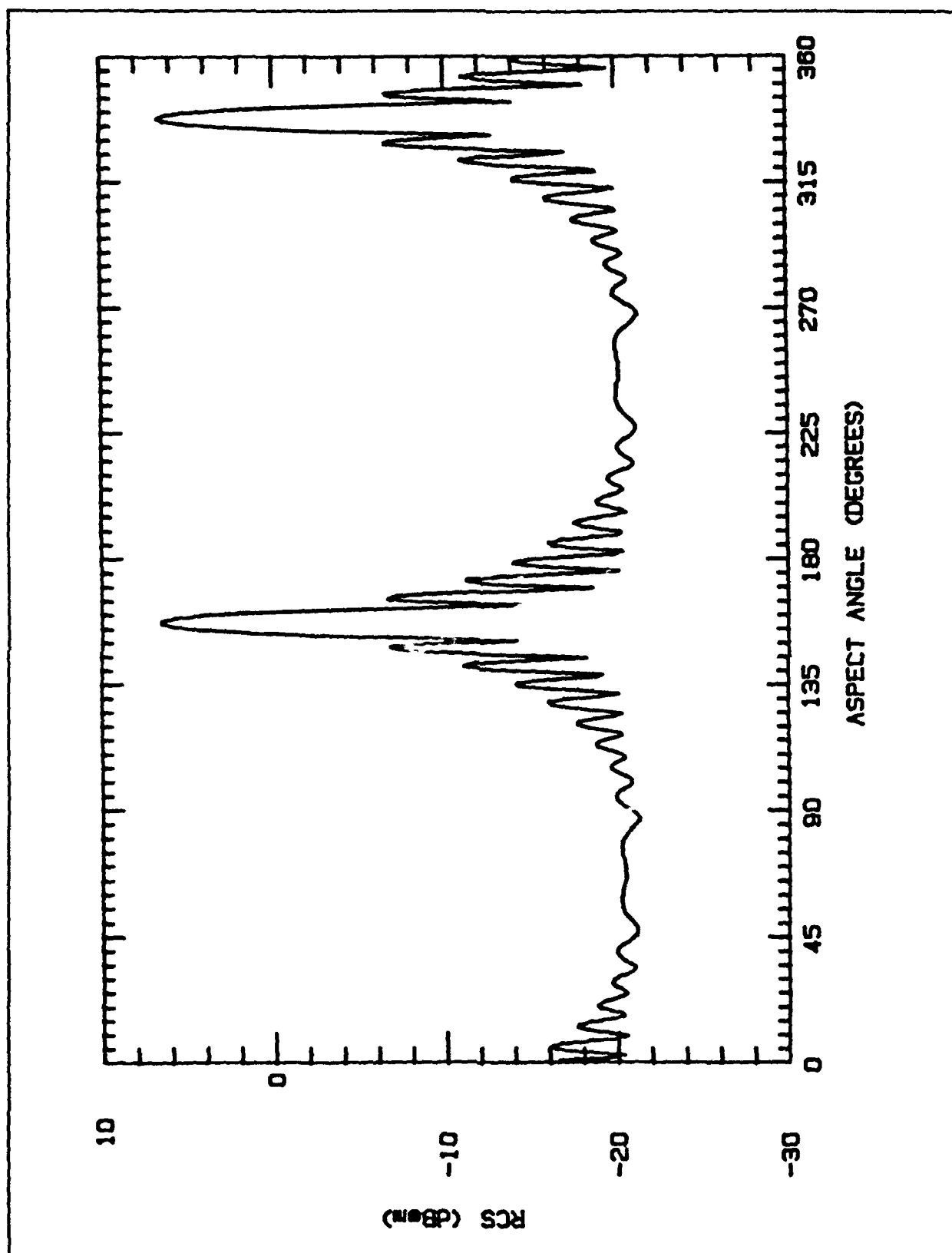


Figure 46. Measured RCS: 6 inch square flat plate,  $\beta = 45^\circ$ , 10 GHz, Vertical Polarization, X-band antenna transmitting

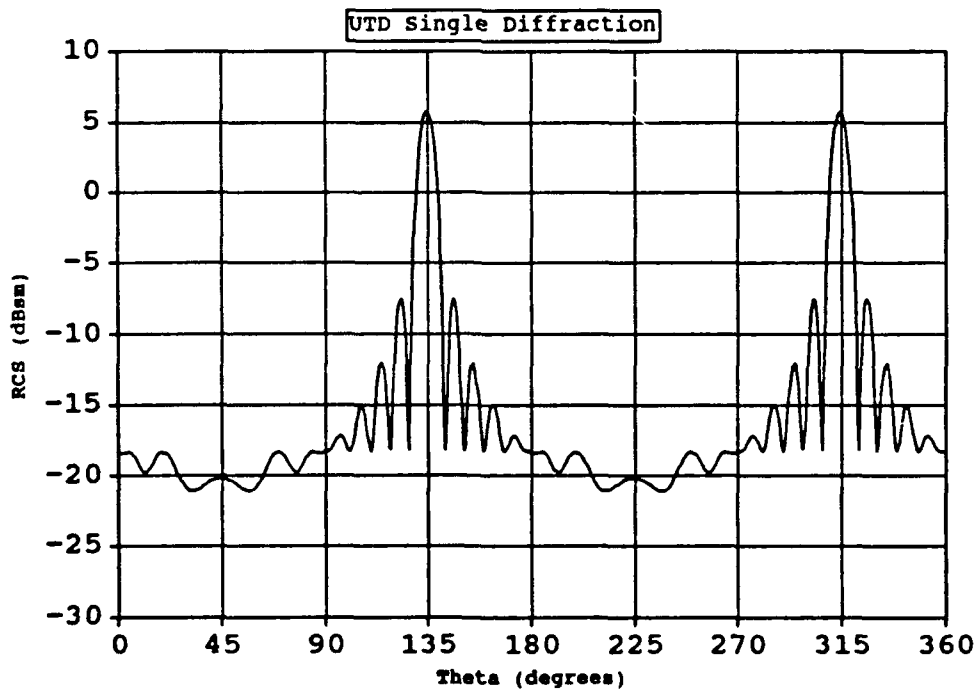
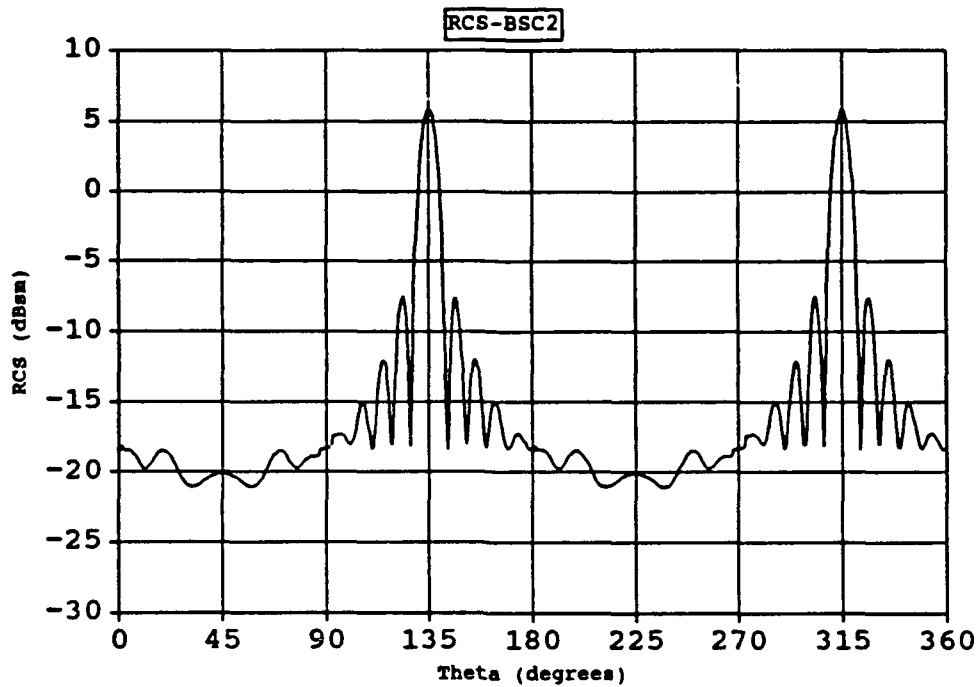


Figure 47. Comparison of bistatic RCS predictions: 6 inch square flat plate,  $\beta = 90^\circ$ , 10 GHz, Vertical Polarization

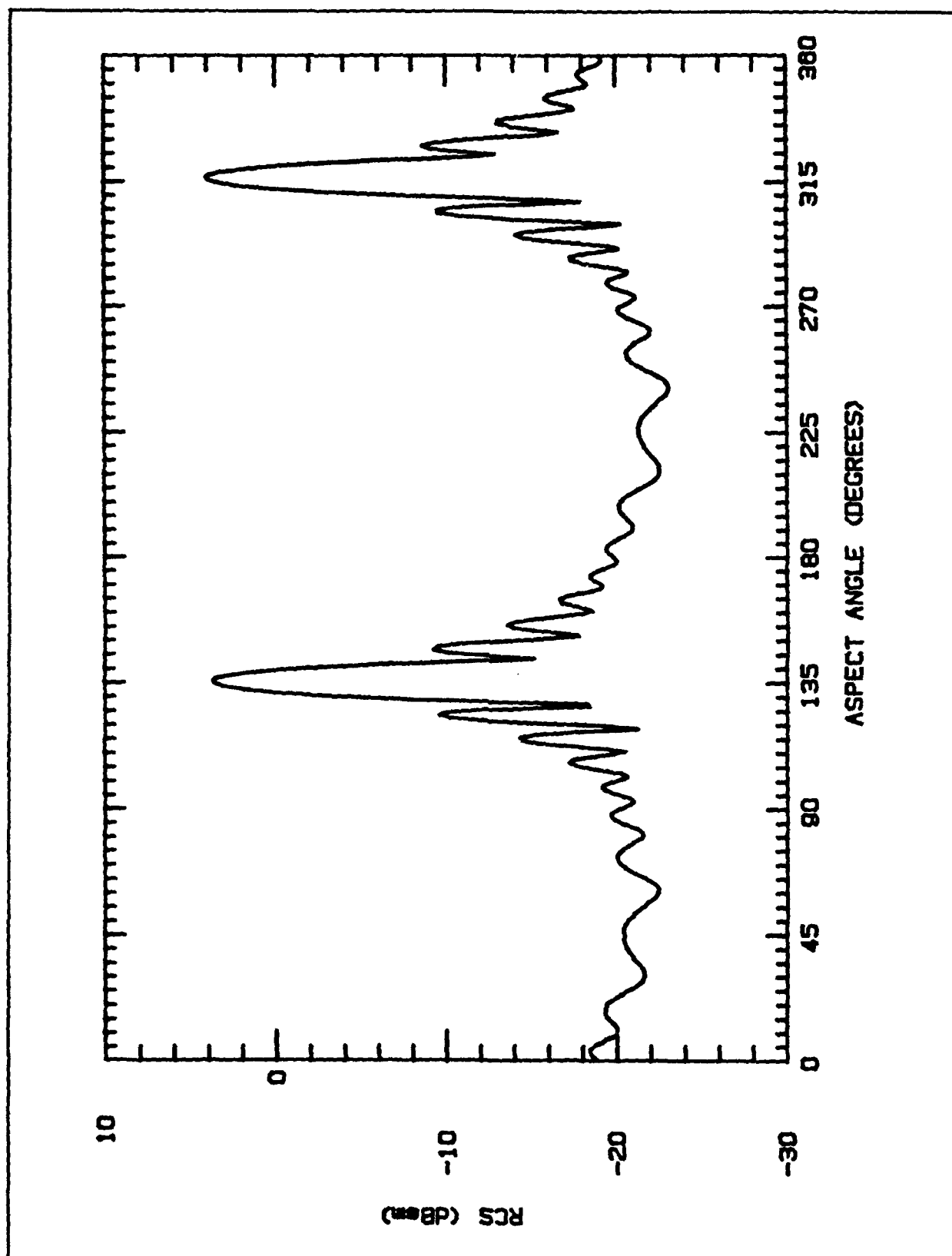


Figure 48. Measured RCS: 6 inch square flat plate,  $\beta = 90^\circ$ , 10 GHz, Vertical Polarization

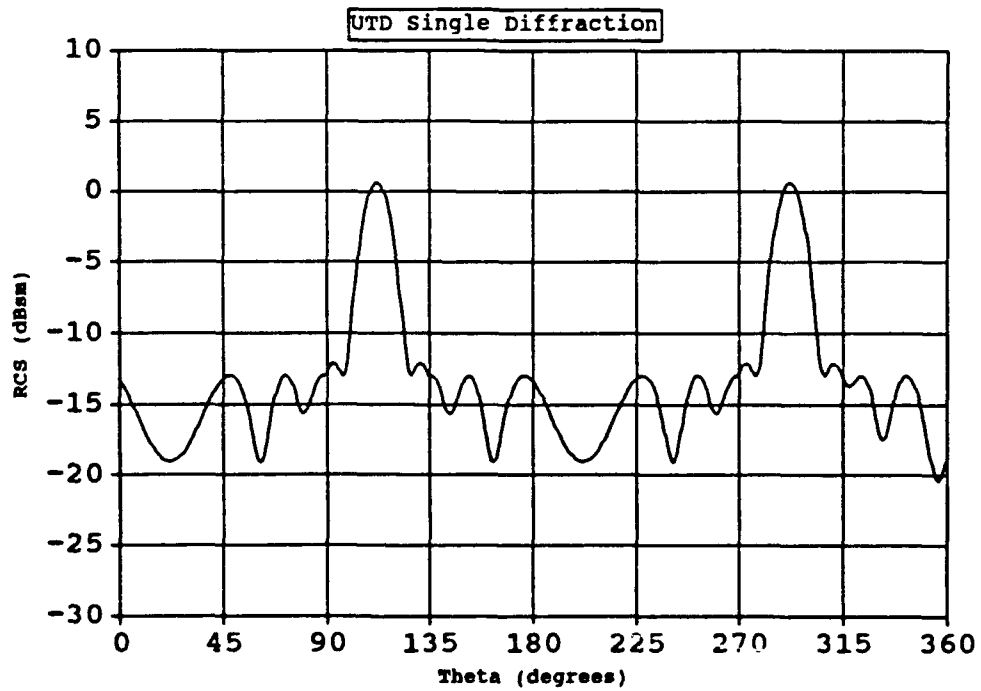
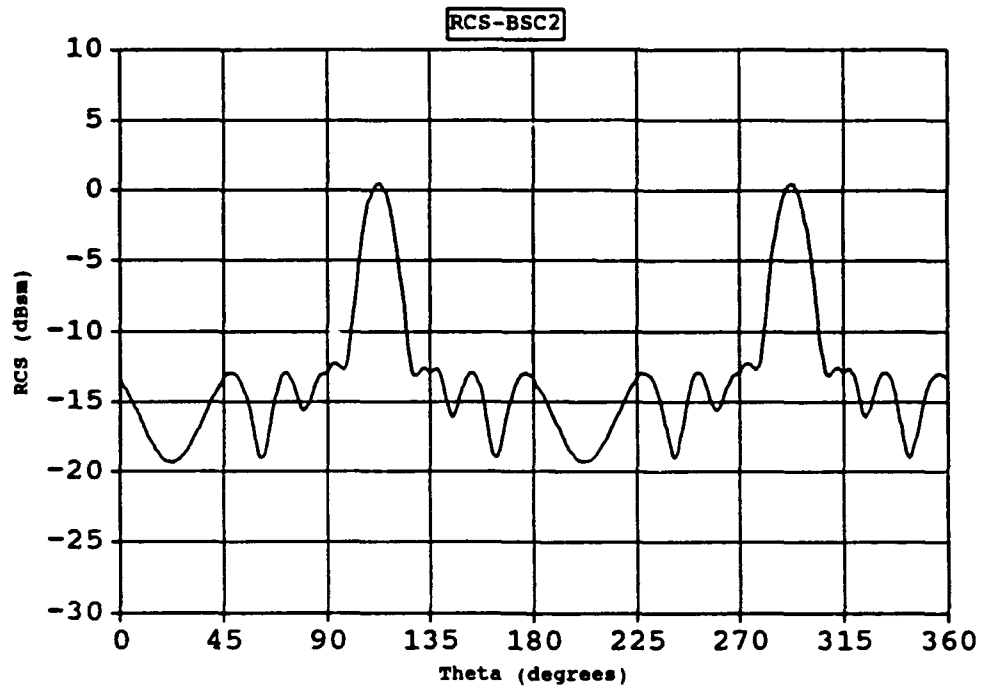


Figure 49. Comparison of bistatic RCS predictions: 6 inch square flat plate,  $\beta = 135^\circ$ , 10 GHz, Vertical Polarization

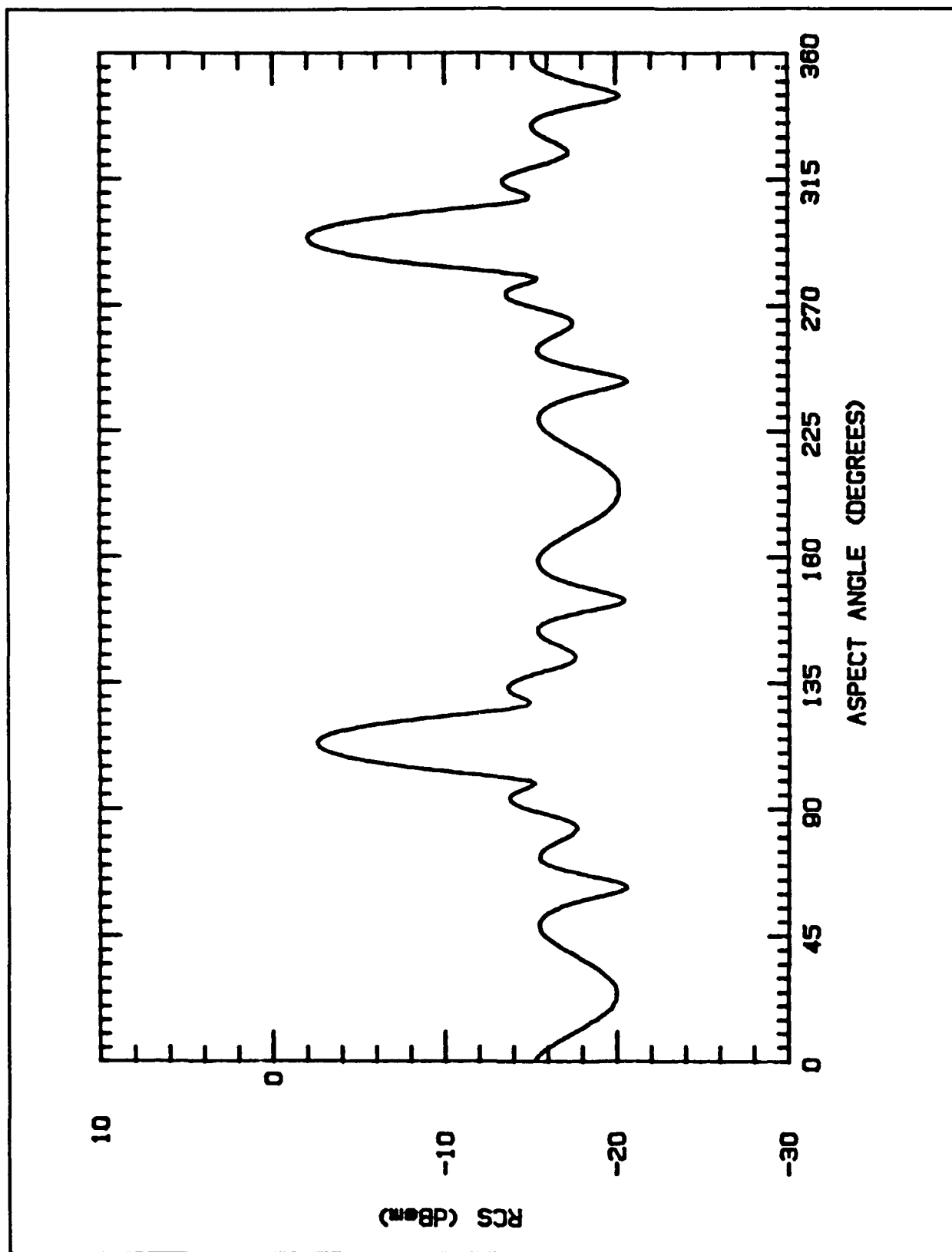


Figure 50. Measured RCS: 6 inch square flat plate,  $\beta = 135^\circ$ , 10 GHz, Vertical Polarization

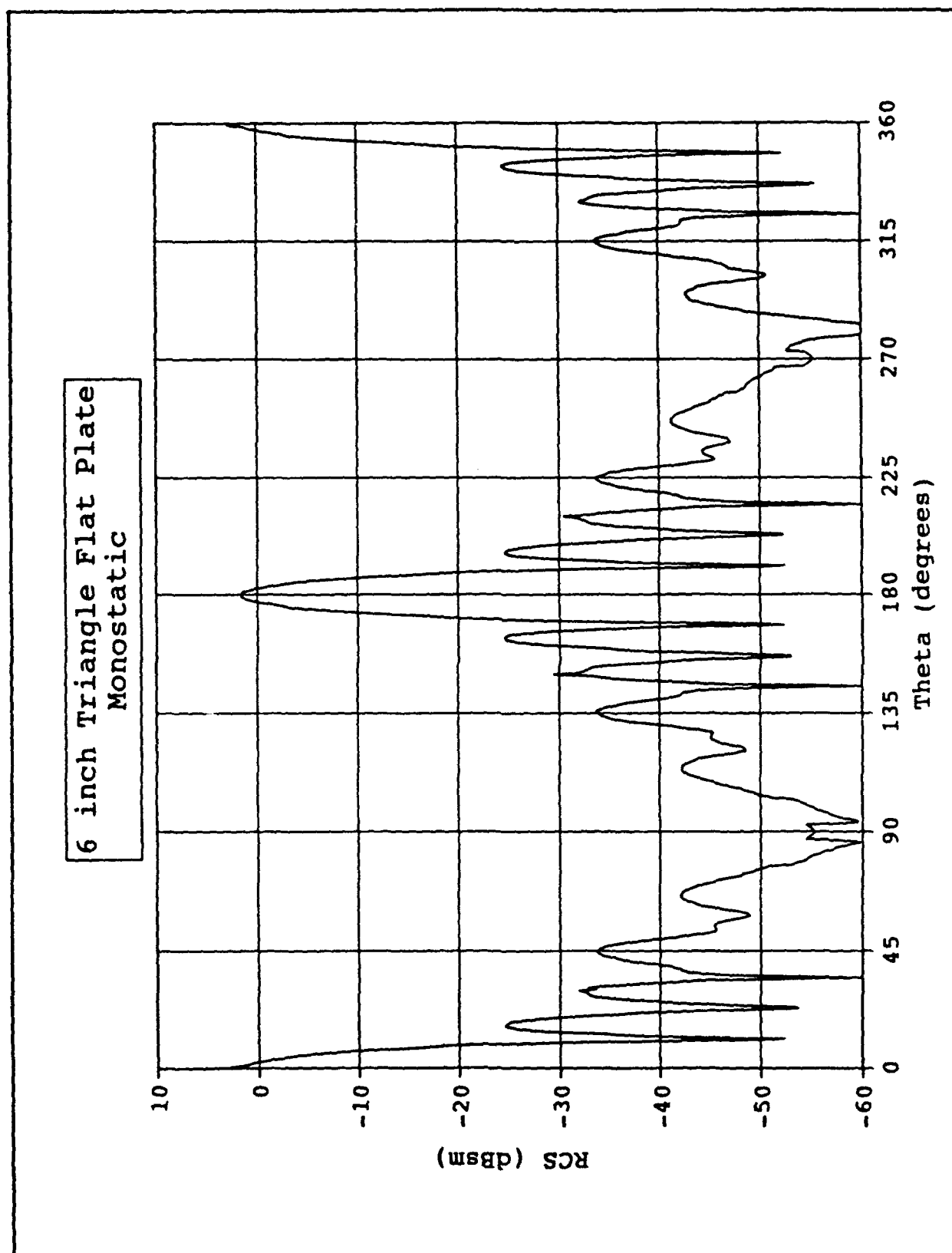


Figure 51. Predicted RCS: 6 inch triangle flat plate, monostatic, 10 GHz, Vertical Polarization



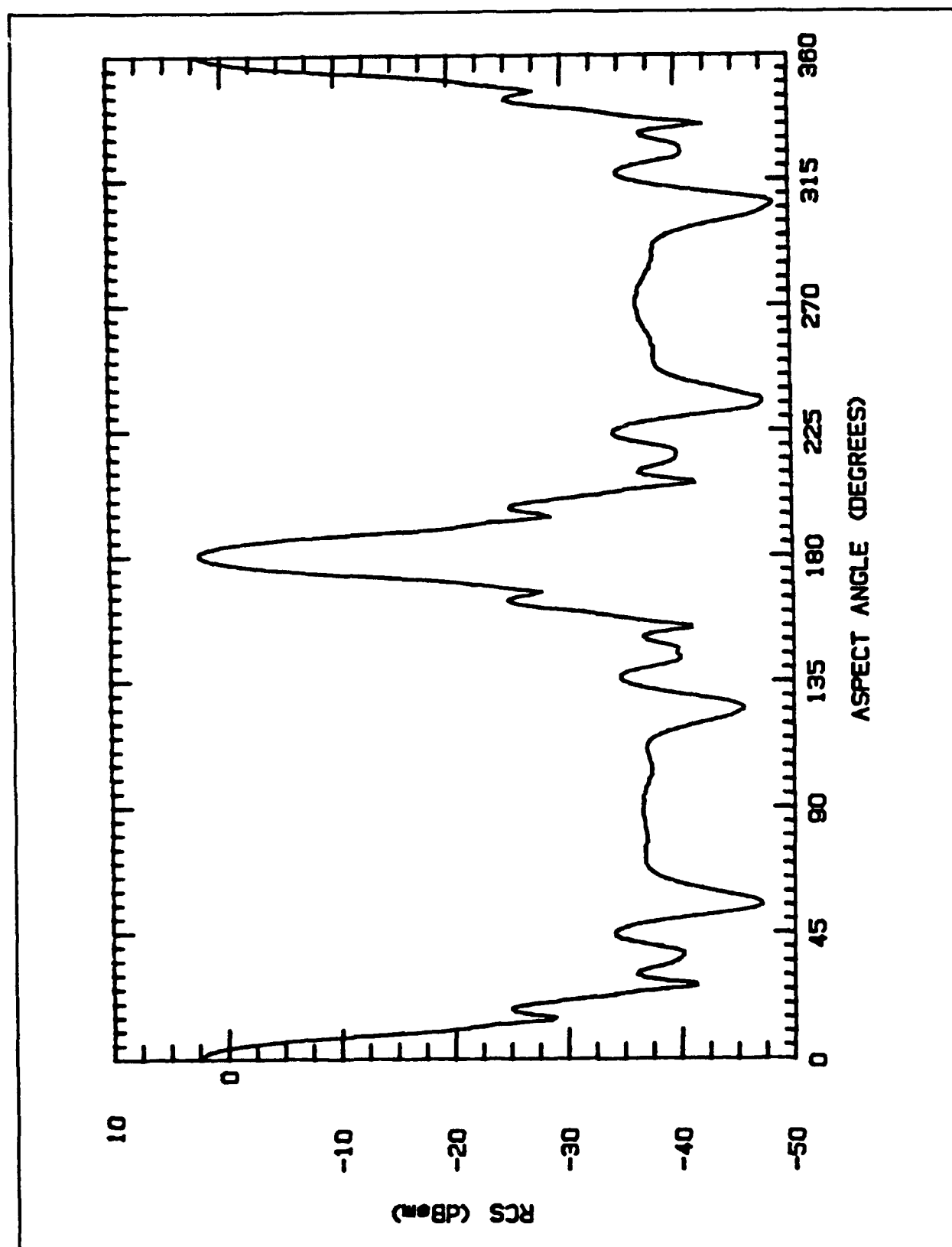


Figure 52. Measured RCS: 6 inch triangle flat plate, monostatic, 10 GHz, Vertical Polarization

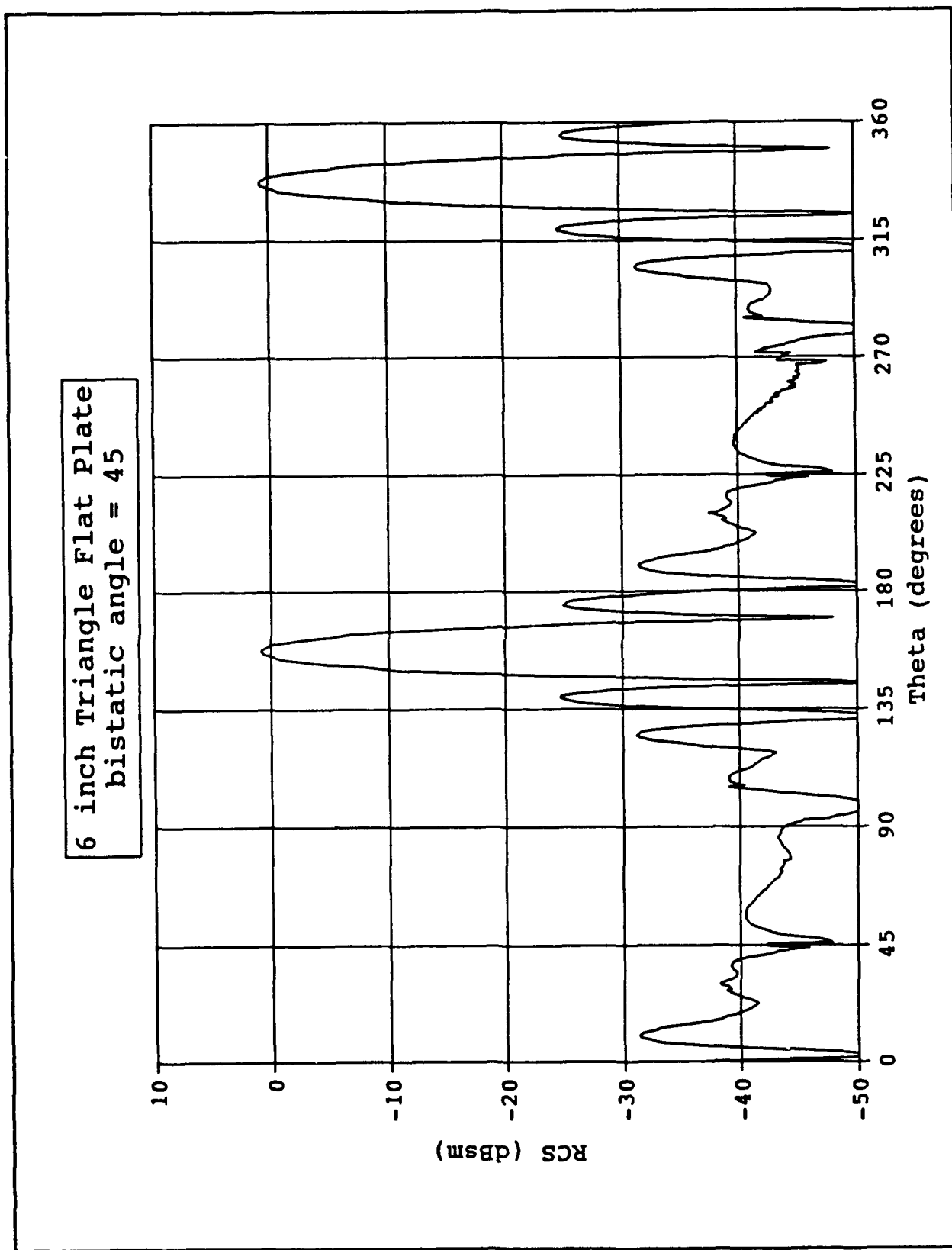


Figure 53. Predicted RCS: 6 inch triangle flat plate,  $\beta = 45^\circ$ , 10 GHz, Vertical Polarization

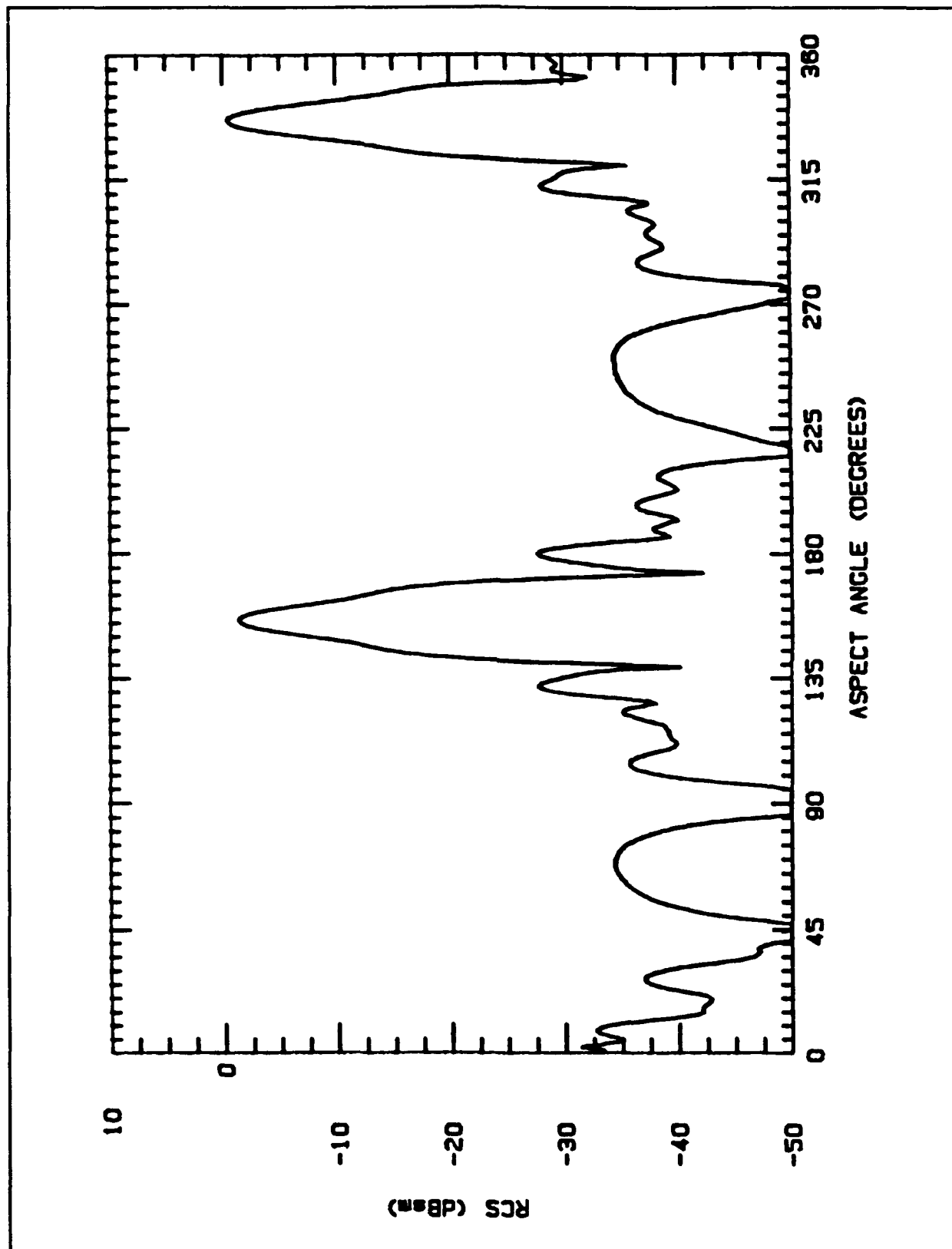


Figure 54. Measured RCS: 6 inch triangle flat plate,  $\beta = 45^\circ$ , 10 GHz, Vertical Polarization

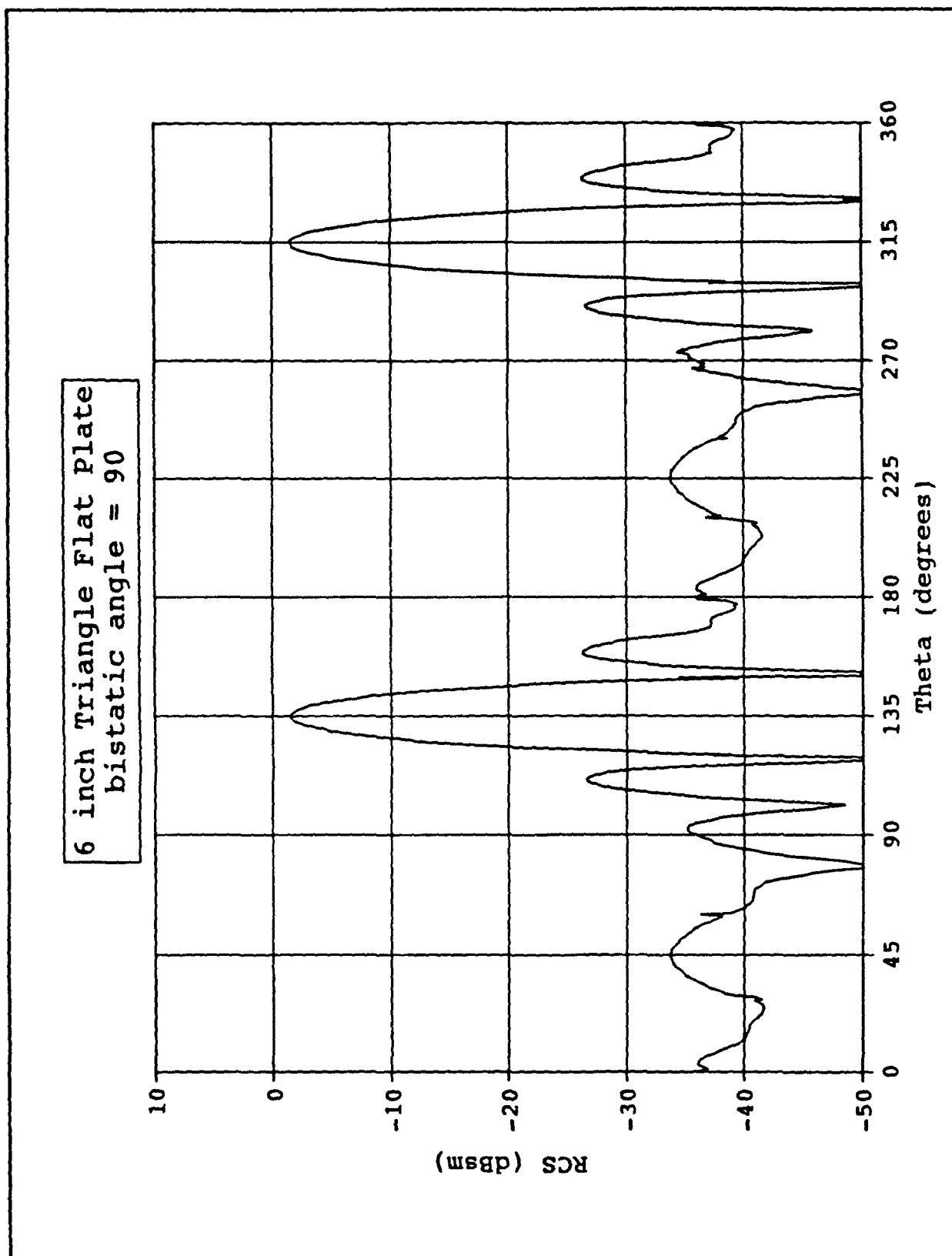


Figure 55. Predicted RCS: 6 inch triangle flat plate,  $\beta = 90^\circ$ , 10 GHz, Vertical Polarization

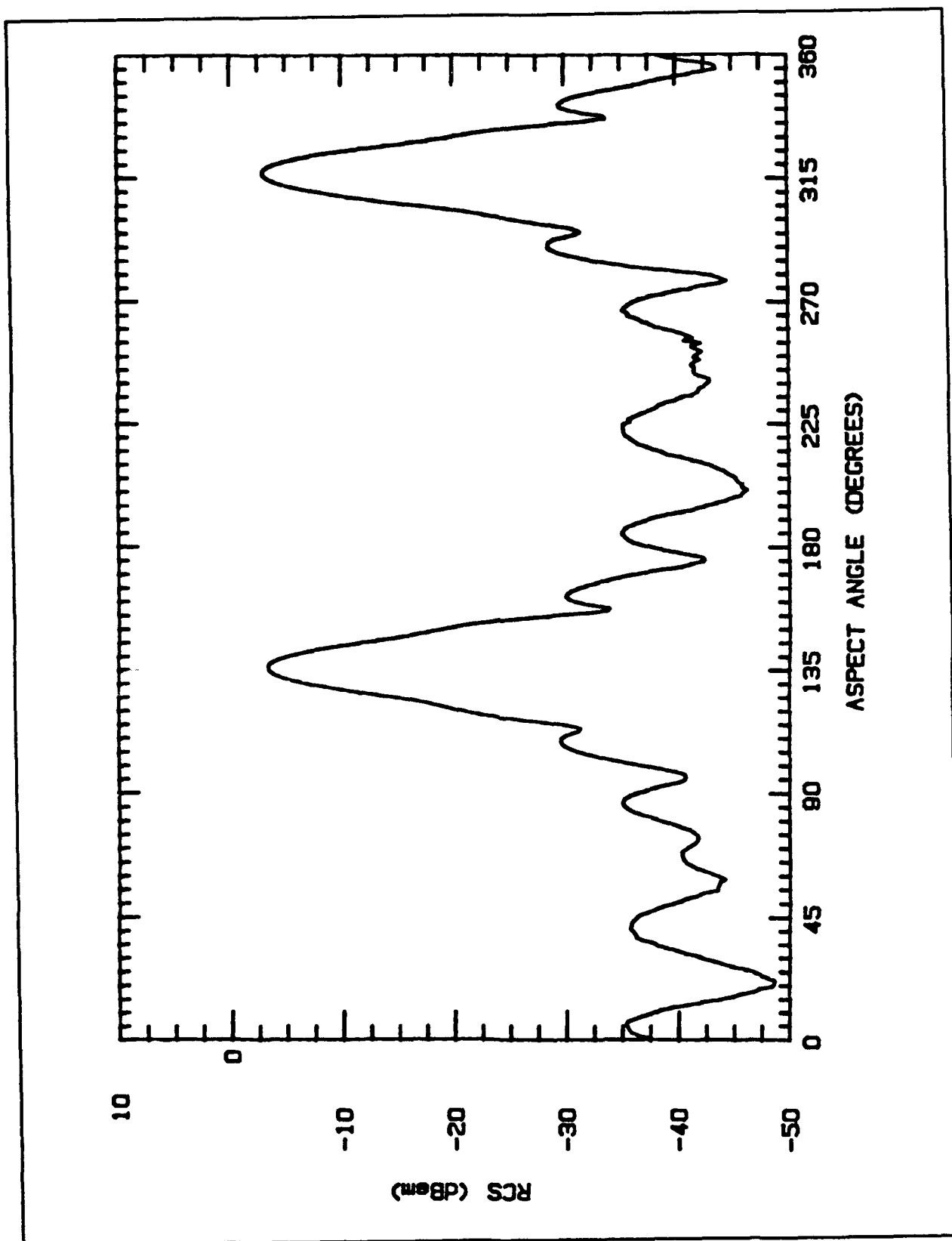


Figure 56. Measured RCS: 6 inch triangle flat plate,  $\beta = 90^\circ$ , 10 GHz, Vertical Polarization

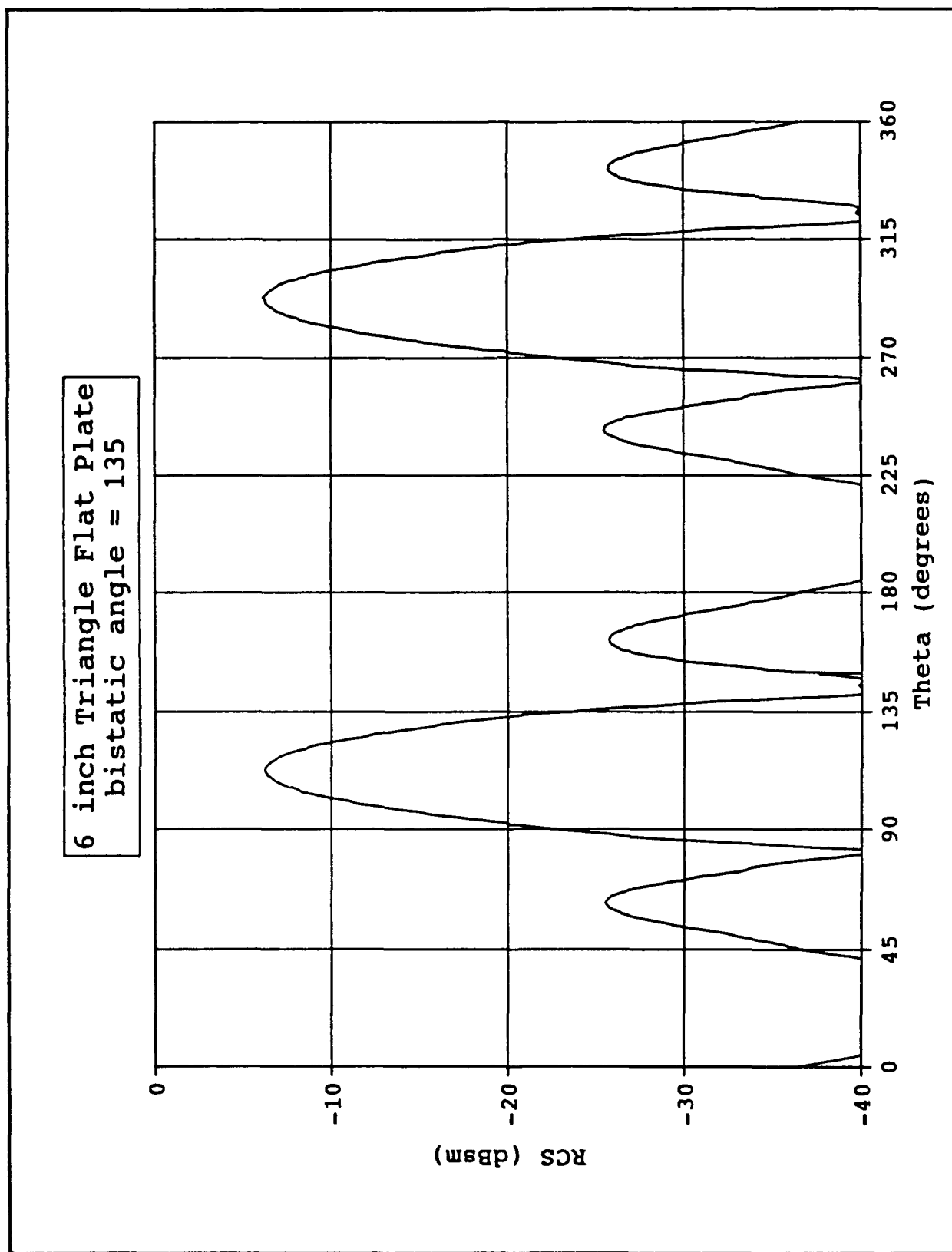


Figure 57. Predicted RCS: 6 inch triangle flat plate,  $\beta = 135^\circ$ , 10 GHz, Vertical Polarization

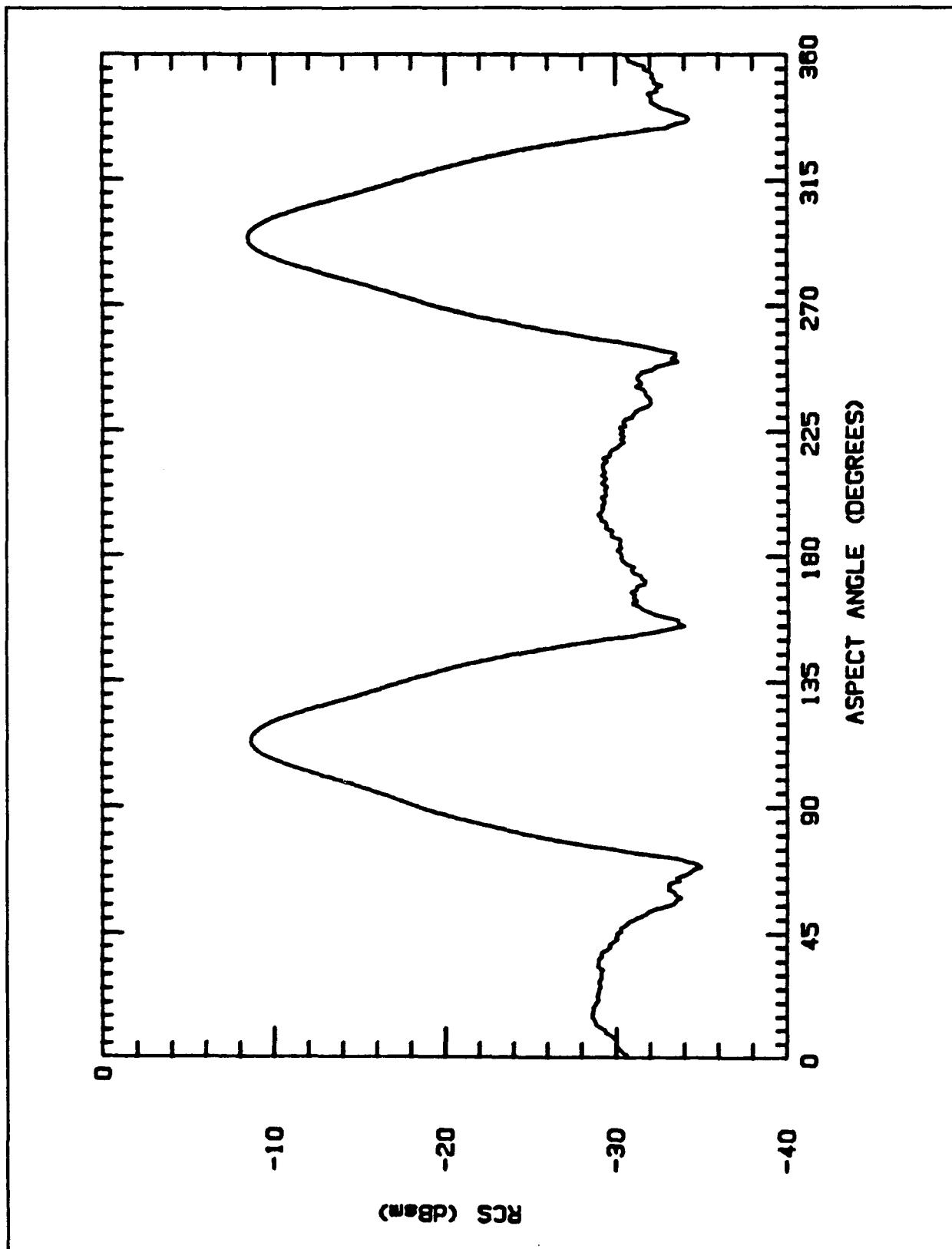


Figure 58. Measured RCS: 6 inch triangle flat plate,  $\beta = 135^\circ$ , 10 GHz, Vertical Polarization

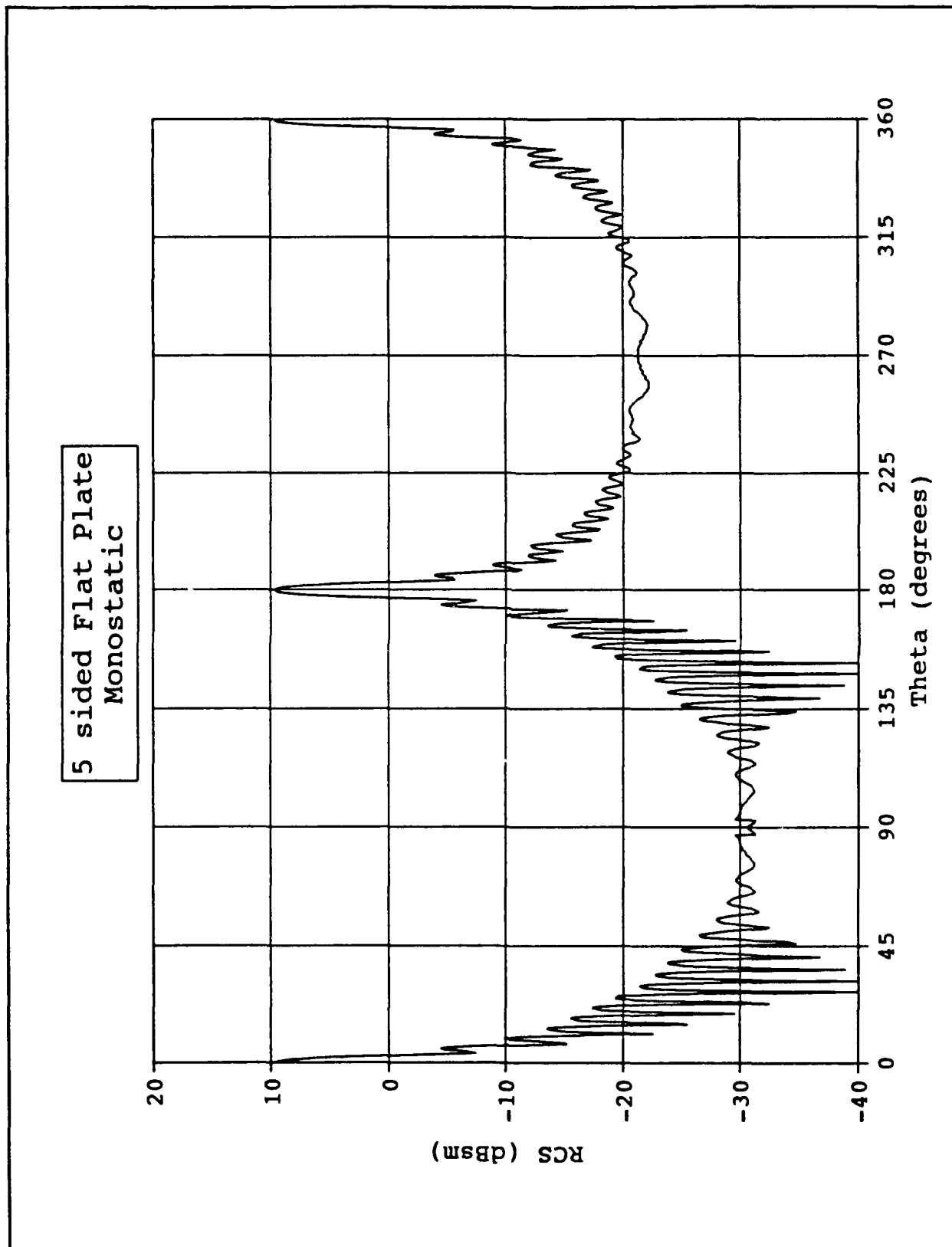


Figure 59. Predicted RCS: Five sided flat plate, monostatic, 10 GHz, Vertical Polarization



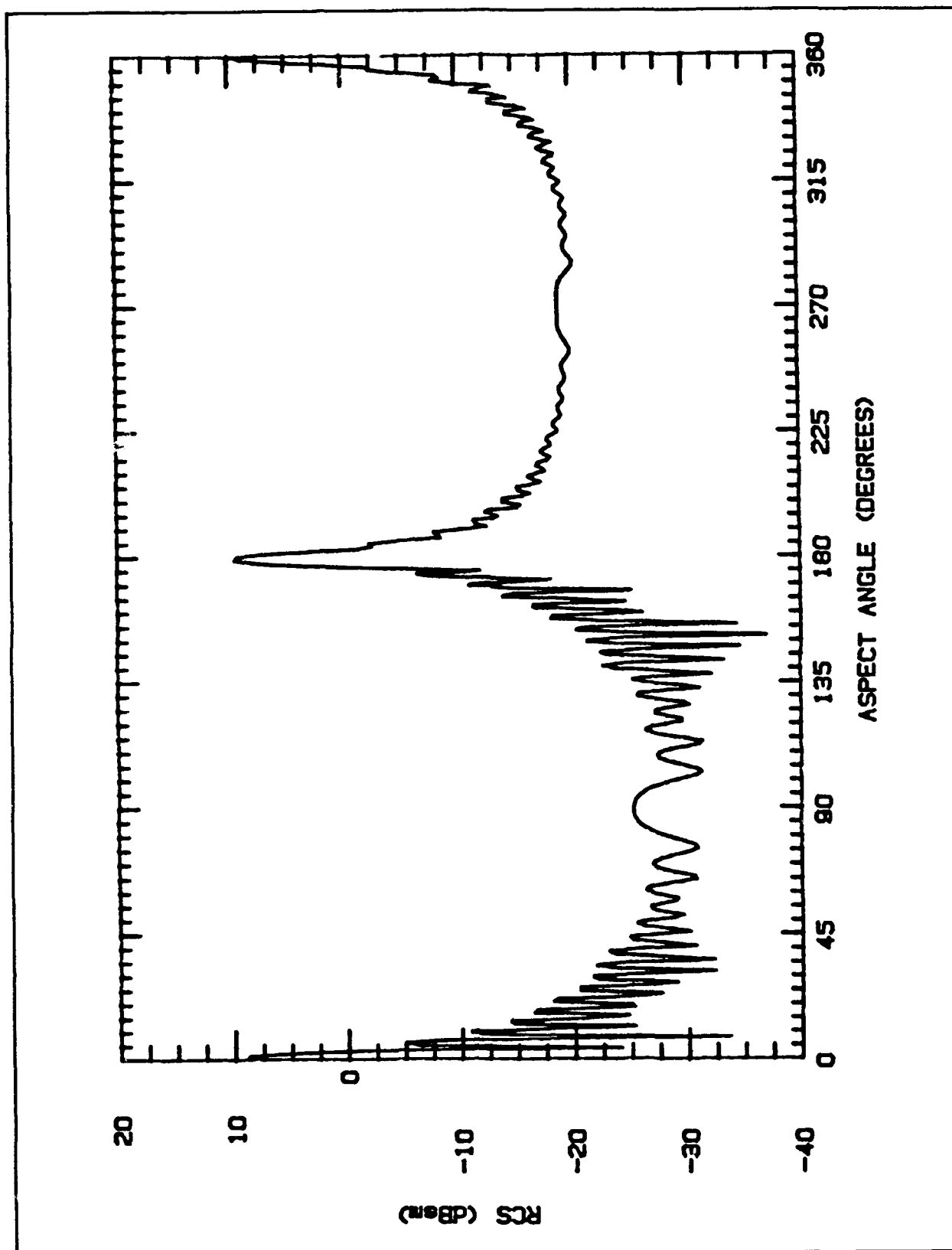


Figure 60. Measured RCS: Five sided flat plate, monostatic, 10 GHz, Vertical Polarization

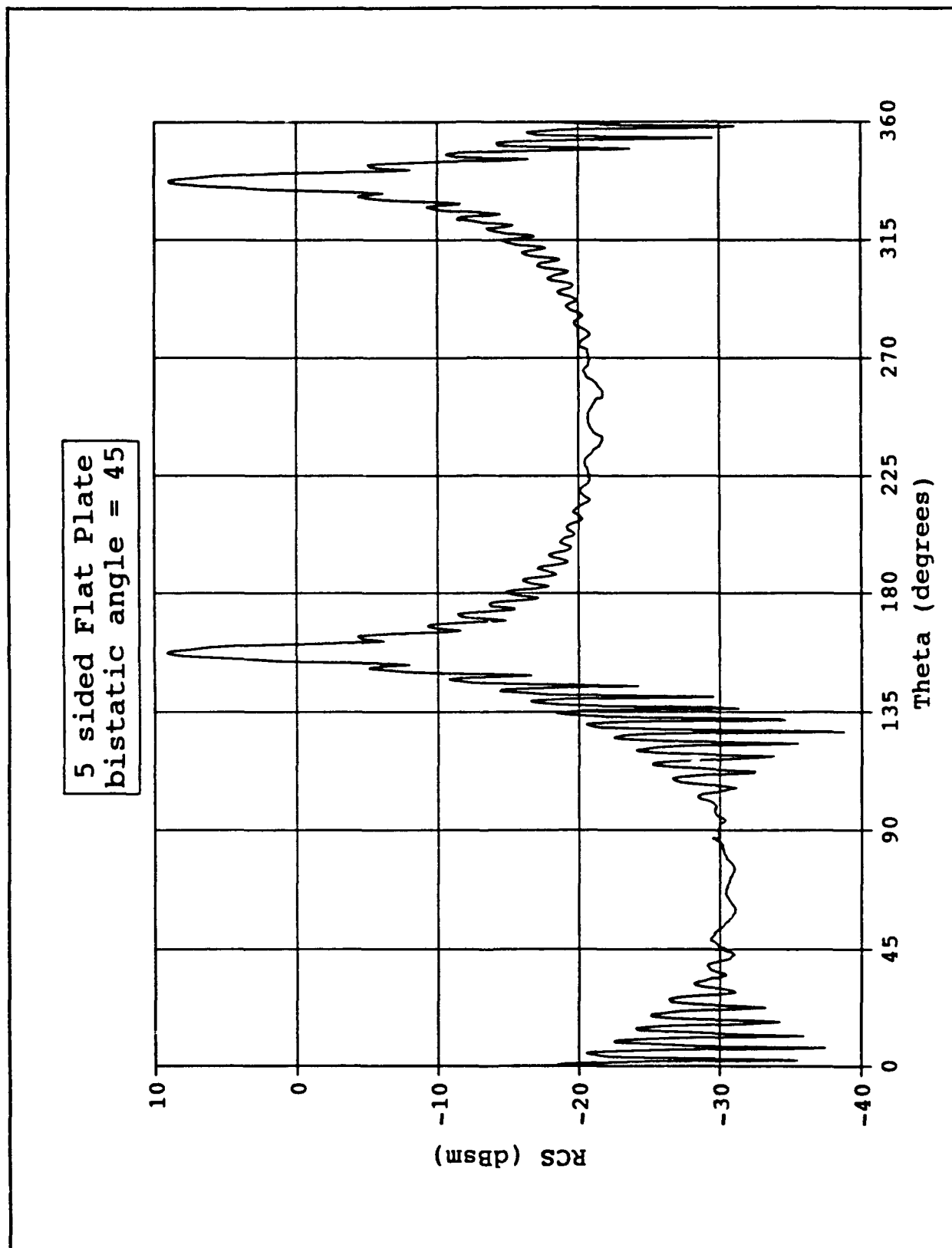


Figure 61. Predicted RCS: Five sided flat plate,  $\beta = 45^\circ$ , 10 GHz, Vertical Polarization

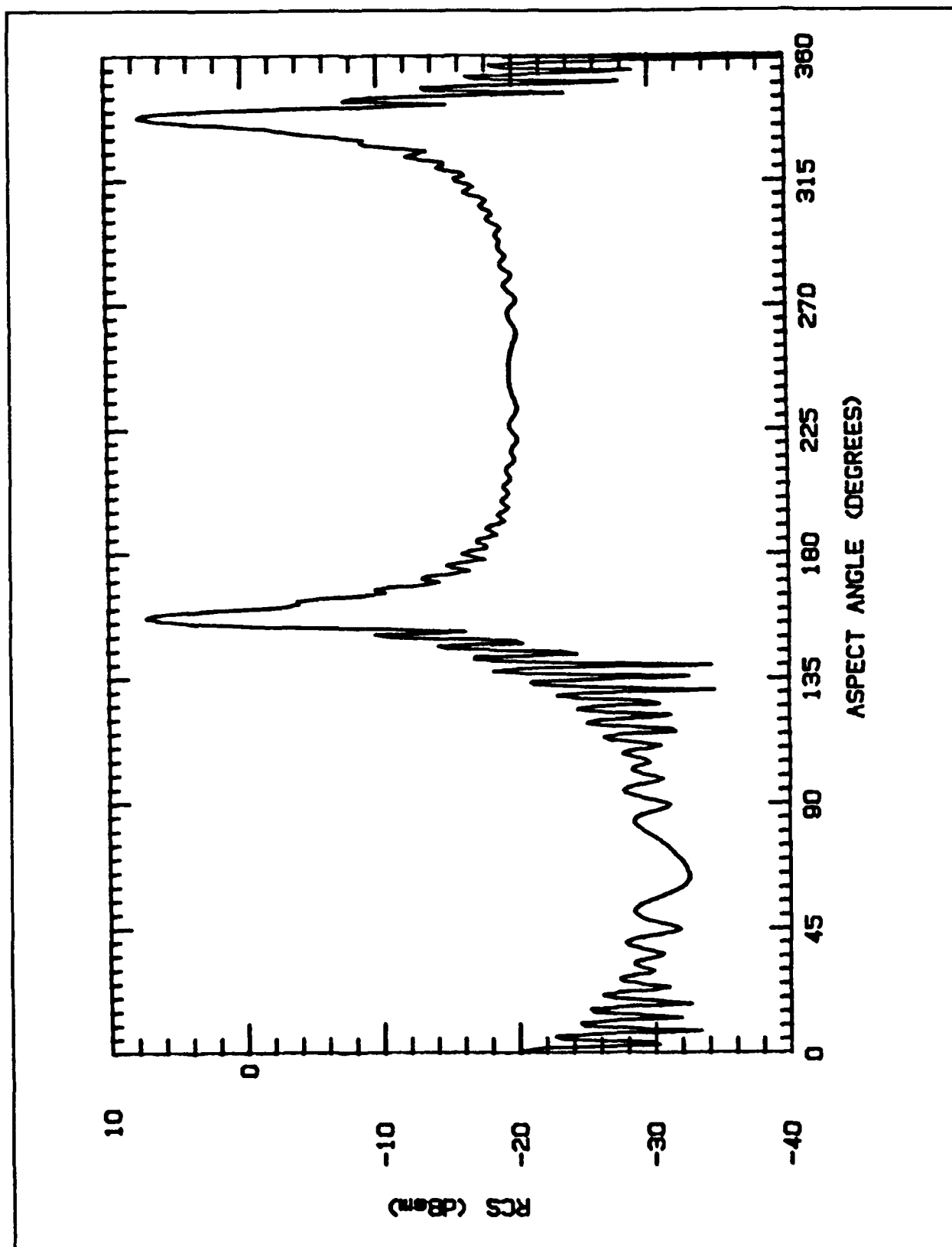


Figure 62. Measured RCS: Five sided flat plate,  $\beta = 45^\circ$ , 10 GHz, Vertical Polarization, X-band antenna transmitting

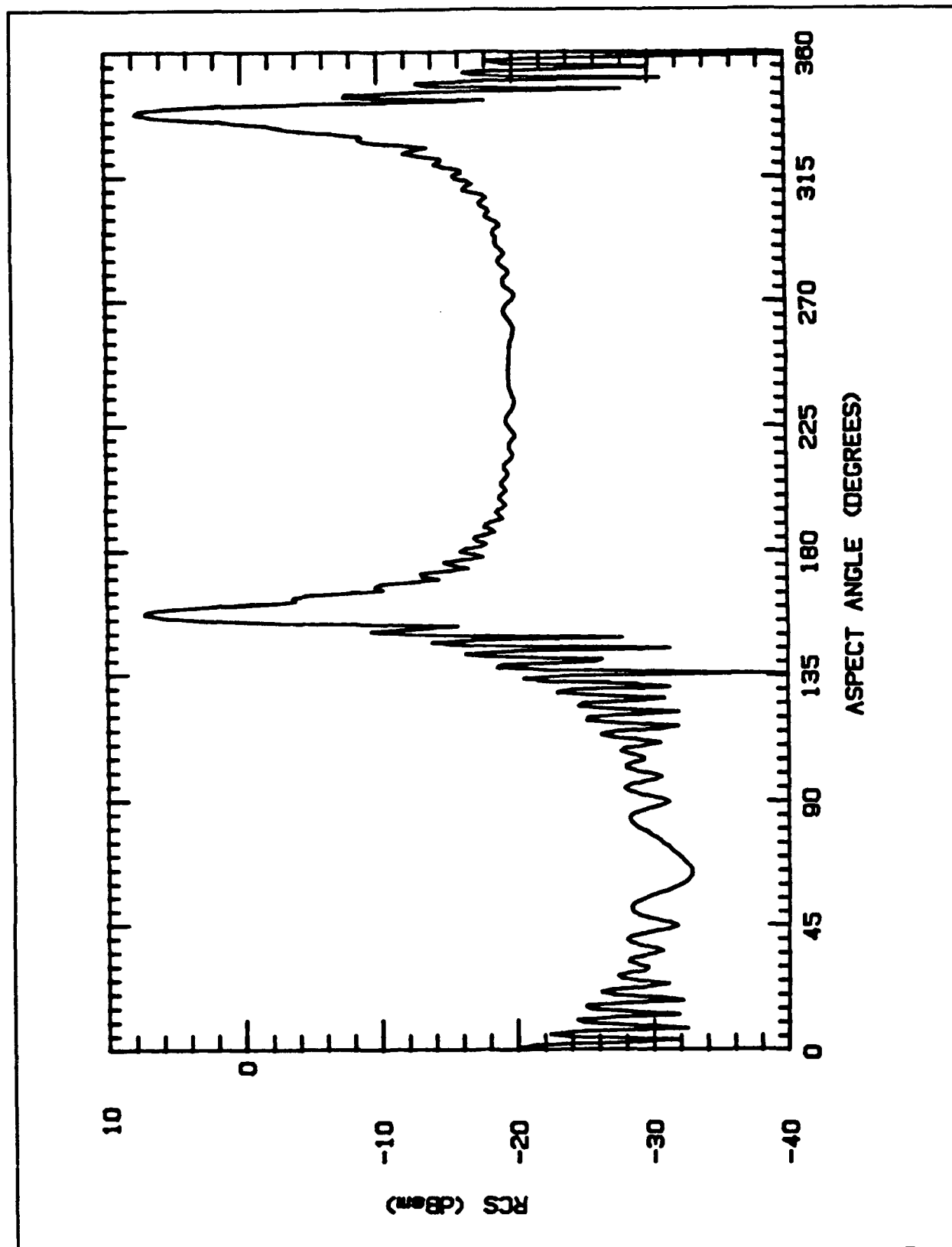


Figure 63. Measured RCS: Five sided flat plate,  $\beta = 45^\circ$ , 10 GHz, Vertical Polarization, Flam and Russell antenna transmitting

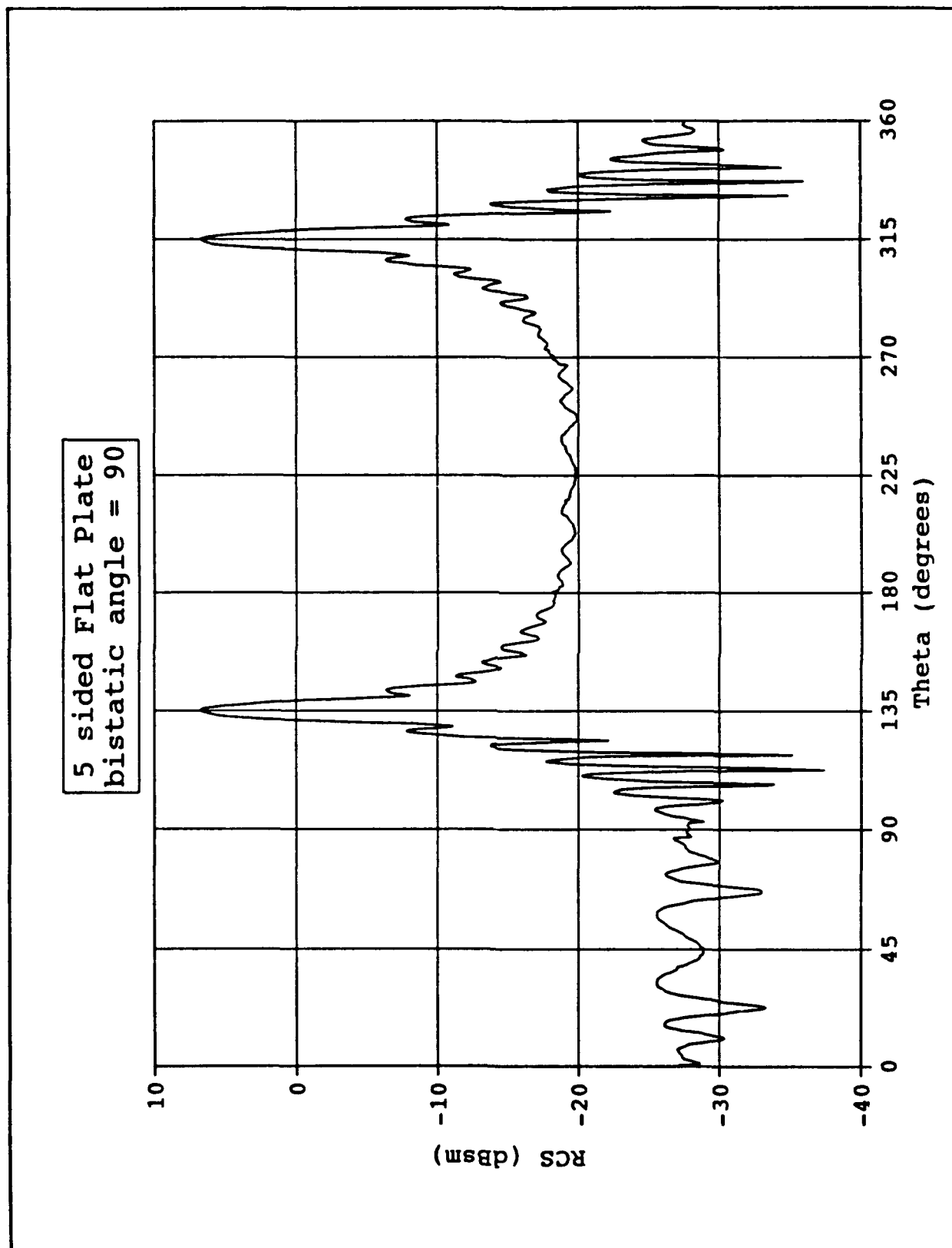


Figure 64. Predicted RCS: Five sided flat plate,  $\beta = 90^\circ$ , 10 GHz, Vertical Polarization

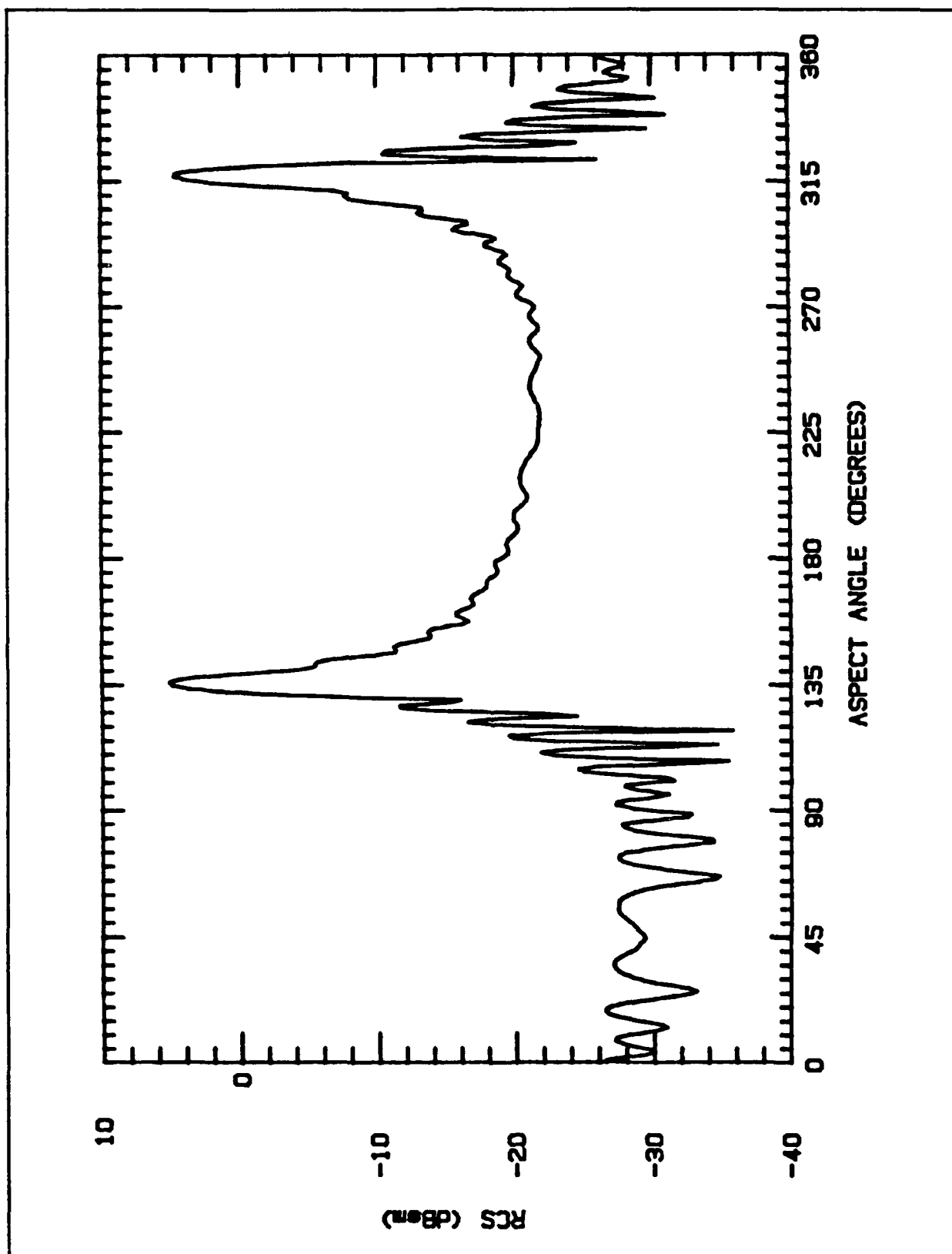


Figure 65. Measured RCS: Five sided flat plate,  $\beta = 90^\circ$ , 10 GHz, Vertical Polarization

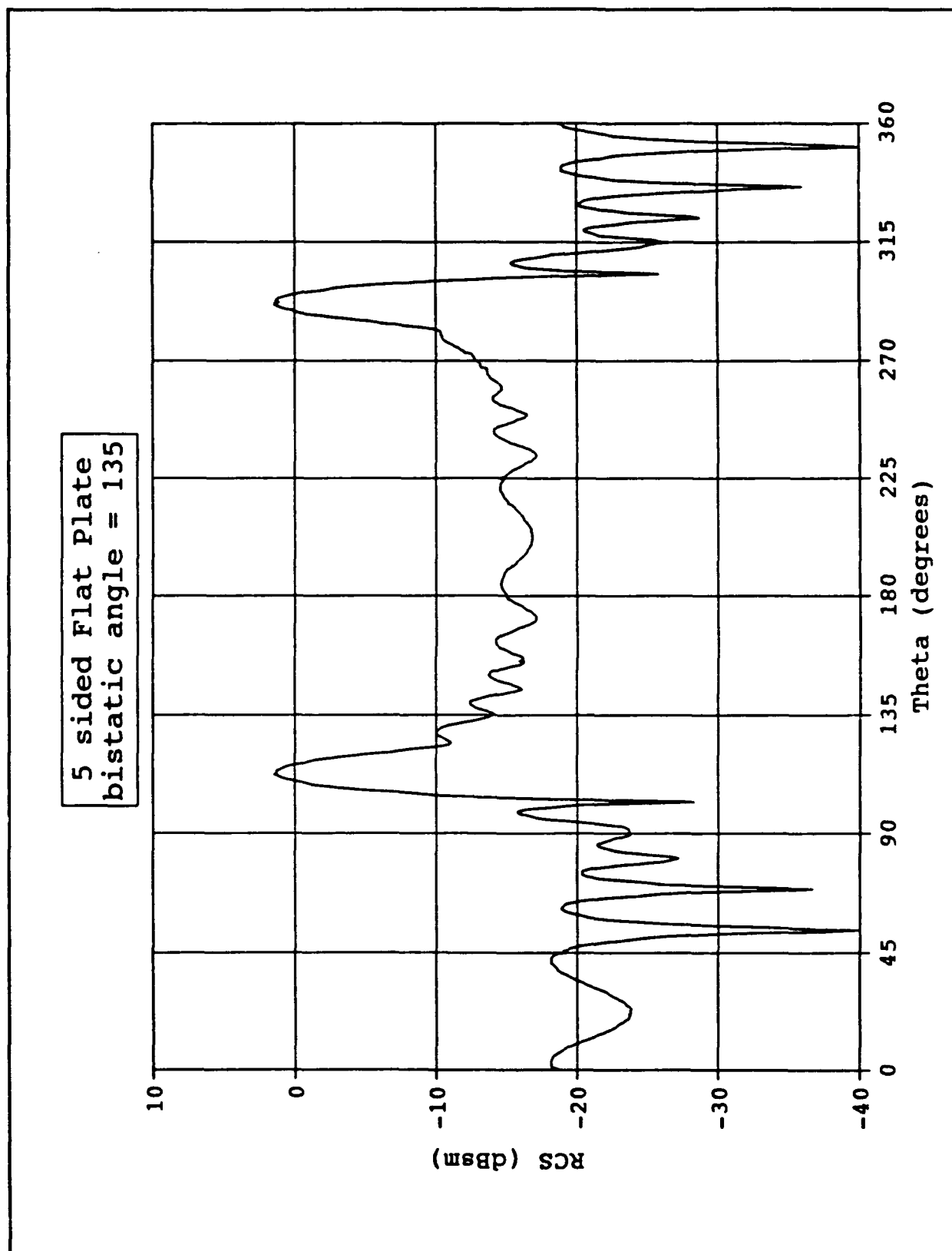


Figure 66. Predicted RCS: Five sided flat plate,  $\beta = 135^\circ$ , 10 GHz, Vertical Polarization

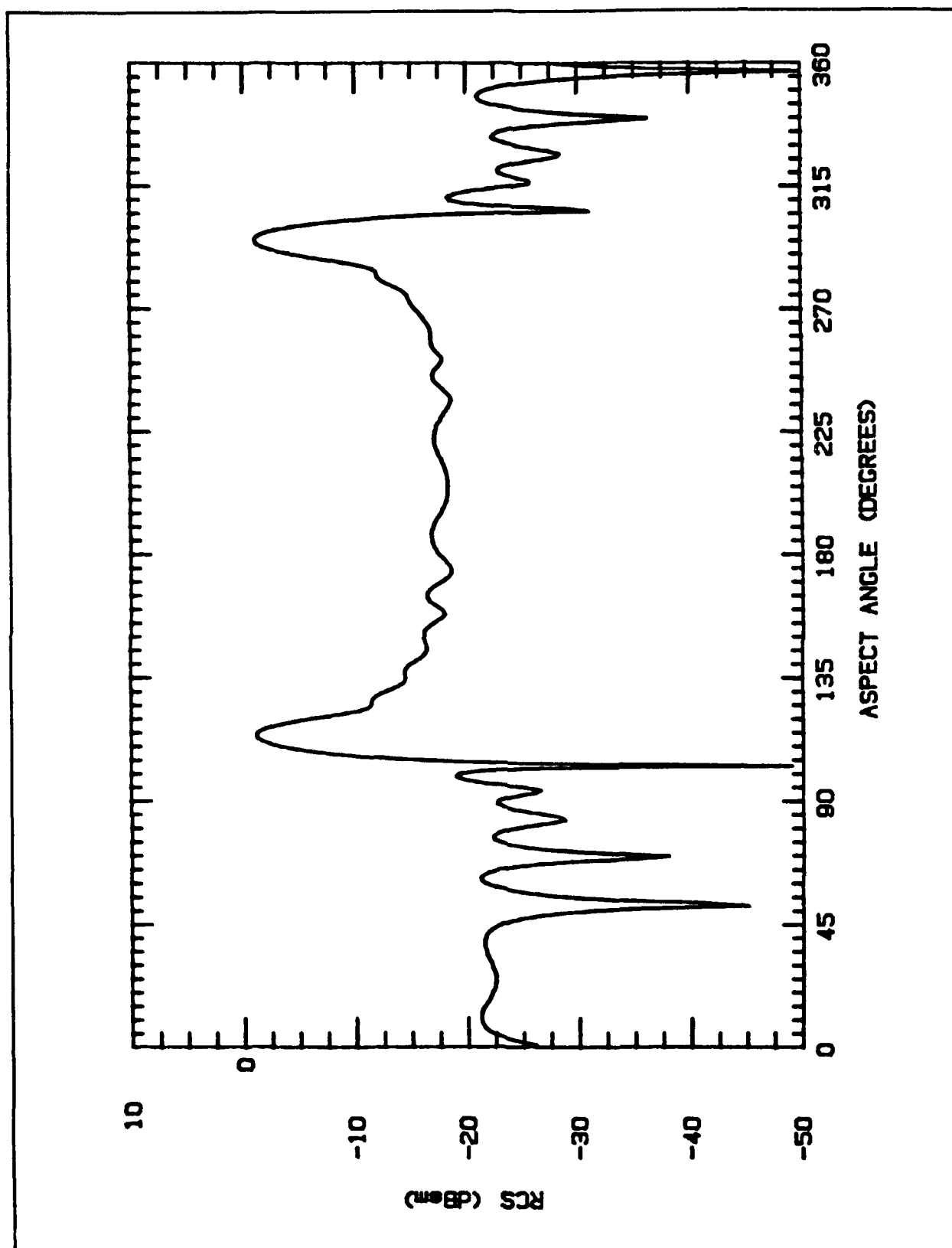


Figure 67. Measured RCS: Five sided flat plate,  $\beta = 135^\circ$ , 10 GHz, Vertical Polarization



## *Appendix B. Procedure for Performing Bistatic Measurements in AFIT's Far-field RCS Chamber*

This appendix contains the general procedure used for the bistatic RCS measurements obtained in this research. First, a "set of instructions" will provide a quick overview of the steps necessary to perform bistatic RCS measurements in the AFIT anechoic chamber. In addition, a precautionary safety procedure used when taking the RCS measurements will be provided. Finally, a list of additional items (hardware, software, etc.) required for bistatic measurements will be given.

### *Set of Instructions - Overview*

This overview assumes that the antennas, antenna mount, cabling, etc are as required for the desired measurements. It provides the basics required for the measurements. For more detail on any of the steps, refer to the main body of this document.

1) The signals in the chamber must be characterized for the desired bandwidth to determine the target signal. This will be used to set the initial instrument settings of the network analyzer (state 8 for monostatic measurements, state 2 for bistatic measurements) for the measurement configuration desired.

2) Load the bistatic ARMS software onto the HP computer. Simply type - LOAD "AUTOPROG" and strike RUN on control pad. The bistatic measurement software will provide the capability to perform either monostatic or bistatic measurements. When the bistatic software is running, the screen will provide a certain amount of detail to help make the measurement easier and ensure that the proper steps are followed. To obtain more accurate results for the monostatic pattern cut RCS measurements, a bistatic pattern cut measurement at  $0^\circ$  (really monostatic) can be performed by using the exact calibration RCS of 5 inch sphere at the desired frequency (for  $\beta = 0^\circ$ ) to obtain better monostatic

results. The current monostatic exact solution is simply  $\pi a^2$ , which is independent of frequency.

3) If frequency response RCS measurements are desired using horizontal polarization, at bistatic angles different than 45, 90, or 135 degrees, or for a frequency range different than 8 to 12.4 GHz, a new exact sphere calibration data file is needed for the measurement configuration that is in HP binary data format. The data file breaks the desired bandwidth into 801 points. The data file must have the 801 real solutions followed by the corresponding 801 imaginary solutions in a single column. The BISPH program provided in Appendix C was used for the exact sphere calibration files generated for this research.

4) Precautionary Safety Procedure - When performing the bistatic measurements, target alignment was crucial. This meant that the amount of the time spent in the chamber was excessive. A precautionary step used was to power the amplifier down to -110 dB before entering the chamber. This is easy to do by going into Local control on the network analyzer and setting the power to the desired level. Beware, though, after exiting the chamber, the equipment must be powered up to 10 dB to obtain valid measurements. After powering back up, the automatic software controlling the measurement will take control as soon as CONTINUE is hit.

### *Additional Items Required*

- 1) Bistatic antenna and mounting structure to put antenna at the desired height
- 2) Long cable to run from bistatic antenna in chamber to measurement equipment
- 3) Bistatic ARMS software
- 4) Trans-232 software to transfer files between Zenith and HP computers if additional calibration data files are required beyond present capability of  $\beta = 45^\circ$ ,  $90^\circ$ , and  $135^\circ$
- 5) Exact sphere calibration data - Program BISPH at WRDC/SNA will work. A listing of the code is in Supplement 1
- 6) The chamber is presently marked for bistatic angles with the antennas in vertical polarization. The bistatic angles must be determined for horizontal polarization since the Flam and Russell antennas rotate  $90^\circ$  when antenna polarization is changed.

## Appendix C. Software Listing

This appendix contains a listing of the software programs used in this research. The appendix has 4 sections. The first section lists the Single Diffraction UTD code resulting from the theoretical development provided in Chapter IV. The second section lists the BISPH code used for the exact RCS for the spheres measured and used for calibration. Section III lists the pattern cut and frequency response RCS measurement software subroutines written for the ARMS software that controls the automatic measurements in the AFIT chamber. The last section provides the software used to transfer the data files between the Zenith computers and the HP computers in the AFIT chamber.

### *Appendix C, Section I. UTD Flat Plate Prediction Code*

This section contains the computer code to predict the bistatic RCS of a 2 dimensional strip geometry using UTD. The 3 dimensional RCS is obtained for either rectangle or square plate geometries by using a scaling factor. The theoretical development for the code is provided in Chapter 4 of the thesis. This code is based on single order diffractions only.

```

C*****C
C
C      BISTATIC SCATTERING FROM A STRIP GEOMETRY      C
C
C      The program will provide the bistatic RCS of a 2 C
C      dimensional strip geometry considering first order C
C      diffractions using UTD. The three dimensional RCS C
C      for flat plates is obtained by using a factor C
C      obtained from a text by Balanis titled Advanced C
C      Engineering Electromagnetics. The RCS is provided C
C      vs aspect angle via a Great Circle Pattern Cut. C
C      The RCS is provided in dBm for 2D and dBsm for 3D. C
C
C*****C
C*****C
C
C      REAL PI,c,FREQ,D,L,DEGINC,DEGSCA,WAVE,K,RADINC,RADSCA
C      REAL DEG,PHI1P,PHI1,PHI2PR,PHI2,PLUS1,MINUS1
C      REAL PLUS2,MINUS2,RCS2,RCS3,RCS3D
C      INTEGER DEGREE,POL,I
C      COMPLEX J,CONST,D1,D2,H1,H2,HTOT
C      CHARACTER*12 OUTPUT
C      PI = 3.14159265358979323846
C      J = CMPLX(0.,1.)
C c is the speed of light divided by 10**9!
C      c = .3
C
C      PROGRAM INPUTS VIA COMPUTER SCREEN
C
C      WRITE(*,*) 'NOTE - REMEMBER DECIMAL POINT!'
C      WRITE(*,*) 'Enter frequency in GHz!'
C      READ(*,10)FREQ
10  FORMAT(F4.1)
C      WRITE(*,20)
20  FORMAT(1X,'
      &
      &                                ')
C
C      WRITE(*,*) 'Enter plate width in meters!'
C      READ(*,30)D
C      WRITE(*,20)
30  FORMAT(F9.6)
C
C      WRITE(*,*) 'Enter plate length in meters!'
C      READ(*,30)L
C      WRITE(*,20)
C
C      WRITE(*,*) 'Enter incident angle in degrees!'
C      WRITE(*,*) 'Normal incidence to plate is 0 degrees!'

```

```

WRITE(*,*) 'NOTE - REMEMBER DECIMAL POINT!'
READ(*,10)DEGINC
WRITE(*,20)
C
WRITE(*,*) 'Enter scattered angle in degrees!'
WRITE(*,*) 'NOTE: SCAT - INC = desired BISTATIC
angle!'
WRITE(*,*) 'NOTE - REMEMBER DECIMAL POINT!'
READ(*,10)DEGSCA
WRITE(*,20)
C
WRITE(*,*) 'Enter degrees of rotation for pattern
cut!'
WRITE(*,*) 'Degrees can be entered from 0 to 360!'
READ(*,40)DEGREE
DEGREE = (2*DEGREE) + 1
WRITE(*,20)
40  FORMAT(I3)
C
WRITE(*,*) 'Enter 1 if Ver Pol or 2 if Hor Pol!'
READ(*,40)POL
WRITE(*,20)
C
WRITE(*,*) 'Type in output filename.'
READ(*,50)OUTPUT
50  FORMAT(a12)
OPEN(3,FILE=OUTPUT,STATUS='NEW')
C
WAVE = c / FREQ
WRITE(*,*)WAVE
k = (2.*PI)/WAVE
CONST = -((CEXP(-J*(PI/4.)))/(2.*SQRT(2.*PI*K)))
C
C
DO 400 I = 1,DEGREE
RADINC = (((FLOAT(I-1))/2)+DEGINC)*(PI/180.))+.0001
RADSCA = (((FLOAT(I-1))/2)+DEGSCA)*(PI/180.))+.0001
DEG = DEGINC +(FLOAT(I-1)/2)
C
IF(RADINC.LE.(270.*(PI/180.))) THEN
    PHI1PR = (90.*(PI/180.)) + RADINC
ELSE
    PHI1PR = RADINC - (270.*(PI/180.))
ENDIF
C
IF(RADSCA.LE.(270.*(PI/180.))) THEN
    PHI1 = (90.*(PI/180.)) + RADSCA
ELSE
    PHI1 = RADSCA - (270.*(PI/180.))
ENDIF
C

```



```

IF(RADINC.LE.(PI/2.)) THEN
    PHI2PR = (270.*(PI/180.)) + RADINC
ELSE
    PHI2PR = RADINC - (PI/2.)
ENDIF
C
IF(RADSCA.LE.(PI/2.)) THEN
    PHI2 = (270.*(PI/180.)) + RADSCA
ELSE
    PHI2 = RADSCA - (PI/2.)
ENDIF
C
C
C
PLUS1 = COS((PHI1+PHI1PR)/2.)
MINUS1 = COS((PHI1-PHI1PR)/2.)
PLUS2 = COS((PHI2+PHI2PR)/2.)
MINUS2 = COS((PHI2-PHI2PR)/2.)
C
C
IF(POL.EQ.1) THEN
    D1 = CONST * ((1./MINUS1)-(1./PLUS1))
    D2 = CONST * ((1./MINUS2)-(1./PLUS2))
ELSE
    D1 = CONST * ((1./MINUS1)+(1./PLUS1))
    D2 = CONST * ((1./MINUS2)+(1./PLUS2))
ENDIF
C
C
H1 = CEXP(J*k*(d/2.)*sin(RADINC))*D1*
&    CEXP(J*k*(d/2.)*sin(RADSCA))
C
H2 = CEXP(-J*k*(d/2.)*sin(RADINC))*D2*
&    CEXP(-J*k*(d/2.)*sin(RADSCA))
C
C
HTOT = H1 + H2
RCS2 = 2.*PI*((cabs(HTOT))**2)
RCS2D = 10.*alog10(RCS2)
C
C
RCS3 = RCS2*(2.*(L**2))/WAVE
RCS3D = 10.*alog10(RCS3)
WRITE(3,500)DEG,RCS3D
500  FORMAT(2PE20.7)
400  CONTINUE
CLOSE(3,STATUS='keep')
C
C
END

```

## *Appendix C, Section II. BISPH Code*

This section contains the computer code that provided the exact solution for the 2.5 inch, 5 inch, and 6 inch spheres used throughout this research effort. The code provides the exact solution for both monostatic and bistatic situations. The code is used by WRDC/SN in their compact range at WPAFB, OH to provide the exact sphere solution used in their RCS measurements. Data from BISPH is provided in Table 11 for a 5 inch sphere at 10 GHz and vertical polarization. The data shows how the exact RCS is dependant on the bistatic separation angle between the two antennas. The variation in RCS for a one degree bistatic angle change indicates the importance of knowing the exact placement of the antennas in the measurement procedure.

-----<< SWSP82.FOR >>-----

THIS PROGRAM GENERATES SPHERE CALIBRATION DATA FOR THE SWEEP  
FREQUENCY SYSTEM.

KEITH SHUBERT/CHARLEY RHOADS                    MODIFICATIONS - NORMAN LI  
.....23-OCT-78.....                    \* \* \*    16-AUG-82    \* \* \*

OUTPUT-----MAGNITUDE: 20 DEG LOG(SQRT(RCS)); RCS IN SQUARE CM  
                  PHASE       : RADIANS; WITH RESPECT TO THE SPHERE CENTER

MODIFICATIONS: THIS PROGRAM WAS MODIFIED FOR USE ON A PDP-11/23.  
                  OUTPUT IS NOW STORED IN ONE 2-DIMENSIONAL ARRAY  
                  YM. THE PHASE IS GIVEN IN RADIANS. OUTPUT GOES  
                  TO AN UNFORMATTED FILE. LEGIBILITY WAS ALSO IM-  
                  PROVED.

COMMON BUFF,NDIM,ANST,AINC  
COMPLEX ETH,EPH  
character\*50 vertitle  
character\*50 hortitle  
character\*50 header  
character\*20 output\_file  
data vertitle /'RCS'(dBSM)'/  
data hortitle /'Bistatic Angle (deg)'/  
REAL KA  
DIMENSION AM(2000),PH(2000),xdata(2000)  
INTEGER\*2 INFILE(15)  
BYTE BUFF(35000)  
LOGICAL VHP,LBK,plt  
DATA PI/3.141593/  
DATA LT,LF/-1,0/  
CONST=2.\*PI\*1.E9/300.E6  
RTD=180./PI

----- DEFINE RANGE GEOMETRY  
SPHERICAL SCATTERING

WRITE(5,\*) 'INPUT T FOR VERTICAL AND F FOR HORIZONTAL POLARIZATION'  
ACCEPT \*, VHP  
WRITE(5,\*) 'INPUT ANTENNA start SEPARATION IN DEGREES'  
ACCEPT \*, ASD  
asdp=asd  
write(5,\*) 'Input Antenna stop separation in Degrees'  
accept \*, asdl  
THB=180.-ASD  
THBp=thb  
PHB=-90.  
IF(VHP) PHB=180.  
write(5,\*) 'Input antenna separation increment >= 1 degree'  
accept \*, dela  
nba=(asdl-asd)/dela+1.01  
  
WRITE(5,\*) 'INPUT SPHERE DIAMETER IN INCHES'  
ACCEPT \*, SDI

```

WRITE(5,*) 'INPUT MIN FREQ. (GHZ): '
ACCEPT *, FMIN
ANST=FMIN*1000.
WRITE(5,*) 'INPUT MAX FREQ. (GHZ): '
ACCEPT *, FMAX
WRITE(5,*) ' FREQUENCY INCREMENT (GHZ): '
ACCEPT *, DELF
write(5,*) 'Type in output filename'
read(5,15) output_file
15  format(a20)
write(5,*) 'Plot data (T=yes, F=no)'
accept *, plt
if(plt) then

write(5,*) ' Enter a title/header of 50 chars or less'
read(5,123)header
123  format(x,a50)
endif
NF=(FMAX-FMIN)/DELF+1.1
NDIM=NF

C
SRCM=SDI*2.54/2.
SRM=SRCM/100.
AREACM=4.*PI*SRCM**2
AINC=DELF*1000.
CKA=CONST*SRM
FREQ=FMIN-DELF

C
C ---- START OF LOOP ----
C
C*****
C BISTATIC SCATTERING FROM A SPHERE
C*****
open(unit=10,file=output_file,status='new',err=100)
write(10,*) ' sph.      Sep. Angle      freq      Bistatic'
write(10,*) ' size      (deg)          (Ghz)      RCS'
write(10,*) ' (in)              (dBsm)      (Phase)'
DO 40 I=1,NF
    FREQ=FMIN+(I-1)*DELF
    KA=CKA*FREQ
    asd=asd
    thb=thbp
do 45 jj=1,nba
    asd=asd+(jj-1)*dela
    thb=180.-asd
    CALL FIELD(1.,KA,THB,PHB,ETH,EPH,IER)
    IF(VHP) THEN
        RCS=AREACM*CABS(ETH)**2
        PH(I)=CATAN2(ETH)*RTD
    ELSE
        RCS=AREACM*CABS(EPH)**2
        PH(I)=CATAN2(EPH)*RTD
    END IF
    AM(jj)=10.*ALOG10(RCS)-40.
    xdata(jj)=jj-1
    write(10,50) sdi,asd,freq,AM(jj),PH(I)

```

```

45      continue
      write(10,*) ' '
40      CONTINUE
      goto 101
100     write(6,*) 'Filename already exists!!!'
50     FORMAT (f5.2,2X,f12.4,2X,f12.8,2X,f12.8,2X,f13.8)
101     continue
      if(plt)then

C       call plotscr(xdata,am,nba,header,vertitle,hortitle)
      endif
      STOP
      END

C -----
      FUNCTION CATAN2(Z)
      COMPLEX Z
      RZ=REAL(Z)
      FIZ=AIMAG(Z)
      CATAN2=ATAN2(FIZ,RZ)
      RETURN
      END

C -----
C -----
C -----
      SUBROUTINE GPS(VHP,KA,EV,ETH,EPH)
      COMPLEX ETH,EPH,ETHT,EPHT,ETHI,EPHI
      REAL KA
      LOGICAL VHP
      IF(VHP) THEN
      THT=180.
      PHT=180.
      CALL FIELD(1.,KA,THT,PHT,ETHT,EPHT,IER)
      ETH=ETHT
      THI=180.-2.*EV
      PHI=180.
      CALL FIELD(1.,KA,THI,PHI,ETHI,EPHI,IER)
      ETH=ETH+ETHI
      ELSE
      THT=180.
      PHT=-90.
      CALL FIELD(1.,KA,THT,PHT,ETHT,EPHT,IER)
      EPH=EPHT
      THI=180.-2.*EV
      PHI=90.
      CALL FIELD(1.,KA,THI,PHI,ETHI,EPHI,IER)
      EPH=EPH+EPHI
      END IF
      RETURN
      END

C -----
C -----
C -----
C -----
C -----
      BISTATIC-BACKSCATTERED FIELD OF A SPHERE

      SUBROUTINE FIELD(TIMCON,KA,THE,PHI,GTHE,GPHI,IER)

```

```

C
C      TIMCON=TIME CONVENTION
C          =+1.0 FOR HARRINGTON (-JWT)
C          =-1.0 FOR STRATTON  (+JWT)
C
C      COMPLEX J,GTHE,GPHI,SGTHE,SGPHI,BN,CN
C      DIMENSION SJ(150),SY(150),DSJ(150),DSY(150),DP(150)
C      DOUBLE PRECISION TPCERR,ANGDIF,P(151),DEF,U,DCOS,DSIN,V
C      REAL KA
C
C ---- DEFINE CONSTANTS
C      J=SQRT(-1)
C      TPCERR=TOTAL % CHANGE ERROR ALLOWABLE BETWEEN
C      SUCCESSIVE ITERATIONS TO DEVINE CONVERGENCE.
C      TPCMAG=TOTAL % CHANGE EN MAGNIU
C      ACTUALLY OCCURRING BETWEEN SUCCESSIVE LOOPS.
C      DATA PI,J,TPCERR,ANGDIF/3.141593,(0.,1.),1.0D-20,1.0D-2/
C      -----
C
C ---- INITIALIZE VARIABLES
C      GTHE=CMPLX(0.,0.)
C      GPHI=CMPLX(0.,0.)
C      SGTHE=CMPLX(0.,0.)
C      SGPHI=CMPLX(0.,0.)
C
C      MO=150
C      CALL SPHBES(KA,SJ,SY,DSJ,DSY,MO,MAX)
C ---- ELIMINATE ZERO ORDER TERMS FROM THE ARRAYS
C      MAX=MAX-1
C      DO 5 L=1,MAX
C          L=L+1
C          SJ(L)=SJ(LL)
C          SY(L)=SY(LL)
C          DSJ(L)=DSJ(LL)
C          DSY(L)=DSY(LL)
5      CONTINUE
C
C      CHKTHE=ABS(180.-THE)
C      IF (CHKTHE .LT. ANGDIF) GOTO 20
C      IF (ABS(THE) .LT. ANGDIF) GOTO 15
C      U=DCOS(DBLE(THE*PI/180.))
C      V=DSIN(DBLE(THE*PI/180.))
C      MAXN=MAX+1
C      M=1
C      DEF=-1.D0
C      CALL POLY2(DEF,U,M,MAXN,P)
C      DO 10 N=1,MAX
C          DP(N)=(FLOAT(N+1)*U*P(N)-FLOAT(N-M+1)*P(N+1))
C          & *V/(1.-U**2)
C ---- NO LONGER NEED P(N)
C      P(N)=P(N)/V
10      CONTINUE
C      GOTO 40
15      DO 16 N=1,MAX
C          FN=FLOAT(N)
C          DP(N)=.5*FN*(FN+1.)

```

```

P(N)=(-1.)*DP(N)
16 CONTINUE
GOTO 40
20 DO 30 N=1,MAX
FN=FLOAT(N)
P(N)=0.5*FN*(FN+1.)*(-1.)**N
DP(N)=P(N)
30 CONTINUE
C
40 DO 50 N=1,MAX
AN=(-1.)*FLOAT(2*N+1)/FLOAT(N**2+N)
BN=AN*(SJ(N)+KA*DSJ(N))/(SJ(N)+KA*DSJ(N)-J*
& (SY(N)+KA*DSY(N)))
CN=AN*SJ(N)/(SJ(N)-J*SY(N))
GTHE=GTHE+BN*DP(N)-CN*P(N)
GPHI=GPHI+BN*P(N)-CN*DP(N)
AA=CABS(GTHE-SGTHE)
BB=CABS(GTHE)
CC=CABS(GPHI-SGPHI)
DD=CABS(GPHI)
IF (BB .NE. 0.) GOTO 44
AA=0.
BB=1.
44 IF (DD .NE. 0.) GOTO 45
CC=0.
DD=1.
45 TPCMAG=AA/BB+CC/DD
IER=N
IF (TPCMAG .LE. TPCERR) GOTO 60
SGTHE=GTHE
SGPHI=GPHI
50 CONTINUE
IER=0
C
60 GTHE=TIMCON*GTHE*J*COS(PHI*PI/180.)/KA
GPHI=TIMCON*GPHI*J*SIN(PHI*PI/180.)/KA
RETURN
END
C
C -----
C
SUBROUTINE SPHBES(X,BJ,BY,BP,YP,IDM,MAX)
C
C X=ARGUMENT
C BJ=SPHERICAL BESSEL FUNCTION ARRAY
C BY=SPHERICAL NEUMAN FUNCTION ARRAY
C BP=PRIMED BESSEL FUNCTION ARRAY
C YP=PRIMED NEUMAN FUNCTION ARRAY
C IDM=MAX NUMBER OF ORDERS TO BE COMPUTED
C MAX=MAX NUMBER OF ORDERS ACTUALLY COMPUTED
C
C COMPUTATION IS STOPPED WHEN THE VALUE OF A NEUMAN
C FUNCTION MAGNITUDE IS GREATER THAN FMAX WHICH IS
C DEFINED INTERNALLY TO THE PROGRAM.
C
C DIMENSION BJ(1),BY(1),BP(1),YP(1)

```

```

FMAX=1.E35
FMIN=1.E-38
SX=SIN(X)/X
CX=COS(X)/X
FF1=SX
FF2=SX/X-CX
YY1=-CX
YY2=-(CX/X+SX)
BY(1)=YY1
BY(2)=YY2
BYB=YY1
BYC=YY2
I=2
20  BYA=BYB
    BYB=BYC
    BYC=(2.*I-1.)*BYB/X-BYA
    L=I+1
    IF (L .LE. IDM) BY(L)=BYC
    AY1=ABS(BYC)
    I=I+1
    IF (AY1 .LT. FMAX) GOTO 20
    MAX=I-1
    BJB=0.
    BJA=FMIN
    I=MAX
50  I=I-1
    BJC=BJB
    BJB=BJA
    BJA=(2.*I+3.)*BJB/X-BJC
    L=I+1
    IF (L .LE. IDM) BJ(L)=BJA
    IF (I .GT. 0) GOTO 50
    ALF=BJ(2)/FF2
    IF (ABS(FF1) .GT. ABS(FF2)) ALF=BJ(1)/FF1
    ALF=1./ALF
    K=MAX
    IF (K .GT. IDM) K=IDM
    DO 60 I=1,K
60  BJ(I)=BJ(I)*ALF
    BP(1)=-BJ(2)
    YP(1)=-BY(2)
    DO 80 I=2,K
    IM=I-1
    FAC=I/X
    BP(I)=BJ(IM)-FAC*BJ(I)
80  YP(I)=BY(IM)-FAC*BY(I)
    RETURN
    END

```

C  
C  
C  
C  
C  
C  
C  
C

-----

ASSOCIATED LEGENDRE POLYNOMIAL SUBROUTINE

FOR HARRINGTON'S DEFINITION OF THE ASSOCIATED  
LEGENDRE POLYNOMIAL-----> DEF=-1.



```

C      FOR THE OTHER DEFINITION OF THE ASSOCIATED
C      LEGENDRE POLYNOMIAL=====> DEF=1.
C
C      SUBROUTINE POLY2(DEF,X,M,MAXN,P)
C      DOUBLE PRECISION DEF,X,P(1),SQ,DSQRT,DBLE,FL1,FL2,FL3
C      SQ=DSQRT(1.D0-X**2)
C      P(1)=1.D0
C      IF (M.EQ.0) GOTO 1
C      DO 2 L=1,M
C      P(1)=DEF*DBLE(FLOAT(2*L-1))*SQ*P(1)
2      CONTINUE
1      P(2)=DBLE(FLOAT(2*M+1))*X*P(1)
C      DO 3 K=3,MAXN
C      I=K-1
C      J=K-2
C      N=M+K-1
C      FL1=DBLE(FLOAT(N+N-1))
C      FL2=DBLE(FLOAT(N+M-1))
C      FL3=DBLE(FLOAT(N-M))
C      P(K)=(FL1*X*P(I)-FL2*P(J))/FL3
3      CONTINUE
C      RETURN
C      END
C -----
C      FUNCTION ACOS(X)
C      DOUBLE PRECISION DSQRT
C      DATA PI/3.141593/
C      IF (X .GE. 1.) GOTO 1
C      IF (X .LE. -1.) GOTO 2
C      ACOS=(PI/2.)-ATAN(X/DSQRT(1.D0-X*X))
C      RETURN
1      ACOS=0.
C      RETURN
2      ACOS=PI
3      RETURN
C      END
C -----

```

### *Appendix C, Section III. ARMS Bistatic Code*

Section III contains the computer code required to automate bistatic RCS measurements in AFIT's far-field RCS measurement chamber. Only the two subroutines from ARMS that were changed are provided here. For the rest of the ARMS program, refer to Reference (14).

### FREQUENCY RESPONSE SUBROUTINE

```
550  !
560  ! THIS SUBROUTINE IS THE MAIN MENU FOR THE FREQUENCY
RESPONSE.
570  !
580  SUB Fr(Date$)
590  ASSIGN @Nwa TO 716
600  ASSIGN @Nwa_data TO 716;FORMAT OFF
610  OPTION BASE !
620  INTEGER Preamble,Size,Cals,No_points,Dm,Bis
630  DIM Bkgdt(801,2),Bkgtr(801,2),Reference(801,2),
Target(801,2),Cal_tgt(801,2),Ex_sphere(801,2),Cal_tgt2(801,2
),
E_data(1602)
640  DIM Data(801,2),Bkgdr(801,2),S_data(1605),
Referenc1(801,2)
650  E_data(1)=0
660 New: CALL Clear_crt
670  PRINT "FREQUENCY RESPONSE can be done for either
MONOSTATIC or BISTATIC measurements!"
680  Bis=0
690  PRINT ""
700  PRINT "      K0 - MONOSTATIC FREQUENCY RESPONSE"
710  PRINT ""
720  PRINT "      K4 - BISTATIC FREQUENCY RESPONSE"
730  ON KEY 0 LABEL "MONOSTATIC FR" GOTO 723
740  ON KEY 4 LABEL "BISTATIC FR" GOTO 689
750  ON KEY 1 GOTO Idle
760  ON KEY 2 GOTO Idle
770  ON KEY 3 GOTO Idle
780  ON KEY 5 GOTO Idle
790  ON KEY 6 GOTO Idle
800  ON KEY 7 GOTO Idle
810  ON KEY 8 GOTO Idle
820  ON KEY 9 GOTO Idle
830 Idle:  DISP "Please hit the appropriate soft key."
840  GOTO Idle
850  OFF KEY
860  Bis=1
870  CALL Clear_crt
880  PRINT "You have selected a BISTATIC FREQUENCY RESPONSE
(BFR)!"
890  PRINT ""
900  PRINT "BFR CURRENTLY works ONLY for bistatic angles of
45, 90, & 135 deg from 8 to 12.4 GHz AND V-Pol!"
910  PRINT ""
920  PRINT "IMPORTANT NOTE: This requires a correct
instrument state setting on HP-8510!"
930  PRINT ""
940  PRINT "NOTE: Another freq range or bistatic angle will
```

```

require a DIFFERENT sphere file to obtain valid
measurements!"
950   PRINT ""
960   PRINT "Refer to T. McCool's (Class GE-90D) thesis for
help on instrument state or exact sphere file!!"
970   PRINT ""
980   Ans$="N"
990   INPUT "Do you want to start over? (Enter Y, or Default
is NO)",Ans$
1000  IF Ans$="Y" THEN GOTO 660
1010  CALL Clear_crt
1020  PRINT "Select the desired bistatic angle>"
1030  PRINT ""
1040  PRINT ""
1050  PRINT "Enter"
1060  PRINT ""
1070  PRINT "  45 ... Bistatic angle = 45 degrees!"
1080  PRINT "  90 ... Bistatic angle = 90 degrees!"
1090  PRINT " 135 ... Bistatic angle = 135 degrees!"
1100  PRINT ""
1110  INPUT Bsa
1120  IF Bsa<>45 AND Bsa<>90 AND Bsa<>135 THEN GOTO 1010
1130  OUTPUT @Nwa;"RECA2;POIN801;"
1140  CALL Clear_crt
1150  OFF KEY
1160  IF Bis=1 THEN GOTO 1410
1170  OUTPUT @Nwa;"RECA8;POIN801;"
1180  PRINT "Choose the range for your frequency response."
1190  PRINT ""
1200  PRINT ""
1210  PRINT "ENTER"
1220  PRINT ""
1230  PRINT "  2 ..... 8 to 12.4 GHz."
1240  PRINT "  3 ..... 6 to 18 GHz."
1250  PRINT ""
1260  PRINT "Default is 8 to 12.4 GHz."
1270  PRINT ""
1280  Frange=2
1290  INPUT Frange
1300  IF Frange<>2 AND Frange<>3 THEN GOTO 660
1310  Pol$=""
1320  INPUT "Type the polarization of the field (H or V:
Default is horizontal).",Pol$
1330  IF Pol$=<>"H" AND Pol$=<>"V" AND Pol$=<>" THEN GOTO
1320
1340  IF Pol$="" OR Pol$="H" THEN
1350    Pol$="HORIZONTAL"
1360    Pol=0
1370  ELSE
1380    Pol$="VERTICAL"
1390    Pol=1
1400  END IF

```

```

1410 Pol$="VERTICAL"
1420 Sweep$=""
1430 INPUT "Type 'S' for step sweep, or 'R' for ramp sweep
(Ramp is default).",Sweep$
1440 IF Sweep$<>"S" AND Sweep$<>"R" AND Sweep$<>" " THEN
GOTO 1430
1450 IF Sweep$="S" THEN Sweep$="STEP"
1460 IF Sweep$="R" OR Sweep$="" THEN Sweep$="RAMP"
1470 Aver=32
1480 INPUT "Enter the averaging factor. (Between 1 and
4096:
32 is default)",Aver
1490 IF Aver<1 OR Aver>4096 THEN GOTO 960
1500 Tmegte=7
1510 INPUT "What time gate do you want (ns)? (Default is 7
ns)",Tmegte
1520 Pre_gate$=VAL$(Tmegate)
1530 IF Bis=1 THEN GOTO 1630
1540 IF Frange=2 THEN 1590
1550 Fmin=6
1560 Fmax=18
1570 Df$="ES6TO18"
1580 GOTO 1730
1590 Fmin=8
1600 Fmin=12.4
1610 Df$="ES8TO12P4"
1620 GOTO 1730
1630 Fmin=8
1640 Fmax=12.4
1650 IF Bsa=45 THEN GOTO 1680
1660 IF Bsa=90 THEN GOTO 1700
1670 IF Bsa=135 THEN GOTO 1720
1680 Df$="BA45"
1690 GOTO 1730
1700 Df$="BA90"
1710 GOTO 1730
1720 Df$="BA135"
1730 CALL Clear_crt
1740 IF Bis=0 THEN GOTO 1780
1750 PRINT "          BISTATIC FREQUENCY RESPONSE"
1760 PRINT ""
1770 IF Bis=1 THEN GOTO 1790
1780 PRINT "          MONOSTATIC FREQUENCY RESPONSE"
1790 PRINT ""
1800 PRINT "The data you have selected is:"
1810 PRINT ""
1820 PRINT ""
1830 IF Bis=0 THEN GOTO 1850
1840 PRINT "Bistatic Angle is          ",Bsa,"degrees."
1850 PRINT "Data File is                    ",Df$,"."
1860 PRINT "Start frequency is              ",Fmin,"GHz."
1870 PRINT "Stop frequency is               ",Fmax,"GHz."

```

```

1880 PRINT "Polarization is          ",Pol$,"."
1890 PRINT "The oscillatoor is in    ",Sweep$,"mode."
1900 PRINT "The gate width is       ",Tmegte,"Nsec."
1910 Print " The averaging is       ",Aver,"."
1920 PRINT ""
1930 PRINT ""
1940 PRINT "      ARE THE CORRECT ANTENNAS INSTALLED?"
1950 Ans$="N"
1960 INPUT "Do you want to change anything? (Enter Y, or
Default is NO).",Ans$
1970 IF Ans$="Y" THEN GOTO 660
1980 !
1990 ! SEND THE INPUT INFORMATION TO THE HP 8510.
2000 !
2010 PRINT ""
2020 PRINT "      PLEASE WAIT"
2030 OUTPUT @Nwa;"STAR";Fmin;"GHZ;STOP";Fmax;"GHZ;"
2040 OUTPUT @Nwa;"GATESPAN";Tmegte;"ns;"
2050 IF Sweep$="RAMP" THEN
2060     OUTPUT @Nwa;"RAMP;"
2070 ELSE
2080     OUTPUT @Nwa;"STEP;"
2090 END IF
2100     OUTPUT @Nwa;"ENTO;"
2110 WAIT 5
2120 !
2130 ! THE FOLLOWING LINES CALL THE HEADER AND MEASUREMENT
SUBROUTINES.  THE DATA COMES IN 801 REAL/IMAGINARY DATA
PAIRS.
2140 !
2150 Measurement$="fr"
2160 CALL Ref_hdr(Pol$,Measurement$)
2170 CALL Measure(Reference(*),Aver,Sweep$)
2180 BEEP
2190 CALL Refbkgnd_hdr(Pol$,Measurement$)
2200 CALL Measure(Bkgdr(*),Aver,Sweep$)
2210 BEEP
2220 PRINT ""
2230 Same: Bck$="N"
2240 PRINT "Do you want to measure a separate target
background?"
2250 INPUT "Enter Y or N:  default is no.",Bck$
2260 CALL Clear_crt
2270 IF Bck$="Y" OR Bck$="y" THEN
2280     CALL Tgtbkgnd_hdr
2290     CALL Measure(Bkgdt(*),Aver,Sweep$)
2300     BEEP
2310 ELSE
2320     FOR K=1 TO 2
2330         FOR L=1 TO No_points
2340             Bkgdt(L,K)=Bkgdr(L,K)
2350         NEXT L

```

```

2360     NEXT K
2370 END IF
2380 CALL Clear_crt
2390 CALL Target_hdr(Bck$)
2400 CALL Measure(Target(*),Aver,Sweep$)
2410 !
2420 !THE FOLLOWING LINES SUBTRACT THE REFERENCE AND TARGET
BACKGROUNDS FROM REFERENCE AND TARGET MEASUREMENTS,
RESPECTIVELY.
2430 !
2440 PRINT "Please wait while the system is number
crunching."
2450 No_points=801
2460 FOR I=1 TO 2
2470     FOR J=1 TO No_points
2480         Target(J,I)=Target(J,I)-Bkgdt(J,I)
2490         Referenc1(J,I)=Reference(J,I)-Bkgdr(J,I)
2500     NEXT J
2510 NEXT I
2520 !
2530 ! THE FOLLOWING LINES CALCULATE (Target-Bkgnd)/
(Reference-Bkgnd).
2540 !
2550 FOR L=1 TO No_points
2560 Den=Referenc1(L,1)^2+Referenc1(L,2)^2
2570 Cal_tgt(L,1)=(Target(L,1)*Referenc1(L,1)+Target(L,2)*
Referenc1(L,2))/Den
2580 Cal_tgt(L,2)=(Target(L,2)*Referenc1(L,1)-Target(L,1)*
Referenc1(L,2))/Den
2590 NEXT L
2600 !
2610 !THE FOLLOWING LINES READ IN THE EXACT SOLUTION FOR
THE
5 INCH SPHERE.
2620 !
2630 IF E_data(1)<>0 THEN 2740
2640     ASSIGN @Dt TO Df$
2650     ENTER @Dt;E_data(*)
2660     ASSIGN @Dt TO *
2670 FOR I=1 TO No_points
2680     Ex_sphere(I,1)=E_data(I)
2690     Ex_sphere(I,2)=E_data(I+No_points)
2700 NEXT I
2710 !
2720 ! THE NEXT LINES CALCULATE (exact_sphere*sub_fields)
2730 !
2740 FOR K=1 TO No_points
2750     Cal_tgt2(K,1)=Cal_tgt(K,1)*Ex_sphere(K,1)-
Cal_tgt(K,2)
*Ex_sphere(K,2)
2760
Cal_tgt2(K,2)=Cal_tgt(K,1)*Ex_sphere(K,2)+Cal_tgt(K,2)

```

```

*Ex_sphere(K,1)
2770 NEXT K
2780 !
2790 !SEND TO HP8510. SE*(Target-Bkgdt)/(Reference-Bkgdr)
2800 !
2810 OUTPUT @Nwa;"FORM3;OUTPDATA"
2820 ENTER @Nwa_data;Preamble,Size,Bkgtr(*)
2830 OUTPUT @Nwa;"AVEROFF;GATEOFF"
2840 Dm=1
2850 OUTPUT @Nwa;"HOLD;"
2860 OUTPUT @Nwa;"FORM3;INPURAW1"
2870 OUTPUT @Nwa_data;Preamble,Size,Cal_tgt2(*)
2880 BEEP
2890 CALL Fr_menu(Fmin,Fmax,Pol,Cal_tgt2(*) ,Date$,
Pre_gate$,Return)
2900 IF Return=1 THEN GOTO New
2910 IF Return=2 THEN GOTO Same
2920 CALL Clear_crt
2930 SUBEND

```

#### PATTERN CUT SUBROUTINE

```

4680 !
4690 !THIS SUBROUTINE IS THE MAIN MENU FOR THE PATTERN CUT.
4700 !
4710 SUB Pc(Date$)
4720 OPTION BASE 1
4730 DIM A(2),Pcbkgdt(365,2),Pcreference(365,2),
Plot_dt(365),Pcplot(370)
4740 DIM View(365),View2(365),Ptrace_data(365),Pdata(365)
4750 ASSIGN @Nwa TO 716
4760 ASSIGN @Nwa_data1 TO 716;FORMAT OFF
4770 INTEGER Preamble,Size,B,Bsa,Bis
4780 New_pc: Call Clear_crt
4790 PRINT "PATTERN CUTS can be done for either MONOSTATIC
or BISTATIC RCSs!!"
4800 Bis=0
4810 PRINT ""
4820 PRINT "      K0 - MONOSTATIC RCS"
4830 PRINT ""
4840 PRINT "      K4 - BISTATIC RCS"
4850 ON KEY 0 LABEL "MONOSTATIC PC" GOTO 5360
4860 ON KEY 4 LABEL "BISTATIC PC" GOTO 4970
4870 ON KEY 1 GOTO Idle
4880 ON KEY 2 GOTO Idle
4890 ON KEY 3 GOTO Idle
4900 ON KEY 5 GOTO Idle
4910 ON KEY 6 GOTO Idle
4920 ON KEY 7 GOTO Idle
4930 ON KEY 8 GOTO Idle

```



```

4940  ON KEY 9 GOTO Idle
4950 Idle:  DISP "Please hit appropriate soft key."54920
GOTO Idle
4960  OFF KEY
4970  Bis=1
4980  OUTPUT @Nwa;"RECA2;POIN801;"
4990  CALL Clear_crt
5000  PRINT "You have selected a BISTATIC RCS pattern
cut!!!"
5010  PRINT ""
5020  PRINT "If monostatic measurements are desired, you can
enter SHIFT RESET and start over OR enter exact monostatic
RCS
later."
5030  PRINT ""
5040  PRINT "For bistatic measurements, the chamber must be
configured with transmit and receive antennas at the desired
bistatic angle."
5050  PRINT ""
5060  PRINT "IMPORTANT NOTE:  For bistatic measurements, a
new instrument state must be saved on the HP_8510."
5070  PRINT ""
5090  PRINT "This program will call instrument state 2 for
bistatic measurements therefore INSTRUMENT STATE 2 MUST BE
SET
CORRECTLY!"
5100  PRINT ""
5110  PRINT "Refer to T. McCool's (Class GE-90D) thesis for
setting correct instrument state."
5120  PRINT ""
5130  PRINT ""
5140  PRINT "NOTE:  Bistatic angle should be between 0 and
180 degrees!"
5150  INPUT "ENTER the bistatic angle between transmit and
receive antenna.",Bsa
5160  IF Bsa<0 OR Bsa>180 THEN GOTO 5150
5170  IF Bsa=0 THEN
5180      GOTO 5220
5190  ELSE
5200      GOTO 5230
5210  END IF
5220  OUTPUT @Nwa;"RECA1;POIN801;"
5230  CALL Clear_crt
5240  PRINT "The exact sphere calibration IS NEEDED for
the desired FREQUENCY, POLARIZATION, BISTATIC ANGLE and
SPHERE DIAMETER!"
5250  PRINT ""
5260  PRINT "The Bistatic Manual contains data for a 5 inch
sphere from a program obtained from the BARN titled BISPH."
5270  PRINT ""
5280  PRINT "If you hit ENTER or entered 0 when prompted
for the bistatic angle, the program will default to a

```

```

monostatic measurement."
5290 PRINT ""
5300 PRINT "For monostatic measurements, ENTER -18.973
dBsm. NOTE: This is the exact solution for a 5 inch sphere!"
5310 PRINT ""
5320 PRINT "OTHERWISE ---"
5330 PRINT "provide exact bistatic sphere RCS!"
5340 INPUT "ENTER exact bistatic sphere RCS!",Rcs
5350 CALL Clear_crt
5360 OFF KEY
5370 PRINT "At present, only the 360 degree option is
active."
5380 CALL Clear_crt
5390 PRINT "Input the parameters for the pattern cut."
5400 PRINT ""
5410 PRINT ""
5420 INPUT "Operating frequency?(Between 2 and 18
GHz)",Freq
5430 IF Freq<2 OR Freq>18 THEN GOTO 5420
5440 CALL Clear_crt
5450 INPUT "What gate do you want (ns)? (Default is 7
ns)",Tmegte
5460 IF Tmegte=) THEN Tmegte=7
5470 Pre_gate$=VAL$(Tmegte)
5480 Pol$=""
5490 INPUT "Polarization? (Enter V or H: Default is
Horizontal)",Pol$
5500 IF Pol$<>" " AND Pol$<>"H" AND Pol$<>"V" THEN GOTO 5490
5510 IF Pol$="H" OR Pol$="" THEN
5520     Pol$="Horizontal"
5530     Pol=0
5540 ELSE
5550     Pol$="Vertical"
5560     Pol=1
5570 END IF
5580 CALL Clear_crt
5590 Speed=2.0
5600 Angle1=0
5610 Angle=360
5620 Resolution=1
5630 !INPUT "Starting aspect angle?",Angle1
5640 CALL Clear_crt
5650 !INPUT "Ending aspect angle?",Angle2
5660 CALL Clear_crt
5670 !INPUT "Angular resolution? (Default is 1 degree)",
Resolution
5680 IF Resolution=0 THEN Resolution=1
5690 CALL Clear_crt
5700 PRINT "You have input the following parameters."
5710 PRINT ""
5720 PRINT ""
5730 IF Bis=0 THEN GOTO 5760

```

```

5740 PRINT "Bistatic Angle .....",Bsa,"degrees."
5750 PRINT "Bistatic calibration RCS .",Rcs,"dBsm."
5760 PRINT "Operating frequency .....",Freq,"GHz."
5770 PRINT "Gate width .....",Tmegte,"nsec."
5780 PRINT "Polarization .....",Pol$,"."
5790 PRINT "Starting aspect angle ....",Angle1,"degrees."
5800 PRINT "Ending aspect angle .....",Angle2,"degrees."
5810 PRINT "Angular resolution .....",Resolution,"degree."
5820 PRINT ""
5830 PRINT ""
5840 Ans$=""
5850 INPUT " Do you want to change anything? (Enter Y of N:
Default is no)",Ans$
5860 IF Ans$<>" " AND Ans$="Y" AND Ans$<>"N" THEN GOTO 5850
5870 IF Ans$="Y" THEN GOTO 4780
5880 !
5890 ! THE FOLLOWING LINES SEND THE INPUT INFORMATION TO
THE HP8510.
5900 !
5910         OUTPUT @Nwa;"MARK1";Freq;"GHz;"
5920         OUTPUT @Nwa;"GATESPAN";Tmegte;"ns;"
5930         OUTPUT @Nwa;"ENTO;"
5940 No_degs=Angle2-Angle1
5950 No_incrmts=No_degs/Resolution
5960 PRINT "PLEASE WAIT"
5970 WAIT 3
5980 !
5990 ! THE NEXT SECTION CALLS THE HEADER AND MEASUREMENT
SUBROUTINES.
6000 !
6010 Measurement$="PC"
6020 CALL Refbkgn_d_hdr(Pol$,Measurement$)
6030 Rep$=""
6040 CALL Background_meas(Rep$)
6050 CALL Ref_hdr(Pol$,Measurement$)
6060 CALL Ref_meas(Sphamp)
6070 !
6080 ! ASK IF THERE IS A DIFFERENT TARGET BACKGROUND
6090 !
6100 New_tgt: PRINT "Do you need a separate target
background?"
6110 PRINT ""
6120 Rep$=""
6130 INPUT "Enter Y or N (Default is no).",Rep$
6140 IF Rep$="N" OR Rep$="" THEN GOTO 6190
6150 IF Rep$<>"Y" THEN GOTO 6130
6160 CALL Clear_crt
6170 CALL Tgtbkgn_d_hdr
6180 CALL Background_meas(Rep$)
6190 CALL Tgt_hdr
6200 CALL Tgt_meas(Pdata(*),No+incrmts,Speed)
6210 !

```

```

6220 ! THE FOLLOWING LINES CALCULATE THE RCS FO THE TARGET.
6230 !
6240 ! Plot_dt(J) .... RCS of the target (dBsm)
6250 ! Rcs ..... exact RCS of the 5 inch sphere
      (dBsm)
6260 ! Pdata(J) ..... target - target background (dBSM)
6270 ! Sphamp ..... reference target - reference target
background (dBSM)
6280 !
6290 IF Bis=1 THEN
6300 GOTO 6370
6310 ELSE
6320 GOTO 6340
6330 END IF
6340 Diam=5
6350 Rcs=10*LGT(PI*(Diam*.0254/2)^2)
6360 FOR J=1 TO 360
6370     Plot_dt(J)=Rcs+Pdata(J)-Sphamp
6380     Next J
6390 !
6400 ! THIS SUBROUTINE DISPLAYS THE PATTERN CUT ON THE CRT.
6410 !
6420 CALL Show_crt(Freq,Pol,Date$,Pre_gate$,Choice,
Plot_dt(*))
6430 IF Choice=1 THEN GOTO New_pc
6440 IF Choice=2 THEN GOTO New_tgt
6450 CALL Clear_crt
6460 SUBEND

```

### *Appendix C, Section IV. Data Transfer Code - Zenith to HP*

This section contains the computer code required to transfer ASCII data from a DOS operating system to an Hewlett-Packard system. This code will transfer the data into binary data (BDAT) format for use with the automatic software used to perform the frequency response RCS measurements in the AFIT anechoic chamber.

Trans - 232

```

10    OPTION BASE 1
20    DIM Array(1602)
30    MASS STORAGE IS ":INTERNAL,4,0"
40    CALL Clear_crt
50    CALL Transfer(Array(*))
60    FOR J=1 TO 1602
70    PRINT J,Array(J)
80    NEXT J
90    PAUSE
100   CALL Clear_crt
110   PRINT ""
120   PRINT ""
130   PRINT "INSERT STORAGE DISK INTO THE RIGHT HAND DRIVE"
140   PRINT ""
150   PRINT "PRESS";CHR$(129);"CONTINUE";CHR$(128);"WHEN
YOU ARE READY."
160   PAUSE
170   CALL Clear_crt
180   INPUT "ENTER THE FILE NAME FOR THE CURRENT SET OF
DATA.",Dt_file1$
190   CREATE BDAT Dt_file1$,1,12880
200   ASSIGN @Dt_file1 TO Dt_file1$
210   OUTPUT @Dt_file1;Array(*)
220   ASSIGN @Dt_file1 TO *
230   END
240   SUB Clear_crt
250       OUTPUT KBD;"K"; ! THE INVERSE VIDEO 'K' DOES NOT
APPEAR ON THE HARDCOPY BEFORE THE K.
260   SUBEND
270   SUB Transfer(REAL Array(*))
280       ON ERROR GOTO Err
290       CALL Clear_crt
300       PRINT ""
310       PRINT "The Baud rate is set at 4800."
320       PRINT ""
330       PRINT "Insure that the RS-232 cable is connected."
340       PRINT ""
350       PRINT "On the Z-248 enter the SMARTCOM directory;
SCOM is the executable file"
360       PRINT " Choose 1 - BEGIN COMMUNICATION; Choose
O(riginate); Choose C - Z-248 TO HP"
370       PRINT Choose F1; Choose 5 - Send file: push
ENTER; enter drive: file name"
380       PRINT ""
390       PRINT "PRESS";CHR$(129);"CONTINUE";CHR$(128);
"when the HP is ready to receive data."
400       PAUSE

```

```

410    ASSIGN @Rs232 to 9;FORMAT ON
420    ENABLE INTR 9
430    CONTROL 9,0;1
440    CONTROL 9,3;4800
450    CONTROL 9,4;3
460    CALL Clear_crt
470    ENTER 9;ARRAY(*)
480    OFF ERROR
490    CALL Clear_crt
500    BEEP
510    PRINT "Finished"
520    PRINT ""
530    PRINT ""
540    PRINT "PRESS";CHR$(129);"CONTINUE";CHR$(128);
"when you are ready."
550    PAUSE
560    SUBEXIT
570 Err:CALL Clear_crt
580    OFF ERROR
590    BEEP
600    PRINT ERRM$
610    Ans$="Y"
620    INPUT "Do you want to try again? (Y or N;
Default is Yes)",Ans$
630    IF Ans$<>"Y" AND Ans$<>"N" THEN GOTO 600
640    IF Ans$="Y" THEN GOTO 280
650    SUBEND

```

## *Bibliography*

1. Air Force Systems Command. *Bistatic Radar Cross Section Measurement Considerations*. RATSCAT Project No. 87-07. Holloman AFB, New Mexico: 6858th Test Group, September, 1988.
2. Balanis, Constantine A. *Advanced Engineering Electromagnetics*. New York: John Wiley and Sons, 1989.
3. Blacksmith, P., Jr. et al. "Introduction to Radar Cross-Section Measurements," *Proceedings of the IEEE*, 53: 901-920 (August 1965).
4. Currie, Nicholas C. *Radar Reflectivity Measurement: Techniques and Applications*. Norwood, Massachusetts: Artech House, Inc., 1989.
5. Dybdal, Robert B. "Radar Cross Section Measurements," *Proceedings of the IEEE*, 75: 498-516 (April 1975).
6. Hunka, John F. et al. "A Technique for the Rapid Measurement of Bistatic Radar Cross Sections," *IEEE Transactions on Antennas and Propagation*, AP-25. 243-248 (March 1977).
7. Joseph, Capt Philip J. Course notes in EENG 627, RCS Analysis, Measurement, and Reduction. School of Engineering, Air Force Institute of Technology (AU), Wright-Patterson AFB, OH, Spring 1990.
8. Kell, Robert E. "On the Derivation of Bistatic RCS from Monostatic Measurements," *Proceedings of the IEEE*, 53: 983-988 (August 1965).
9. Knott, Eugene F. et al. *Radar Cross Section*. Norwood, Massachusetts: Artech House, Inc., 1984.
10. Kouyoumjian, R. G. and L. Peters, Jr. "Range Requirements in Radar Cross Section Measurements," *Proceedings of the IEEE*, 53: 920-928 (August 1965).
11. ----- and P. H. Pathak. "A Uniform Geometrical Theory of Diffraction for an Edge in a Perfectly Conducting Surface," *Proceedings of the IEEE*, 62: 1448-1461 (November 1974).



12. Marhefka, R. J. *Radar Cross Section - Basic Scattering Code RCS-BSC (Version 2.0) User's Manual*. Technical Report 718295-15, Contract Number F33615-86-K-1023. The Ohio State University, Columbus, OH, February 1990.
13. McCool, Capt Stephen W. *Bistatic Resonant Scattering Measurements of Special Shapes*. MS Thesis, AFIT/GE/ENG/88D-27. School of Engineering, Air Force Institute of Technology (AU), Wright-Patterson AFB, OH, December 1988.
14. Owens, Capt Scott A. *Automation of an RCS Measurement and its Application to Investigate the Electromagnetic Scattering from Scale Model Aircraft Canopies*. MS Thesis, AFIT/GE/ENG/89D-38. School of Engineering, Air Force Institute of Technology (AU), Wright-Patterson AFB, OH, December 1989.
15. Ruck, George T. et al. *Radar Cross Section Handbook*. New York: Plenum Press, 1970.
16. Sanders, Capt Brian K. *Radar Image Processing for the AFIT Anechoic Chamber*. MS Thesis, AFIT/GE/ENG/90D. School of Engineering, Air Force Institute of Technology (AU), Wright-Patterson AFB, OH, December 1989.
17. Skinner, Paul and Hirsch Chizever. "Bistatic Radar Scattering from Simple Shapes," Technical Memorandum AFWAL-TM-86-23-AAWP. Avionics Laboratory, Air Force Wright-Aeronautical Laboratories, Wright-Patterson AFB, OH, October 1986.
18. Skolnik, Merrill I. *Introduction to Radar Systems*. New York: McGraw-Hill Book Company, 1980.
19. Walls, Major Charles G. *Evaluation of the Bistatic Equivalence Theorem for the Near and Far-Field Radar Cross Section of Complex Targets*. MS Thesis, AFIT/GE/ENG/89J-1. School of Engineering, Air Force Institute of Technology (AU), Wright-Patterson AFB, OH, June 1989.

## Vita

Captain Timothy D. McCool [REDACTED]

[REDACTED] He graduated from Mascoutah Community High School in Mascoutah, Illinois in 1979 and was awarded an Air Force ROTC scholarship. He received his Bachelor of Science Degree in Electrical Engineering from Southern Illinois University at Edwardsville in June of 1984. After being commissioned in the USAF in June of 1984, he entered active duty in November of the same year. Captain McCool's first assignment was to the Deputy for Engineering, Avionics, at Aeronautical Systems Division (ASD) at Wright-Patterson AFB, OH. While at ASD he provided avionics engineering support for airborne electro-optical systems in support of the Deputy for Airlift and Trainer Systems (ASD/AFEA) and the Deputy for Special Operational Forces (ASD/VXEA). In May of 1989 he entered the Air Force Institute of Technology in pursuit of a Master of Science Degree in Electrical Engineering.

[REDACTED] 10 [REDACTED]  
[REDACTED]

REPORT DOCUMENTATION PAGE			Form Approved OMB No. 0704-0188	
Public reporting burden for this collection of information is estimated to average 1 hour per response, including the time for reviewing instructions, searching existing data sources, gathering and maintaining the data needed, and completing and reviewing the collection of information. Send comments regarding this burden estimate or any other aspect of this collection of information, including suggestions for reducing this burden, to Washington Headquarters Services, Directorate for Information Operations and Reports, 1215 Jefferson Davis Highway, Suite 1204, Arlington, VA 22202-4302, and to the Office of Management and Budget, Paperwork Reduction Project (0704-0188), Washington, DC 20503.				
1. AGENCY USE ONLY (Leave blank)	2. REPORT DATE December 1990	3. REPORT TYPE AND DATES COVERED Master's Thesis		
4. TITLE AND SUBTITLE Analysis and Testing of a Bistatic Radar Cross Section Measurement Capability for the AFIT Anechoic Chamber		5. FUNDING NUMBERS		
6. AUTHOR(S)  Timothy D. McCool, Captain, USAF				
7. PERFORMING ORGANIZATION NAME(S) AND ADDRESS(ES)  Air Force Institute of Technology Wright-Patterson AFB, OH 45433		8. PERFORMING ORGANIZATION REPORT NUMBER  AFIT/GE/90D-37 ENG		
9. SPONSORING / MONITORING AGENCY NAME(S) AND ADDRESS(ES)  WRDC/SNA Wright-Patterson AFB, OH 45433		10. SPONSORING / MONITORING AGENCY REPORT NUMBER		
11. SUPPLEMENTARY NOTES				
12a. DISTRIBUTION / AVAILABILITY STATEMENT  Approved for public release; distribution unlimited		12b. DISTRIBUTION CODE		
13. ABSTRACT (Maximum 200 words) This research effort examined the feasibility of performing bistatic radar cross section (RCS) measurements in the AFIT anechoic chamber. The capability was established to measure the bistatic RCS of a target versus frequency and versus target azimuth angle. In either case, one of three bistatic angles (angle between transmit and receive antennas) is available: 45 degrees, 90 degrees, and 135 degrees. Accurate bistatic RCS measurements were obtained using a CW radar and utilizing background subtraction, bistatic calibration, and software range gating. Simple targets were selected for validation purposes since their bistatic RCS could be predicted. These consisted of spheres and flat plates (square, triangle, and five sided). Several computer codes were utilized for system validation. Two codes based on the Uniform Theory of Diffraction were used to predict the scattering from the flat plates. A program using a Mie series solution provided the exact scattering for the spheres, which were used for both RCS predictions and system calibration.				
14. SUBJECT TERMS Bistatic, Bistatic Radar Cross Section, Radar Cross Section, Anechoic Chamber, Far-field Range, Uniform Theory of Diffraction, Calibration, Flat Plates, Spheres			15. NUMBER OF PAGES 163	
			16. PRICE CODE	
17. SECURITY CLASSIFICATION OF REPORT Unclassified	18. SECURITY CLASSIFICATION OF THIS PAGE Unclassified	19. SECURITY CLASSIFICATION OF ABSTRACT Unclassified	20. LIMITATION OF ABSTRACT UL	